LIDAR wind speed measurements from a rotating spinner (SpinnerEx 2009)

Angelou, Nikolas; Mikkelsen, Torben Krogh; Hansen, Kasper Hjorth; Sjöholm, Mikael; Harris, Michael

Publication date:
2010

Document Version
Publisher's PDF, also known as Version of record

LIDAR Wind Speed Measurements from a Rotating Spinner: “SpinnerEx 2009”

Risø-R-Report

Nikolas Angelou, Torben Mikkelsen,
Kasper H. Hansen, Mikael Sjöholm,
Michael Harris

Risø-R-1741(EN)
August 2010

Risø DTU
National Laboratory for Sustainable Energy

Author:
Nikolas Angelou, Torben Mikkelsen, Kasper H. Hansen, Mikael Sjöholm, Michael Harris
Title:
LIDAR wind speed measurements from a rotating spinner (SpinnerEx 2009)
Division: Wind Energy Division (VEA)

Risø-R-1741(EN)
August 2010

Abstract (max. 2000 char.):

In the context of the increasing application of remote sensing techniques in wind energy, the feasibility of upwind observations via a spinner-mounted wind lidar was tested during the SpinnerEx 2009 experiment. The objective was to install a QinetiQ (Natural Power) ZephIR lidar in the rotating spinner of a MW-sized wind turbine, and investigate the approaching wind fields from this vantage point. Time series of wind speed measurements from the lidar with 50 Hz sampling rate were successfully obtained for approximately 60 days, during the measurement campaign lasting from April to August 2009.

In this report, information is given regarding the experimental setup and the lidar's operation parameters. The geometrical model used for the reconstruction of the scanning pattern of the lidar is described. This model takes into account the lidar's pointing direction, the spinner axis's vertical tilt and the wind turbine's yaw relative to the mean wind speed direction. The data analysis processes are documented. A methodology for the calculation of the yaw misalignment of the wind turbine relative to the wind direction, as a function of various averaging times, is proposed, using the lidar's instantaneous line-of-sight radial wind speed measurements.

Two different setups have been investigated in which the approaching wind field was measured at distances of 0.58 Ø and 1.24 Ø rotor diameters upwind, respectively. For both setups, the instantaneous yaw misalignment of the turbine has been estimated from the lidar measurements. Data from an adjacent meteorological mast as well as data logged within the wind turbine's control system were used to evaluate the results.

ISSN 0106-2840
ISBN 978-87-550-3836-3

Contract no.:

Group's own reg. no.: 1130403-01
(Føniks PSP-element)

Sponsorship: Dong Energy and Vestas Wind System

Cover: The NM80 2.5 MW Wind Turbine situated at Tjæreborg Enge equipped with a forward looking wind lidar in the tip of the rotating spinner.

Pages: 79
Tables: 4
References: 6

Information Service Department
Risø National Laboratory for Sustainable Energy
Technical University of Denmark
P.O.Box 49
DK-4000 Roskilde
Denmark
Telephone +45 46774005
bibl@risoe.dtu.dk
Fax +45 46774013
www.risoe.dtu.dk

Table of Contents

Preface

Mikael Rasmussen and Per Hansen from Risø DTU, and Dong Energy are gratefully acknowledged for skilled technical support and for access to the NM80 test turbine at Tjæreborg Enge located in Western Jutland, Denmark. Vestas Wind Systems is acknowledged for safety supervision of the operation of the NM80 research turbine. The SpinnerEx 2009 experiment has been conducted as part of the new Danish research infrastructure facility activities under the auspices of Windscanner.dk. Access to DONG Energy's NM80 Tjæreborg wind turbine and the local met-mast data has been facilitated in collaboration with the simultaneously ongoing DAN-AERO and TOPFARM test activities during the summer of 2009, which is also gratefully appreciated. Meteorology and turbine data was provided by the DAN-AERO MW project, carried out by Vestas, Siemens, LM, DONG Energy and Risø DTU in cooperation, funded partly by EFP-2007 "Experimental Rotor and Airfoil Aerodynamics on MW Wind Turbines" contract nr 33033-0074 and partly by the participants. Since April 2010 support to the analysis was also given via the HTF project "Integration of Wind LIDARs in Wind Turbines for Improved Productivity and Control" (HTF 049-2009-3).

1 Introduction

The objective of the Tjæreborg Enge lidar-in-spinner experiment (SpinnerEx 2009) was to investigate the possibility to perform real-time wind speed measurements using a light detection and ranging (lidar) system installed in the spinner of an operating wind turbine. The feasibility of this application can lead to the achievement of improved wind turbine control through lidar instruments mounted or integrated in wind turbines, with the benefits of enhanced power production performance, as well as increased life time of the wind turbine [Harris et al., 2006]. The optimization of the power production can be achieved through active lidar-controlled yaw, rpm and pitch control of the blades. An increase of the life time of the wind turbine, by protecting the blades from intense bending moments, can be accomplished by timely lidar detection of approaching extreme wind events, e.g. gusts [Harris et al., 2007].

For the needs of this experiment a modified version of the standard QinetiQ (Natural Power) ZephIR lidar was used (see Figure 1.1, left). The standard ZephIR lidar is a commercial available continuous wave coherent Doppler lidar developed by QinetiQ and manufactured by Natural Power, UK. This lidar system is capable of acquiring wind speed measurements at 50 Hz, while scanning radial wind speeds over a conical pattern, at selected distances set by the lidar's focus [Smith et al., 2006]. In the framework of the Windscanner.dk project the lidar system was modified to acquire data at up to 500 Hz sampling rate and was installed into the rotating spinner of the NM80 offshore test wind turbine, belonging to the Danish Dong Energy. The NM80 is a 2.5 MW turbine model, which has a rotor diameter of 80 m and a hub height of 59 m (see Fig. 1.1, right).

Figure 1.1 Photos of the QinetiQ (Natural Power) ZephIR lidar system (left) and the NM80 (Vestas) wind turbine (right).

The aim of the experiment was to study the feasibility of integrating a lidar system, with real time data acquisition, in the spinner of a wind turbine and to analyze the wind speed measurements from different heights and upwind distances away from the rotor plane regarding their usability for wind turbine control.

1.1 Period of experiment

The experiment took place from the beginning of April 2009 until the 11th of September 2009 (see Figure 1.2).

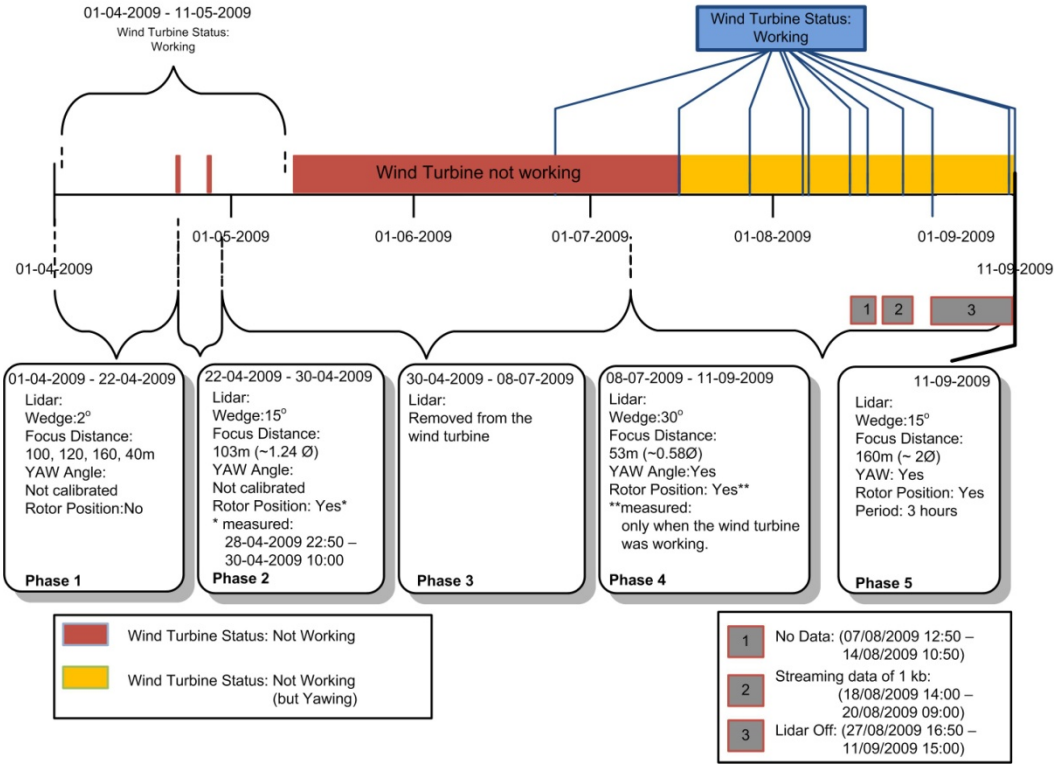

Figure 1.2 Information regarding the ZephIR lidar's and the NM 80 wind turbine's operation throughout the whole period of the experiment.

Throughout the whole period of the experiment, the lidar was scanning upwind at a single preset distance at a time. Based on the lidar's operation parameters the period of the experiment can be separated into 5 different phases:

- In the 1st phase (01/04 – 22/04) the lidar was operating, equipped with a 2° optical wedge prism. Wind speed measurements were acquired at 4 different focus distances[1] (40, 100, 120 and 160 m). During that period the wind turbine was working, but the position of the rotor was not measured. Additionally the wind turbine yaw angle was measured, although the measurements were not calibrated.

- In the 2nd phase (22/04 – 30/04) the lidar was operating, equipped with a 15° optical wedge prism and the focus distance was set to 103 m. The yaw of the wind turbine was still measured without calibration. Nonetheless measurements of the position of the spinner were successfully acquired from the evening of the 28th of April until the 30th of April.

- In the 3rd phase (01/05 – 08/07) the lidar was removed from the wind turbine and transferred to Risø DTU for calibration of the focus parameters.

- In the 4th phase (08/07 – 27/08) the lidar equipped with a 30° optical wedge prism was reinstalled in the spinner of the wind turbine, while the focus distance was set to 53 m. During this phase the wind turbine was operating only when experiments associated with the DAN – AERO MW project were held. In the rest of the period the wind turbine was not operating. Nevertheless it was yawing following the wind direction.

- In the 5th phase (11/09, from 15:00 until 18:00) the focus distance was set to 160 m and a 15° optical wedge was equipped to the lidar. The wind turbine was operating and measurements of the yaw and the position of the rotor were acquired.

[1] Focus distance is defined as the distance between the lidar head and the point where the laser beam is focused

1.2 Terrain Description

The NM80 wind turbine (#2 in Figure 1.3), in which the ZephIR lidar was installed, is placed in Tjæreborg Enge close to the city of Tjæreborg. To the North in a distance of approximately 1 km the city of Tjæreborg is located, while to the south and south-west there is open land to the North Sea. In the area a total number of 8 wind turbines can be found. There can be expected three wind direction sectors, for which the operation of the wind turbine is not affected from wakes produced by the adjacent turbines (assuming no wake expansion). These are:

1. 310^o – 90^o (Wind direction: North – North East)
2. 150^o – 180^o (Wind direction: South – South East)
3. 225^o – 245^o (Wind direction: South West)

A meteorological mast (MET mast) was installed for the purpose of the experiments at a distance approximately 310 m from the wind turbine and towards the direction of ~233^o SSW. The MET mast was equipped with calibrated cup anemometers (at 6 heights: 93, 77, 57, 41, 28.5 and 17 m) and sonic anemometers (at 2 heights: 93 m and 57 m), as well as two resolver-based wind vanes (at 93 m and 57 m).

Figure 1.3 The landscape of the area of the experiment where 8 wind turbines are located (Google Earth©). The lidar was mounted in the NM80 turbine indicated by #2 and the MET mast providing data for the experiment is indicated by M.

2 Experimental Setup

The ZephIR lidar was mounted inside the rotating spinner of a NM80 wind turbine (see Figure 2.1). This wind turbine model has a window in the tip of the spinner. Through a hole made in this window, the laser beam of the wind lidar was emitted and received. The lidar was aligned with the slightly vertically tilted horizontal axis of the wind turbine and it was scanning in its standard conical scan pattern in front of the wind turbine. The mount, made by Risø DTU for holding the lidar in a coaxial position, was quite robust, in order to prevent any movements or vibrations of the lidar due to gravitational forces or spinning acceleration.

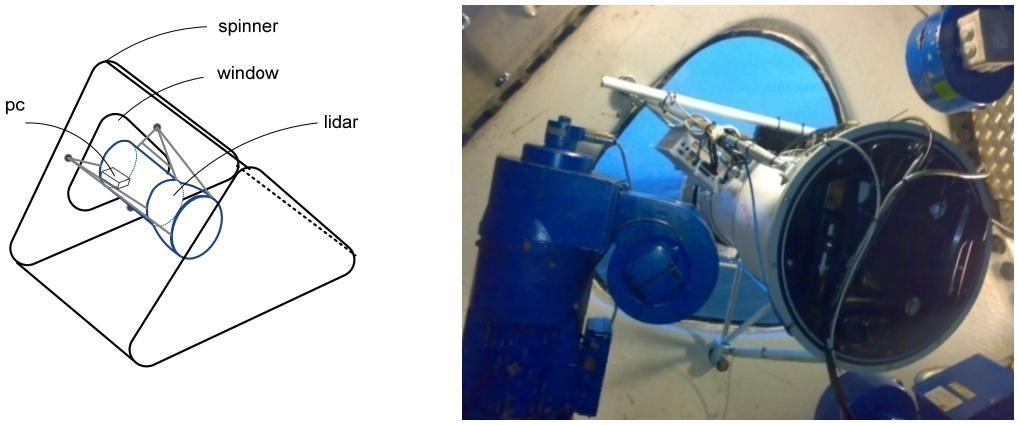

Figure 2.1 Schematics and photo of the ZephIR lidar inside the spinner of the NM80 turbine.

2.1 ZephIR lidar

The particular ZephIR lidar used in this experiment was a hybrid system which consisted by the optical head of a commercial QinetiQ (Natural Power) ZephIR lidar and the electronics part of the experimental windscanner.dk ZephIR lidar [Mikkelsen et al., 2009]. The wavelength of the laser emission is 1575 nm. The radial extent of the lidar's measurement volume is increasing quadratically with the focus distance and is defined as twice the value of the Rayleigh length (z_R). The Rayleigh length for the ZephIR has been found to be equal with $0.0013 \cdot r^2$, where r is the radial distance between the focus point and the ground based scanning lidar [Wagner et. al, 2009].

The ZephIR lidar is emitting and receiving continuously. The coherently detected Doppler shift of the backscattered radiation from the sampling volume, representing the wind speed along the beams radial pointing direction, is sampled at 100 MHz. Partitions of 512

consecutive measurements are then being Fourier transformed to a create power spectrum of 256 bins over a 50 MHz bandwidth.

Approximately 195312 spectra are being measured per second:

$$\text{Number of Spectra} = \frac{\text{Number of received signals}}{\text{Size of the FFT}} = \frac{100\text{x}10^6}{512} = \\ = 195312.5 \ {}^{\text{spectra}}/_{\text{sec}} \tag{2.1}$$

In order to achieve an adequate signal-to-noise ratio, 4000 of the aforementioned spectra are averaged in real-time to form a single Doppler Spectrum for each wind speed measurement. Hence 48.828 Doppler spectra are being streamed from the lidar each second (195312.5/4000 ≅ 48.828 Hz).

The velocity resolution of the Doppler spectrum is defined by the width of the each bin and is equal with,

$$\text{Velocity resolution} = \frac{\text{Bandwidth}}{\text{Number of bins}} = \frac{50\text{MHz}}{256} = 195.3125 \ {}^{\text{kHz}}/_{\text{bin}} \tag{2.2}$$

The ZephIR lidar is scanning in a conically pattern through the deflection of the laser beam from an optical wedge prism. The wedge prism is placed in the tip of the lidar system and it is performing a continuous clockwise rotation (viewed from above/front). For each Doppler spectrum acquired, an azimuth angle of the wedge prism is assigned by the lidar system. This represents the position of the wedge prism during the acquisition of the backscattered signal. For the detection of the position of the lidar's wedge an opto-coupler is used. One full revolution is completed whenever a reference point on the wedge passes an optical sensor, hereafter denoted as the "reset position". Whenever the wedge is found to this reset position the lidar beam is emitted into the anti-diametric direction.

The lidar was connected via an on-board pc through a wireless network to a computer in the base of the wind turbine tower. Thus it was possible to achieve online remote access to the lidar system, in order to control the lidar's operation parameters, as well as to have online real-time access to measured wind speeds.

2.2 Wind Turbine Spinner

The angular position of the spinner was measured by two inductive sensors connected to a data acquisition unit (DAU) in the nacelle. One of the blades (#1) was used as the reference of the angle of the spinner. One sensor counted 397 pulses per revolution. While the other sensor was placed in the upper part of the nacelle, so that whenever the reference blade was passing through, the first counter reset and consequently the spinner position angle was reset. For this reason when the wind turbine was not working, it was not possible to have a precise measurement of the position of the spinner, as the counter was not reset.

In the first and the second phase of the experiment the lidar was placed in such a way that the line-of-sight (LOS) of the lidar, at the optical wedge prism reset position, was found in a direction 65^{o} counterclockwise from the blade #1 (see Figure 2.2). In the case of the phases #4 and #5 the ZephIR lidar was placed in a way that was rotated 120^{o} counterclockwise in comparison with the position that it had during the phases #1 and #2.

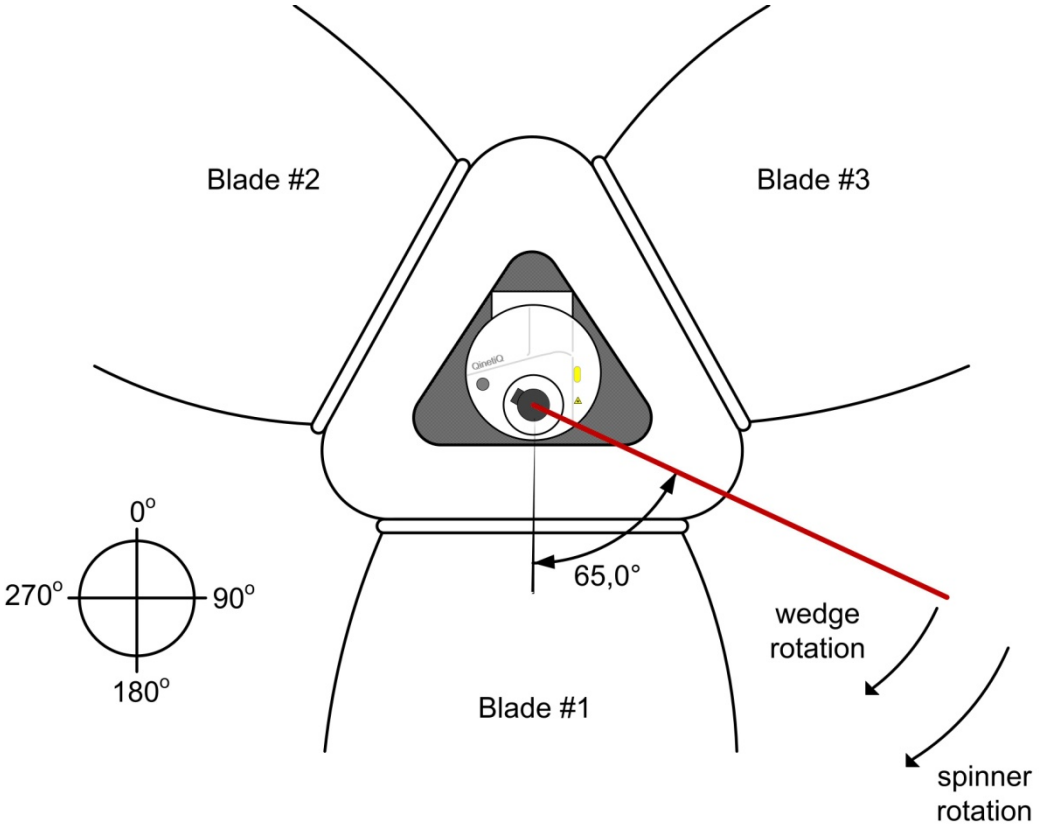

Figure 2.2 Schematic of the LOS direction regarding the reference position of the blade #1 of the wind turbine (corresponds to the 1st and 2nd phase of the experiment).

The azimuth angle (φ) of each measurement was calculated by taking into consideration the optical wedge prism azimuth angle of the lidar (φ_{lidar}), the angle of the spinner (φ_{Blade}) as well as the relative offset angle (φ_{offset}) between the reset points of the φ_{Blade} and $\varphi_{lidar.}$ The angle of the measurement can then be calculated from the equation:

$$\varphi = \varphi_{Blade} + \varphi_{lidar} + \varphi_{offset} \quad (2.3)$$

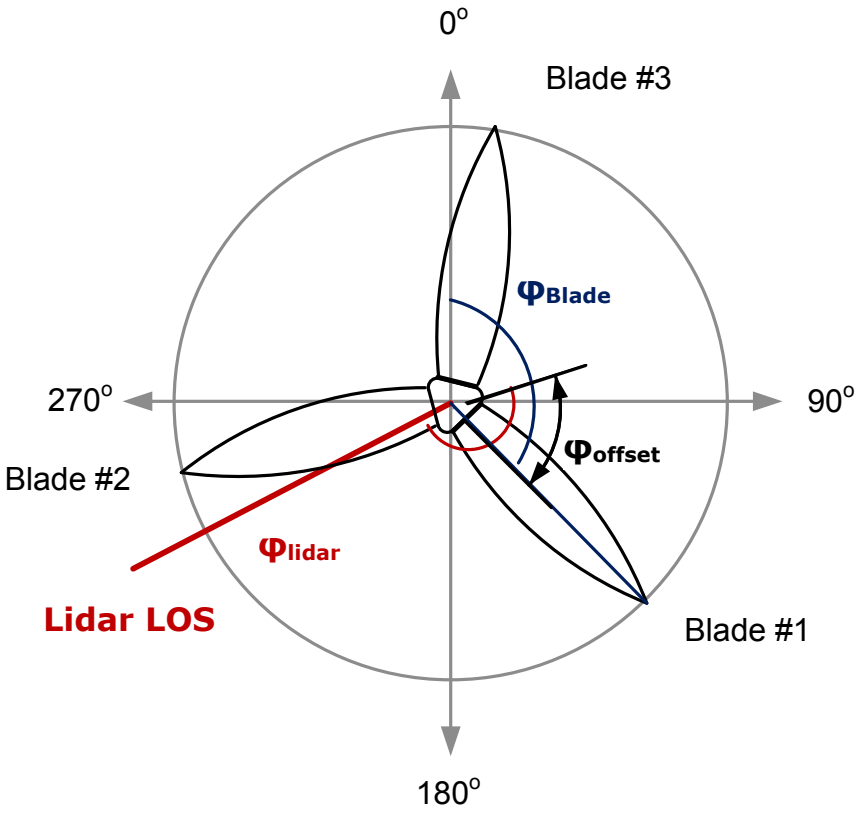

Figure 2.3 Schematic representation of the azimuth angle calculation

2.3 The data path

The ZephIR lidar was located in the spinner along with a personal computer (pc) that received and stored the data streamed from the lidar and the Data Acquisition Unit (DAU). The DAU was located in the nacelle and transmitted data through a Wireless Local Area Network (WLAN) to a ground station that relayed it to the pc in the spinner. Both the data from the ZephIR lidar and the DAU were streamed as packets using the User Datagram Protocol (UDP). The nature of the UDP does not guarantee any stability or chronology in the stream. I.e. if UDP packets are sent there are no guarantees when they will arrive, if they will arrive at all or that they will arrive in order. The only guarantee is that if a packet arrives the integrity of the packet

is guaranteed (i.e. there are no errors in the packet). This is well suited for streaming large amounts of data where the individual packets differ only slightly.

The reliability of the data streams is dependent on the load and signal strength of the wireless link shown in Figure 2.3. Both the pc in the spinner used for this experiment as well as the pc used for experiments that coincided with the SpinnerEx 2009 (such as the DAN-AERO MW and the TOPFARM), used the wireless link for data transfer and were remote controlled over the link. The DAN-AERO MW and TOPFARM experiments did not transmit their data continuously during the recording of the data. Rather they stored the data locally and sent it each time one in a series of experiments was conducted. The turbine was usually stopped after each experiment rendering the data from the SpinnerEx meaningless and thus did not usually affect the SpinnerEx's wireless link capacity. The signal strength of the wireless link was not constant throughout the experiment and seemed to vary depending on the yaw of the turbine. Data transmission related problems were handled by a proper post processing algorithm prior to the data analysis.

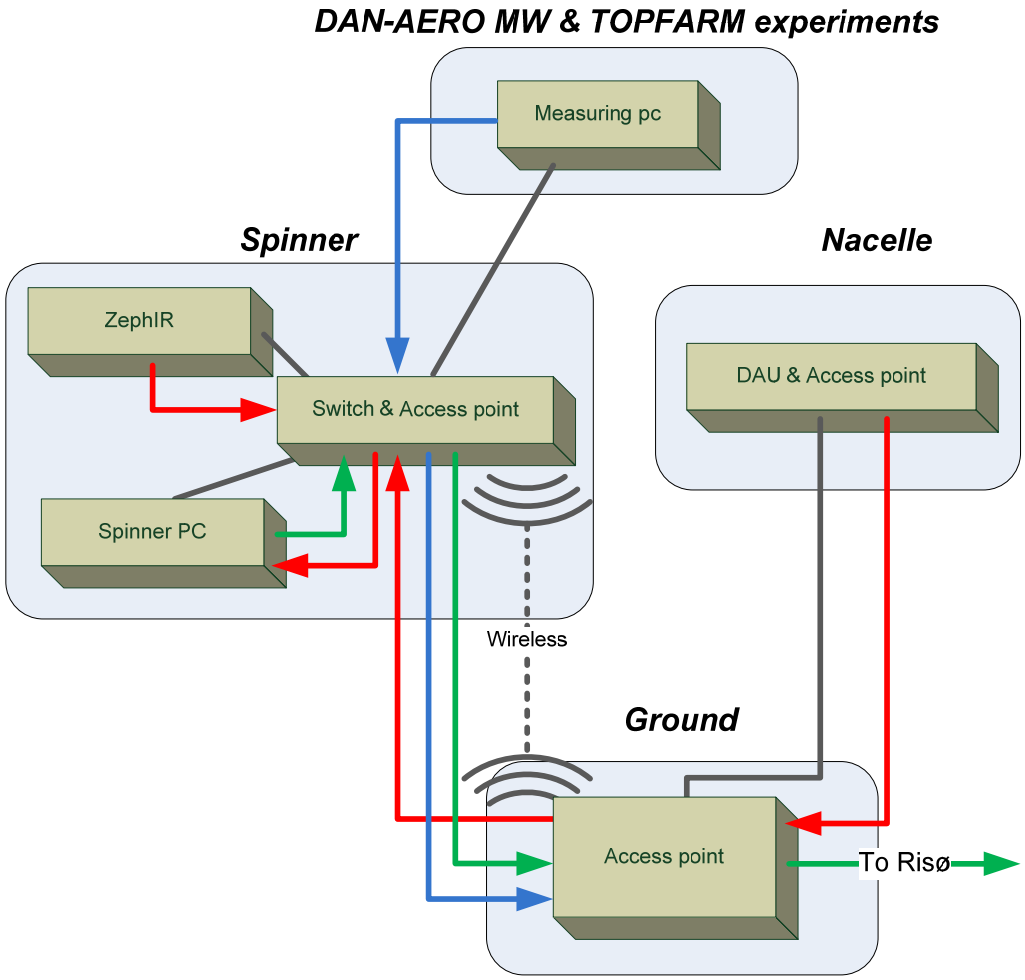

Figure 2.4 Diagram of the relevant data paths. The physical network is marked in gray. Data flow from instruments to the pc are marked in red. Combined data sent to Risø is marked in green and data flow from other experiments are marked in blue.

3 Data Analysis

During the SpinnerEx 2009 experiment the lidar was streaming so-called uncalibrated spectral "raw" data at ~50 Hz. These raw data were separated according to the time of their acquisition and stored in individual data files, each of which represented a 10-minute period. Along with the Doppler spectrum, the prism and the spinner angle, the time stamp and the yaw angle values[2] for each individual measurement were also stored. More information regarding the ZephIR streamed files can be found in Appendix A.

The analysis of the Tjæreborg lidar data therefore involved the following calculations:

i. Azimuth Angle
ii. Height
iii. Radial wind speed
iv. Separation of data according to the height and calculation of the 1 Hz data
v. Yaw misalignment angle
vi. Horizontal wind speed
vii. Comparison between 1 Hz data of the lidar and the anemometers

In this chapter details concerning the first 3 steps (i, ii, iii) will be given. The theoretical aspects of the steps (iv, v, vi) will be described in Chapter 4: *Geometry of the lidar measurements*. While results for the calculations of the yaw misalignment, the horizontal wind speed, as well as for the comparison between the 1 Hz data of the lidar and the anemometers are presented in Chapter 5.

3.1 Azimuth angle

As already mentioned (see Section 2.2), for the calculation of the azimuth angle three parameters were taken into account, the optical wedge prism angle of the lidar, the angular position of the spinner and the relative angle between the lidar and the spinner:

$$\varphi = \varphi_{\text{Blade}} + \varphi_{\text{lidar}} + \varphi_{\text{offset}} \tag{2.3}$$

2 Only for the period when the 30º wedge was used (phase #4)

3.1.1 Optical prism angle (φ_{lidar})

3.1.1.1 Time stamp

A time stamp and a wedge azimuth angle were assigned to each spectrum streamed from the lidar. In order to test the flow of the streamed data, the time step between two consecutive measurements was calculated for several 10-min data sets. Generally it was observed to be constant, taking values either 20 or 21 ms. However, occasional deviations from these values were observed:

Random time step peaks was one type of deviation observed that is attributed to data streaming delay (cf. notification 1 in Figure 3.1, left). Another type of deviation rarely observed was the appearance of zero valued time steps, which is caused by data duplication of some of the data (cf. notification 2 in Figure 3.1, left). These issues were resolved by implementing a special algorithm for sorting the data.

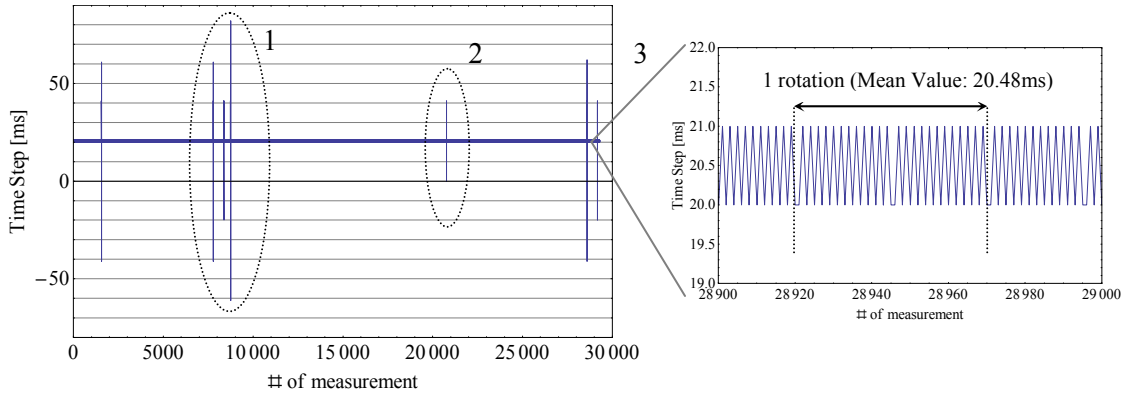

Figure 3.1 Time Step Values of one data file (left) and a magnified area of this plot for 100 of the measurements (right). (Data file: 2009-04-22 13:20).

Figure 3.1 (right, notification 3) presents the time steps of a group of 100 measurements. The mean value of the time step between the measurements of one rotation is 20.48 ms (value which is representative only for this rotation, as small variations of this value are observed), giving a frequency value of 48.828 Hz.

3.1.1.2 Optical prism rotation

The pointing direction of the lidar is described by the value of the azimuth angle of the rotating optical wedge prism. This angle increases linearly as the wedge rotates clockwise at an almost constant rotation speed of approximately one revolution per second, until it reaches the value of 2π, which corresponds to the position where an optical sensor of the wedge is crossing a once-per-revolution reset point (see Figure 3.2, left). In parallel with the time step analysis

previously described, the step between consecutively measured angles was also investigated. Some jitter in the step of the prism's angle values was observed (see Figure 3.2, right).

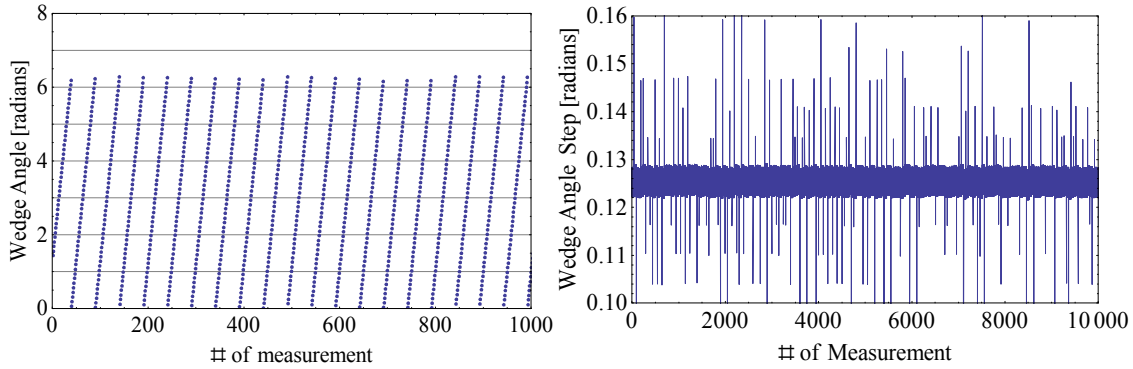

Figure 3.2 Wedge angle values for the first 1000 measurement of the data file (left) and steps for 10000 measurements (right). (Data file: 2009-04-22 13:20).

The calculation of the wedge angle value from the system is based on 3 times:

1. The reset time (t_0)
2. The time that the measurement is being acquired (t_i)
3. The duration of the last full wedge rotation ($\Delta t_{n \to n+1}$)

The wedge angle of each measurement is calculated through the equation (see Figure 3.3, left):

$$\theta_i = (t_i - t_0) \cdot K_n \tag{3.1}$$

where, $K_n = \frac{2\pi}{\Delta t_{n \to n+1}}$.

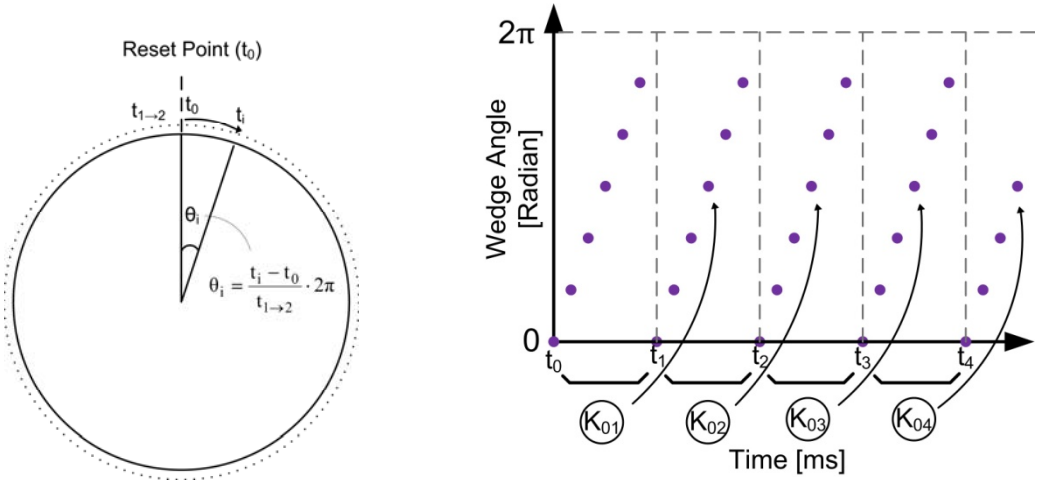

Figure 3.3 Diagram of wedge angle calculation (left) and plot of wedge angle values vs. time (right).

The variations of the angle step between two consecutive measurements can be attributed to the fact that the ZephIR internal system measures the time needed for a full rotation and subsequently use that time for estimating the wedge angle step for the following rotation. This would cause a small jitter error in the cases where the rotation speed of the wedge was not exactly constant. (The ZephIR's build-in wedge scanner DC motor is driven by a dedicated controller).

In order to investigate this phenomenon, a linear fit model was applied to the wedge angle data for each individual rotation. Assuming that the wedge is moving with a constant rotation speed, the wedge angle can be described by a linear equation $\theta_i = K_n\ t+b$ and the solution of this equation (i.e. t_1), for $\theta_i = 0$, would represent the reset time. By applying this method to each of the rotations it was verified that the ZephIR system is using the rotation time of the previous full 360 degree rotation turn to calculate the wedge positions within the current turn.

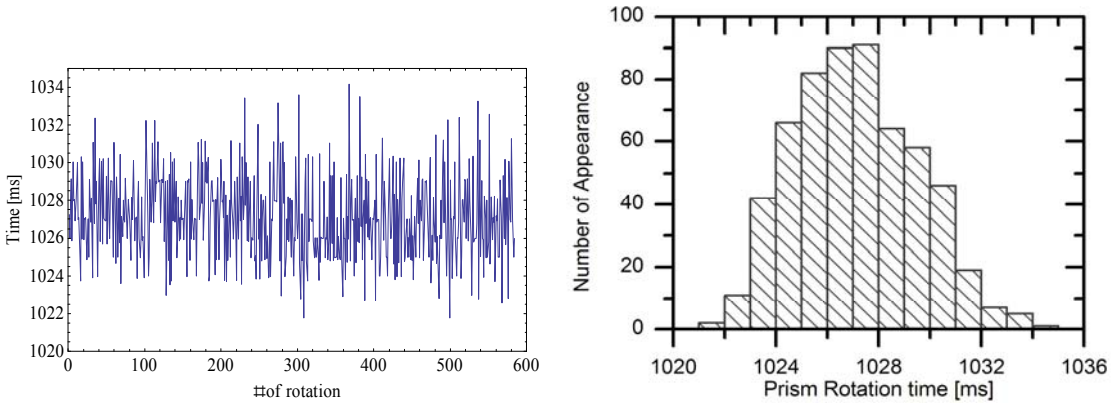

Figure 3.4 Time step values between two consecutive rotations, (left) time series and (right) distribution (Data file: 2009-04-22 01:20).

Figure 3.4 presents the calculated values for the time difference between two reset times for a 10 min period (~600 rotations). From the figure it can be observed that the rotation speed of the wedge is slightly varying. The distribution of times for a full 360 degree rotation seems to be described by a bell-shaped curve centered on the mean value, which for this particular data file is 1027.13 ms per rotation.

In order to correct the observed jitter in the rotation speed, the wedge angle values for each individual rotation were re-calculated. This was achieved by using the time required to complete one full rotation to calculate the characteristic wedge angle step of the same rotation. By using this method, the observed variations in the measured wedge angles could be corrected for as seen in Figure 3.5 where both the measured (blue) as well as the corrected (red) values of the angle step for a period of 10-min are presented.

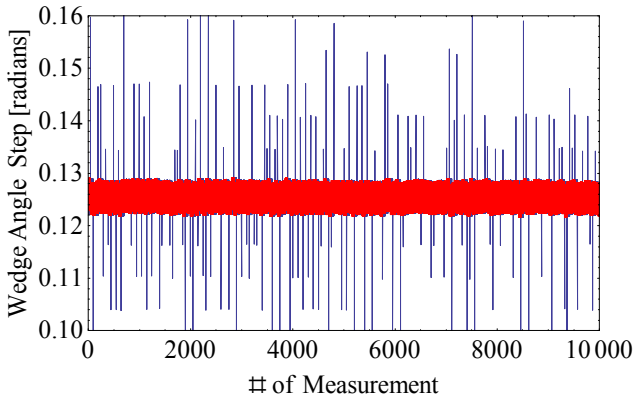

Figure 3.5 Phase step values based: a) on the phase data values (blue color) and b) on the calculated values (red color)

Additionally, it was observed that some rotations were not completed, but instead when the wedge angle reached the value of π it was reset back to 0 (see Figure 3.6a). This can be explained by a missed detection of one rotation's end by the once-per-revolution optical sensor. The result of such a failed detection is that the measured time between two consecutive measurements ($\Delta t_{n\rightarrow n+1}$) becomes twice the expected time for one full rotation. Therefore the lidar system calculated values of the angle step become halved.

$$\theta_i' = (t_i - t_0)\cdot K_n = \frac{t_i - t_0}{2\,\Delta t_{n\rightarrow n+1}}\,2\pi = \frac{1}{2}\,\theta_i \qquad (3.2)$$

By applying the previously described method it was possible to rearrange the data points (see Figure 3.6) and correct this error.

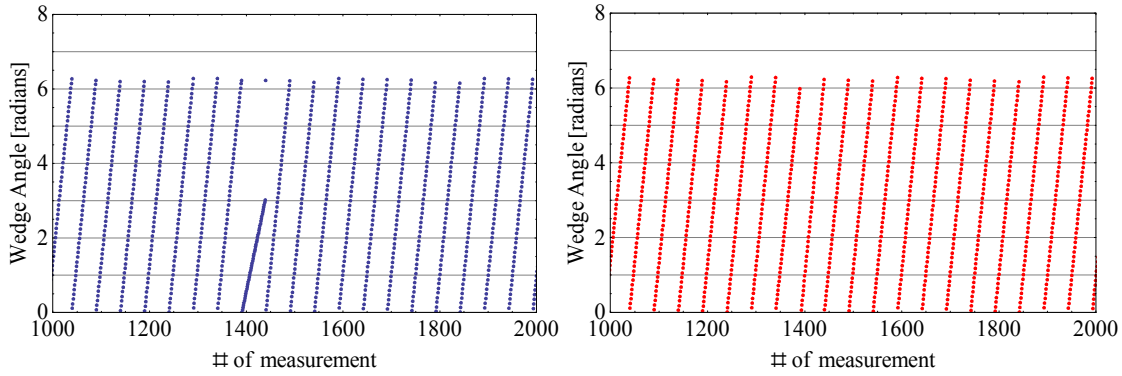

Figure 3.6 Plot of phase values vs. # of measurement for 1000 measurement of the data file 2009-04-23 13:20 (with blue color are the values of data file and with red the post corrected values).

3.1.2 Spinner angle (φ_{Blade})

Regarding the spinner angle of the wind turbine, several errors in the data sequence were observed in forth phase of the experiment (when the lidar was equipped with the 30° optical wedge prism). Three different types of errors have appeared. First, a series of zero values randomly interfere with the measurements (see Figure 3.7, notification 1). Second, the indication of the spinner's position was occasionally fixed in specific values (see Figure 3.7, notification 2). Third, losses of data for small periods were occurring (see Figure 3.7, notification 3).

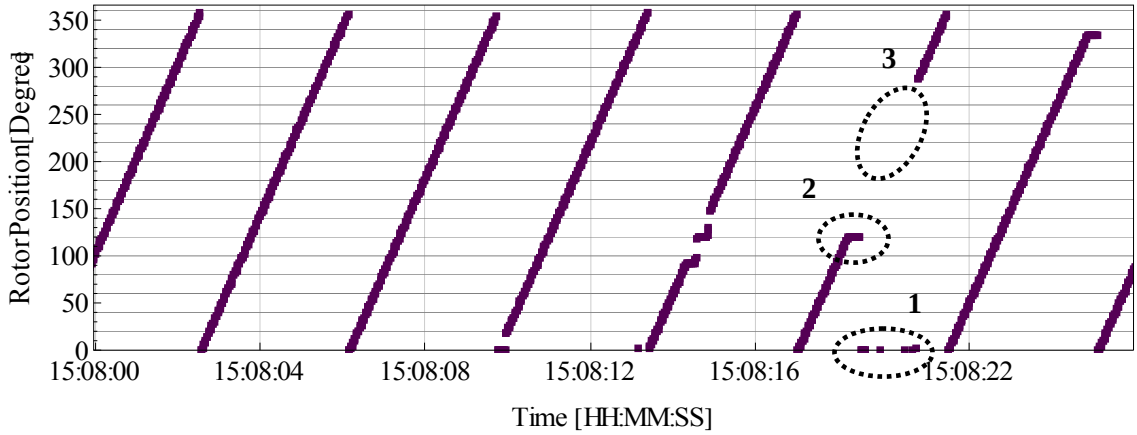

Figure 3.7 Values of the spinner position measurements (data file: 2009-08-06 15:00)

The spinner angle values were corrected by applying an algorithm which operation is based on the assumptions that:

1. It is impossible to have two consecutive measurements of the spinner position with the same angle.
2. Consecutive measurements should always follow an incremented step, moving from 0° to 360°. An exception is when a full rotation of the spinner is being fulfilled.

Figure 3.8 presents the spinner values which were stored in the data (left, purple dots) as well as the corrected ones (right, red dots). It should be mentioned that despite the correction by the algorithm, still there are some voids in the data sequence, resulting from loss of the data.

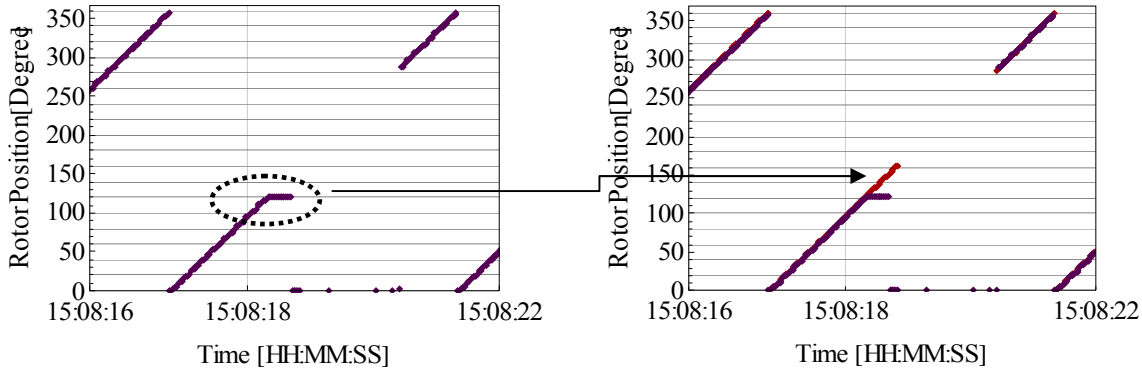

Figure 3.8 Corrected values of the spinner angle measurements (data file: 2009-08-06 15:10)

3.2 Calculation of the LOS wind speed

The lidar was streaming Doppler spectra at an average rate of 48.828 Hz. Each Doppler spectrum represents the mean spectrum averaged over 4000 Fast Fourier Transforms (FFT). The ZephIR build-in (Field-Programmable Gate Array (FPGA) based FFT was set to produce power spectra into 256 bins, where the first bin represents the radial velocity of 0 ms^{-1}. The last bin was excluded from the stored values. Therefore each Doppler spectrum is presented in the range of 255 bins. In the data, by default, the first 10 bins of the backscattered signal values are set to 0, as these bins can be dominated by the background Relative Intensity Noise (RIN) spectrum of the laser. For the calculation of the radial wind speeds from the Doppler spectra, the following steps were followed:

1. RIN spectrum calculation.
2. Thresholding and removal of the RIN spectrum.
3. Estimation of the center frequency.

Step 1: Calculate the RIN spectrum

A series of measurements with the shutter of the lidar being closed were recorded as zero references. This was done at several times during the whole experiment. From these "nul"-series, the RIN background spectrum was calculated following the procedure:

- Mean (M) and Standard Deviation (STD) values are measured between bin 200 and 250, for each individual spectrum (see Figure 3.9 left).
- The corresponding sum M + 5STD, which indicates the threshold of the measurements, is subtracted from each spectrum. If there are negative values they are taken into account as zero values (see Figure 3.9 left).
- The mean and standard deviation values of each bin are calculated. The RIN spectrum is then calculated as $RIN_{Bin} = M_{Bin} + 5STD_{Bin}$ (see Figure 3.9 right).

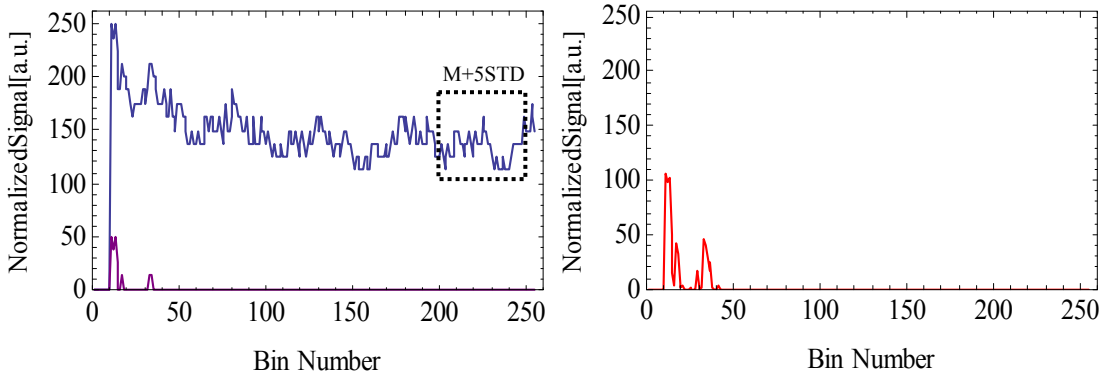

Figure 3.9 Example of a zero background reference spectrum with shutter closed (left) and of the RIN noise spectrum (right). (Data file 2009-04-23 12:10).

Step 2: Thresholding

Mean and Standard Deviation values are measured between bin 200 and 250, for each individual spectrum of the wind speed measurements. The corresponding sum M+5STD is subtracted from each spectrum. If there are negative values they are taken into account as zero values. The factor of 5 STD is used to calculate the threshold so as to include all the possible variations of the backscatter noise without removing any valuable information from the spectrum. The remaining value of each bin is compared with the value of the RIN spectrum in the corresponding bin.

If the condition $Signal_{Bin} > RIN_{Bin}$ is satisfied, then the signal is considered to be part of the Doppler Spectrum and is taken into account. Otherwise if $Signal_{Bin} \leq RIN_{Bin}$ then $Signal_{Bin} = 0$.

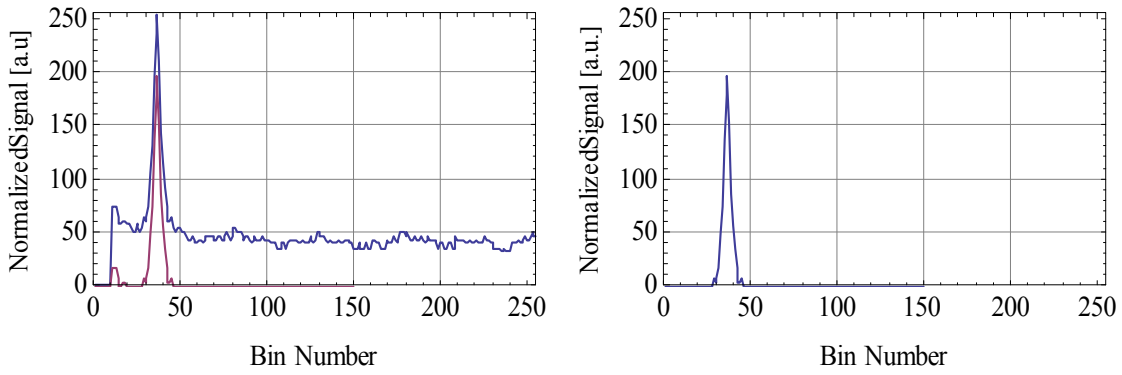

Figure 3.10 Example of a Doppler spectrum measurement, before (blue) and after (purple) the removal of the threshold (left). The same but after also filtering away the RIN noise (right).

Step 3: Wind Speed calculation

For the calculation of the actual wind speed the mean frequency of the Doppler shift is calculated. First the mean frequency shift is found by estimating the representative "mean" bin, using a "median" frequency function. Subsequently Equation 2.1 is applied to convert from bin to frequency:

$$\text{Velocity bin resolution} = \frac{\text{Bandwidth}}{\text{Number of bins}} = \frac{50\text{MHz}}{256} = 195.3125 \ {}^{\text{kHz}}/_{\text{bin}} \qquad (2.1)$$

From the Doppler shift theory it is now possible to derive the wind speed from the mean frequency shift, using the standard Doppler shift equation:

$$\frac{\Delta u}{c} = \frac{1}{2}\frac{\Delta f}{f} \Leftrightarrow \Delta u = \frac{1}{2}\frac{c}{f}\Delta f \Leftrightarrow \Delta u = \frac{1}{2}\lambda\Delta f \tag{3.3}$$

where,

Δu: the wind speed,

C: the speed of light,

f: the frequency of the emitted radiation,

λ: the wavelength of the emitted radiation and

Δf: the Doppler shift.

In the case of the QinetiQ's ZephIR lidar, where the wavelength of emission is $\lambda = 1.575$ µm, the above equation can be written as:

$$\Delta u = \frac{1.575\ \mu m}{2}\ 10^{-6}\Delta f \tag{3.4}$$

4 Geometry of the measurements

4.1 Lidar radial wind speed

The spinner-mounted wind lidar acquired upwind radial wind speed measurements by scanning conically around the wind turbines axis of rotation. In general a lidar measures the wind speed projected along its instantaneous line-of-sight unit point vector, hereby denoted by $\hat{r}$ (see Figure 4.1). This is given by:

$$\hat{r} = (r_x, r_y, r_z) = (\cos\theta_c\,, \sin\theta_c \sin\varphi\,, \sin\theta_c \cos\varphi) \tag{4.1}$$

Where,

θ_c: the lidar's optical wedge prism deflection angle (2, 15 and 30 degrees were used during the SpinnerEx 2009)

φ : the azimuth angle caused by the rotation of the lidar's optical wedge prism.

The x-axis of the Cartesian coordinate system is assumed to be aligned with the main axis of the wind turbine.

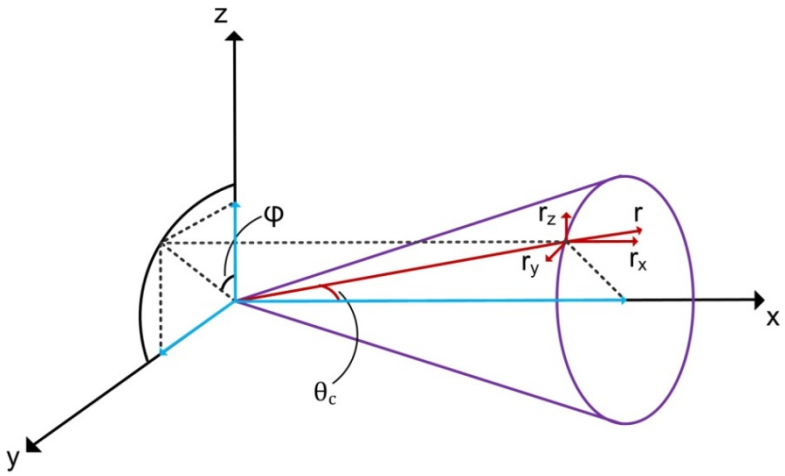

Figure 4.1 Geometry of the lidar measurements in a Cartesian coordinate system.

In this coordinate system the measured wind speed is equal to:

$$U_{Lidar} = \hat{r} \cdot u = (r_x, r_y, r_z) \cdot (u_x, u_y, u_z) \tag{4.2}$$

Where u_x, u_y and u_z are the wind components of the instantaneous wind vector.

In reality, for the NM80 turbine, the axis of rotation of the turbine is tilted in the vertical direction by a fixed angle θ_i (~5°). Furthermore the horizontal orientation is steered by the horizontal plane yaw control of the turbine that tracks the changes in the wind direction. As the turbine is not always perfectly aligned into the wind, it is necessary to introduce an instantaneous yaw misalignment angle (θ_w). This is defined as the angle between the instant pointing yaw direction of the wind turbine and the instantaneous actual horizontal wind direction.

In order to relate the line-of-sight pointing vector in the tilted and yawed reference system to a fixed frame of reference attached to the ground, where also the MET tower is measuring, it is necessary to apply a coordinate transformation consisting of two consecutive rotations:

a) Relative to a fixed coordinate system attached to the ground (x, y, and z) the vertical tilt of the wind turbine is represented by a counter-clockwise rotation about the y-axis of an angle θ_i. (In the case of the NM80 wind turbine it is equal to 5 degrees, see Figure 4.2).

$$\begin{bmatrix} x' \\ y' \\ z' \end{bmatrix} = \begin{bmatrix} \cos\theta_i & 0 & -\sin\theta_i \\ 0 & 1 & 0 \\ \sin\theta_i & 0 & \cos\theta_i \end{bmatrix} \begin{bmatrix} x \\ y \\ z \end{bmatrix} \tag{4.3}$$

After this rotation, the components of the unit pointing vector $\hat{r}$ become:

$$\begin{bmatrix} r_x \\ r_y \\ r_z \end{bmatrix} = \begin{bmatrix} \cos\theta_i \cos\theta_c & 0 & -\sin\theta_i \sin\theta_c \cos\varphi \\ 0 & \sin\theta_c \sin\varphi & 0 \\ \sin\theta_i \cos\theta_c & 0 & \cos\theta_i \sin\theta_c \cos\varphi \end{bmatrix} \tag{4.4}$$

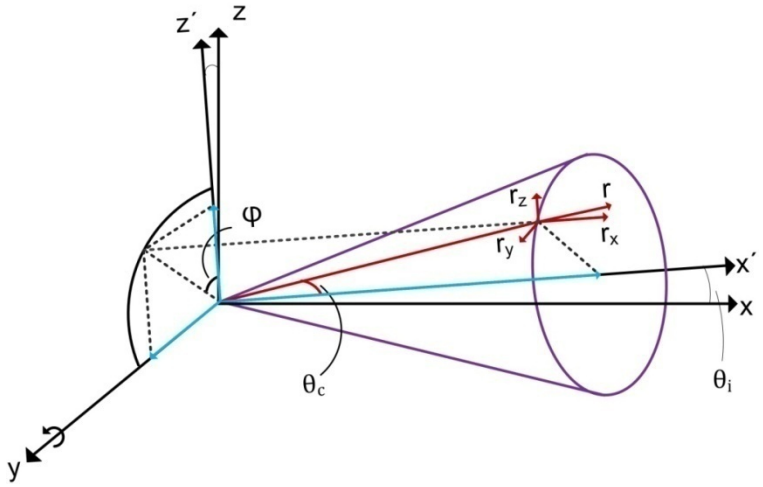

Figure 4.2 Geometry of the lidar measurements in a rotated Cartesian coordinate system.

b) The yaw-misalignment of the wind turbine (θ_w) relative to the x-axis can be represented by a rotation around the z-axis (see Figure 4.3). This rotation is assumed to be counterclockwise, although the relative angle between the yaw angle and the direction of the wind can be either positive or negative.

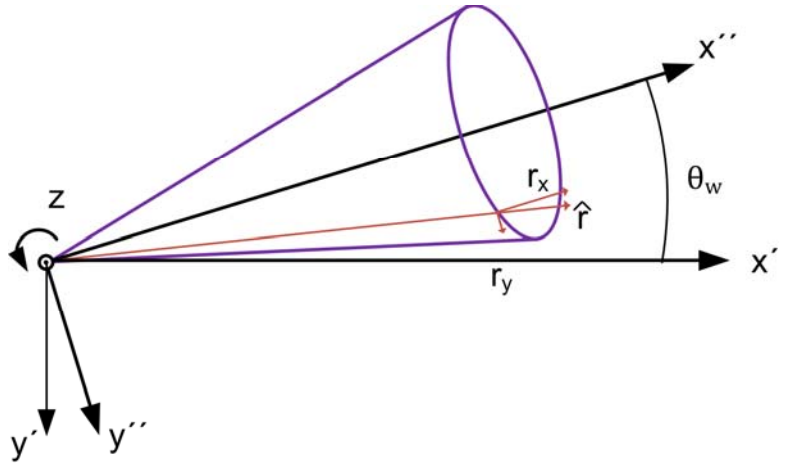

Figure 4.3 Geometry of the lidar measurements (view from above).

$$\begin{bmatrix} x'' \\ y'' \\ z'' \end{bmatrix} = \begin{bmatrix} \cos\theta_w & -\sin\theta_w & 0 \\ \sin\theta_w & \cos\theta_w & 0 \\ 0 & 0 & 1 \end{bmatrix} \begin{bmatrix} x' \\ y' \\ z' \end{bmatrix} \tag{4.5}$$

From the equations (4.3) and (4.5) an expression for the lidar's instantaneous radial wind speed measurement can be derived by relating the pointing vector in equation (4.1) to the fixed frame as function of tilt, azimuth, wedge deflection angle and yaw error.

The instantaneous pointing unit vector of the lidar can in this way be calculated from the equation (4.6) as,

$$\begin{bmatrix} r_x \\ r_y \\ r_z \end{bmatrix} =$$

$$\begin{bmatrix} \cos\theta_w \cos\theta_i \cos\theta_c - \cos\theta_w \sin\theta_i \cos\theta_c \cos\varphi & -\sin\theta_w \sin\theta_c \sin\varphi & 0 \\ \sin\theta_w \cos\theta_i \cos\theta_c - \sin\theta_w \sin\theta_i \cos\theta_c \cos\varphi & \cos\theta_w \sin\theta_c \sin\varphi & 0 \\ 0 & 0 & \sin\theta_i \cos\theta_c + \cos\theta_i \sin\theta_c \cos\varphi \end{bmatrix}$$

4.2 Calculation yaw-error of the wind turbine (θw)

Due to the co-rotation of the optical wedge prism and the spinner of the wind turbine (see Figures 2.2 and 2.3) the lidar was obtaining wind speed measurements in manifold heights during a 10-minute period. The focus distance (R) of the lidar was adjusted to measure in the vicinity of the points contributing most to the power production of the turbine, that is, near the 2/3 cord distance of the blade radius. The altitude (z) of each measurement, which is defined by the azimuth angle (φ) of the optical wedge prism and the focus distance (R) of the laser beam, can be calculated through the equation:

$$z(\varphi) = h_0 + R \cdot \hat{r}(\varphi) \cdot \hat{z} \tag{4.7}$$

$$\Rightarrow z(\varphi) = h_0 + R \cdot r_z$$

$$\overset{(4.6)}{\Longrightarrow} z(\varphi) = R(\sin\theta_i \cos\theta_c + \cos\theta_i \sin\theta_c \cos\varphi) \tag{4.8}$$

Here, h_0 is the hub height (in the case of the NM80 wind turbine it is 57 m), $\hat{r}(\varphi)$ the line-of-sight vector of the lidar measurement and $\hat{z}$ the vertical unity vector.

The lidar is taking measurements between the ~40 m and ~94 m (see Figure 4.4, left). Due to the tilt and the rotation of the spinner the majority of the measurements are retrieved either around 40 or 90 m (see Figure 4.4 right).

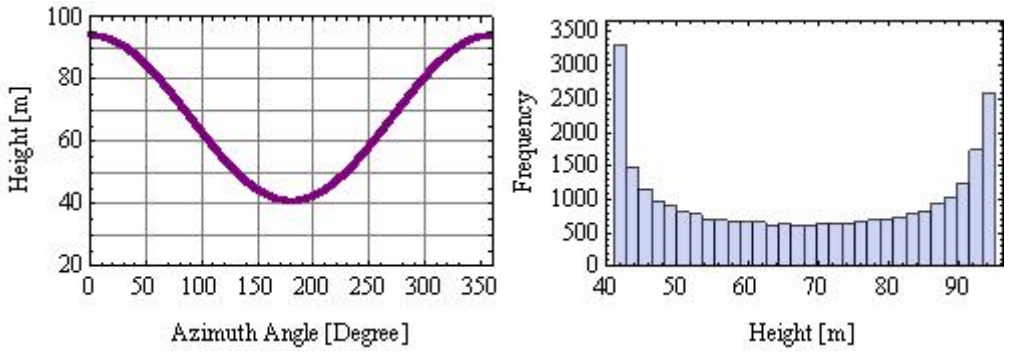

Figure 4.4 Height of measurements over a 10-minutes period (left) and frequency diagram of the number of measurements per height (right).

For the calculation of the yaw misalignment (θ_w) it is assumed that the wind blows homogenously towards the wind turbine in the whole rotor area. This is happening only when the turbine is not affected by wakes of adjacent wind turbines or when there is no horizontal wind shear. Additionally it is expected that wind direction may change with height, therefore the calculation of the angle θ_w is done in several height layers.

The radial wind speed data were grouped in partitions of consecutive seconds. For each partition the data were separated according to the height where each measurement was acquired (and consequently according to the azimuth angle). Based on this separation the misalignment of the yaw angle was estimated in different height layers. The vertical width of the height layers was defined so as to fulfill two criteria:

i. Sufficient amount of data per layer
ii. Adequate spatial resolution

Within vertical layers of 5 meters height the aforementioned criteria appeared to be fulfilled. Therefore the scanning circle was separated into 11 different layers, between 40 m and 95 m (see Figure 4.5).

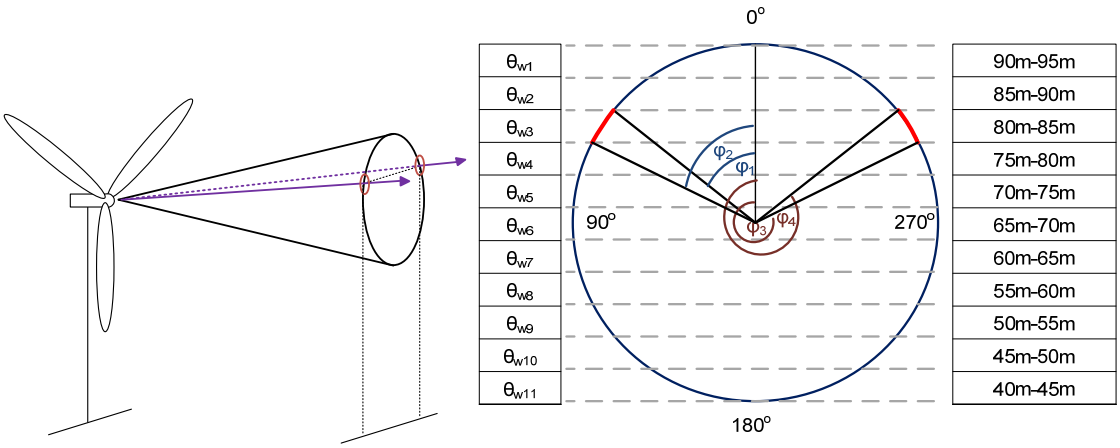

Figure 4.5 Scanning pattern of the lidar

The lower (z1) and the upper (z2) limits of each layer, are defined by 4 different azimuth angles, $z_1(\varphi_1)$ the lower and $z_2(\varphi_2)$ for the higher in the angular interval 0^o – 180^o, and $z_1(\varphi_3)$ and $z_2(\varphi_4)$ for the angular interval between 180^o – 360^o, respectively. The aforementioned data sets were spatial averaged, so as to create pairs of 1 Hz time series of the radial wind speed for each layer. The outcome of the aforementioned procedures resulted in the creation of pairs of time series, acquired within the same height layers but at different conjugated azimuth angles.

The radial wind speed measured from the lidar (U_L) is:

$$U_L = \hat{r} \cdot u = (r_x, r_y, r_z) \cdot (u_x, u_y, u_z) = u_x r_x + u_y r_y + u_z r_z \quad (4.2)$$

Assuming that the mean wind direction is along the x-axis, the equation (4.2) is simplified to:

$$U_L = u_x r_x \overset{(4.6)}{\Longrightarrow}$$

$$U_L = u_x(\cos\theta_w \cos\theta_i \cos\theta_c - \cos\theta_w \sin\theta_i \cos\theta_c \cos\varphi - \sin\theta_w \sin\theta_c \sin\varphi) \quad (4.10)$$

A yaw misalignment of an angle θ_w at a height (z), would differ the line-of-sight pointing vector of the lidar measurements for two conjugative angles. The radial wind speed values represent the projection of the wind speed to the pointing vector of the lidar. Hence, an angle of θ_w between the cone axis of the lidar and the wind direction would result in the observation of different radial wind speed measurements for the same mean horizontal wind speed.

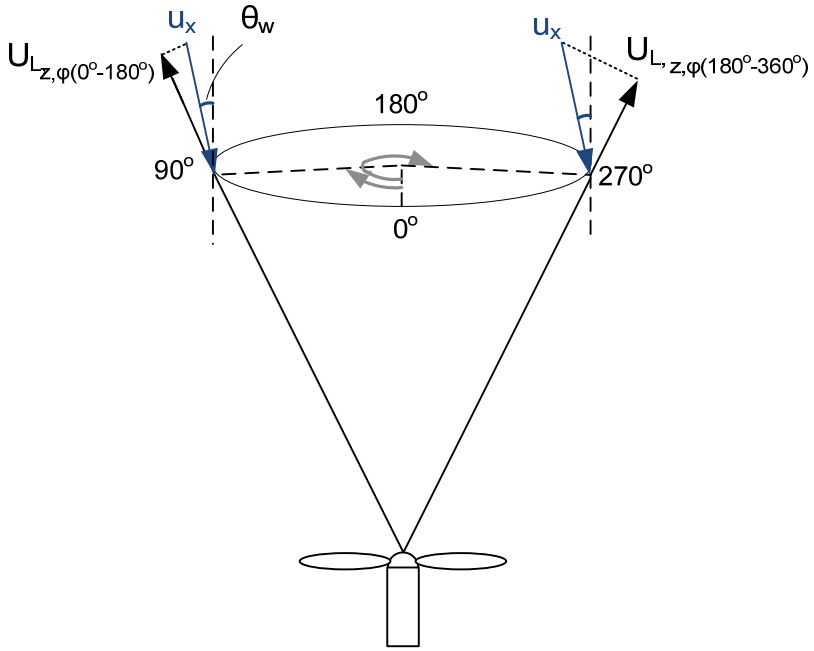

Figure 4.6 Scanning cone of the lidar (view from above).

Thus, it is feasible to estimate the instantaneous yaw misalignment using the mean radial wind speed measurements, through the following equation:

$$u_x = {}^{U_{L_{z,\varphi(0^o-180^o)}}}\Big/_{r_{x_{z,\varphi(0^o-180^o)}}} = {}^{U_{L_{z,\varphi(180^o-360^o)}}}\Big/_{r_{x_{z,\varphi(180^o-360^o)}}} \qquad (4.11)$$

An important parameter of the yaw misalignment study is the time interval in which the mean radial wind speed is calculated. When the wind turbine rotor is perpendicular to the incoming wind flow, the lidar which at all times is focused in one fixed distance, is acquiring measurements at the same horizontal distance from the rotor, for all the azimuth angles (see Fig. 4.7a). However, when there is a relative angle between the wind direction and the instantaneous yaw direction, the lidar is measuring in different phases of the wind flow in different parts of the scanning circle (see Fig. 4.7b). This may lead to the phenomenon of observing differences in lidar-measured wind speed and turbulence within the same scanning circle.

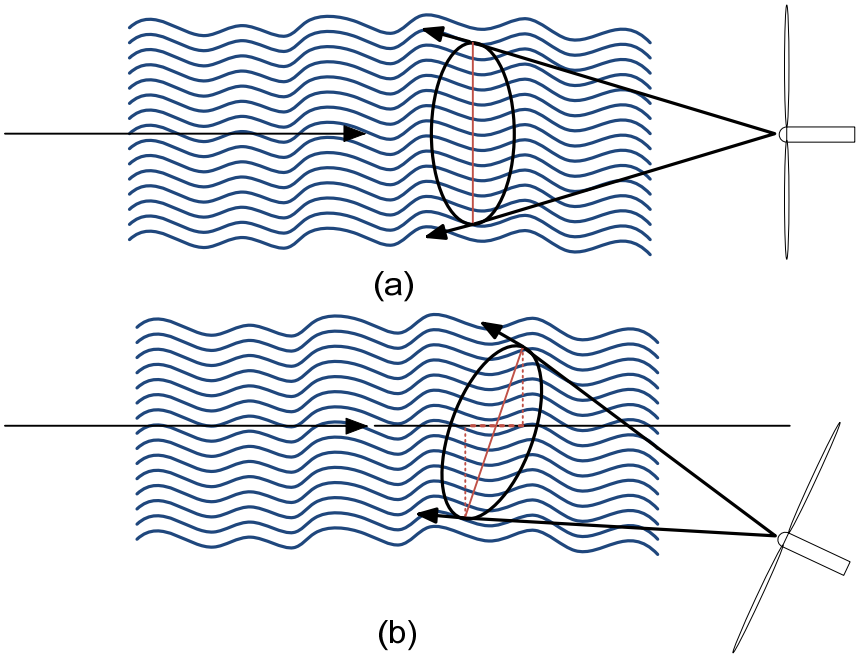

Figure 4.7 Diagram of the scanning cone of the lidar, (a) when the wind turbine rotor plane is perpendicular to the wind flow, (b) when a yaw error exists.

The difference between the horizontal distances (*dhd*), away from the wind turbine rotor plane, where two time series of the radial wind speed, in a given height, are being acquired can be calculated from the following equation:

$$dhd = CD = DB - CB = GH - CB = AG\cos(\theta_c - \theta_w) - AC\cos(\theta_c + \theta_w) =$$

$$= L\,[cos(\theta_c - \theta_w) - cos(\theta_c + \theta_w)] = L \cdot 2 \cdot \sin\theta_c \cdot \sin\theta_w$$

$$\Leftrightarrow \quad dhd = 2 \cdot L \cdot \sin\theta_c \cdot \sin\theta_w \tag{4.12}$$

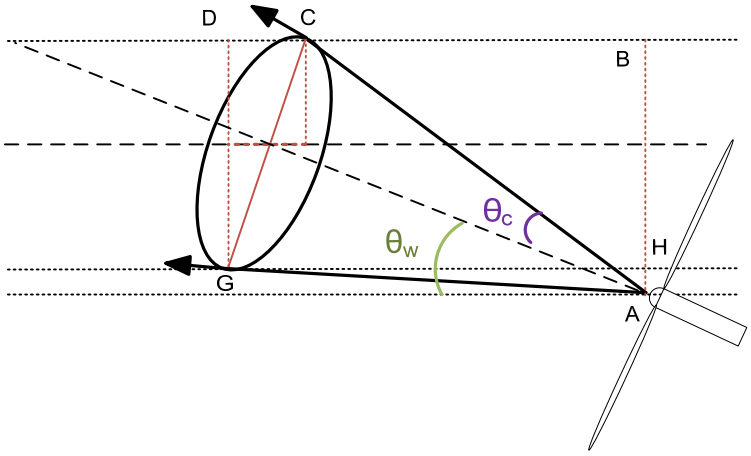

Figure 4.8 Calculation of the spatial lag between the lidar measurements.

From the equation (4.12) it is noticed that the distance dhd is dependent on the half angle (θ_c) of the scanning cone and on the misalignment angle (θ_w). Figure 4.9 presents the values of the distance dhd, in the case were the cone half angle is 15 degree and the focus distance 103 m, for different yaw misalignment angles. It can be seen that the larger the relative angle is the longer is the distance between the positions of the two measurements.

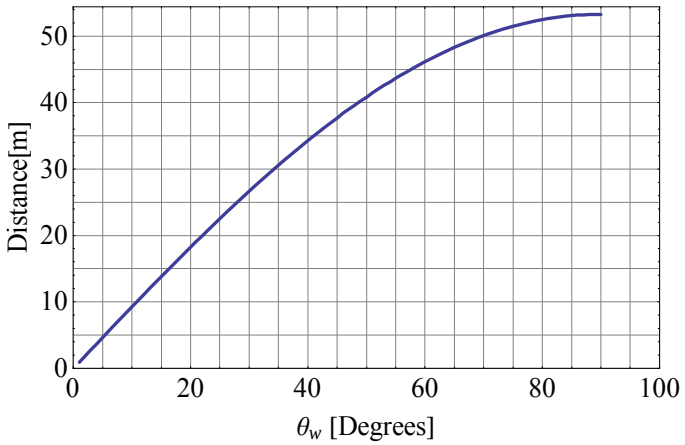

Figure 4.9 Distance vs. Yaw Error (L=103m, θ_c= 15°).

Furthermore it should be noted that the expected error in the yaw misalignment calculations depends on the height layer of investigation. This can be explained by two factors: First that the lidar is scanning in a circular pattern, meaning that the measurements acquired at the zenith ($\varphi = 0^o$) or the nadir ($\varphi = 180^o$) of the circle for two conjugate angles, have a small horizontal distance between them. Therefore the two air volumes scanned will be relatively close. In the contrary as the lidar line-of-sight is moving away from the zenith and the nadir of the scanning circle, the horizontal distance along the wind between the two conjugate azimuth measurement angles increases. Thus increasing the probability that the scanned air volumes will not have the same characteristics, e.g. different mean wind speed and turbulence (see Figure 4.10).

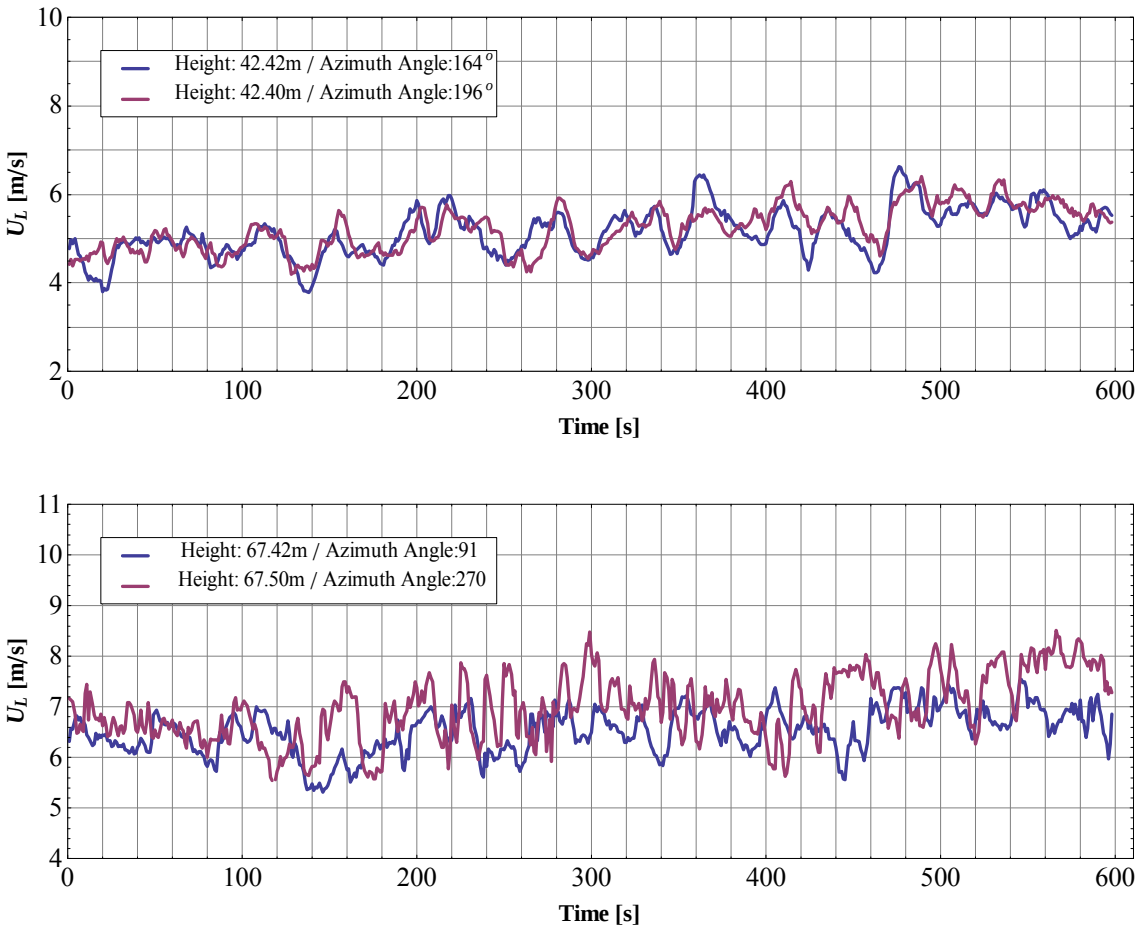

Figure 4.10 Radial wind speed time series measured at 42 m (upper panel) and 67.5 m (lower panel) for two conjugate azimuth angles, for the same 10-minute period.

Secondly, when no yaw misalignment is observed, the values of the horizontal component of the line-of-sight vector of the lidar measurements r_x are characterized by a symmetry (see Figure 4.11). This symmetry is degraded as the yaw misalignment

increases. Thus larger differences are expected between the horizontal components of the r vector of conjugated azimuth angles around 90° and 270° than those around the zenith and nadir of the scanning circle. Hence an existing yaw misalignment will induce smaller differences in the radial wind speed time series of two conjugate azimuth angles at the zenith or the nadir than in the rest of the scanning circle. In order to reduce the level of uncertainty in the calculations of the yaw misalignment angles, average values of the radial wind speed measurements were used. The data averaging was done for 6 different time intervals (0.5, 1, 2, 3, 5 and10 minutes).

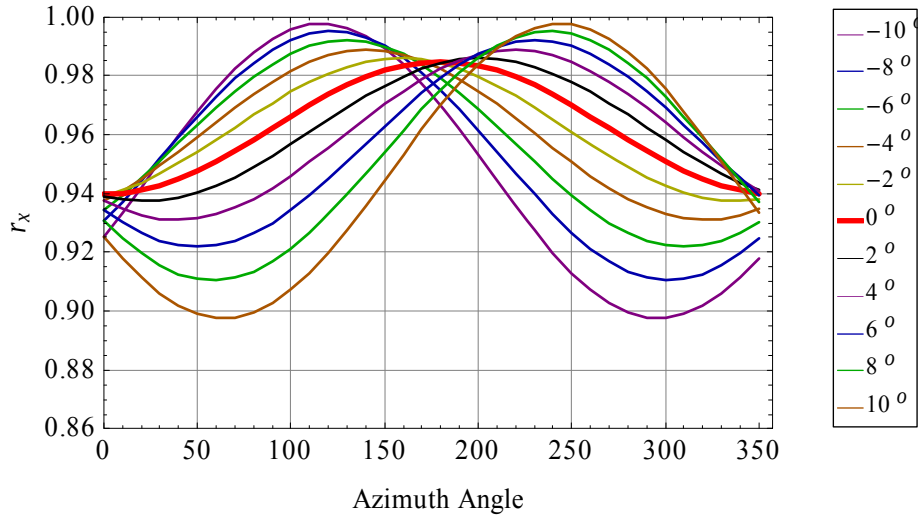

Fig. 4.11 Horizontal component of the lidar's radial pointing vector for various yaw misalignment angles.

5 Results

During the phases #1, #2 and #4 of the Tjæreborg SpinnerEx 2009 experiment, three different optical wedge prisms were constructed and used for the deflection of the laser beam with angle of deflection 2°, 15° and 30°, respectively. The objective of the latter two prisms was to focus upwind near the 2/3 maximum extracted power rotor radius (Ø) of the blades. As mentioned in Section 1.1, during the periods when the 15° and 30 ° prisms were used, the focus distance was set to 103 m and 53 m, respectively (see Figure 5.1). These two different setups enabled the possibility of investigating the wind flow at two horizontal distances away from the wind turbine, 1.24 Ø and 0.58 Ø respectively. Table 1 presents the operation parameters of the lidar during these two periods.

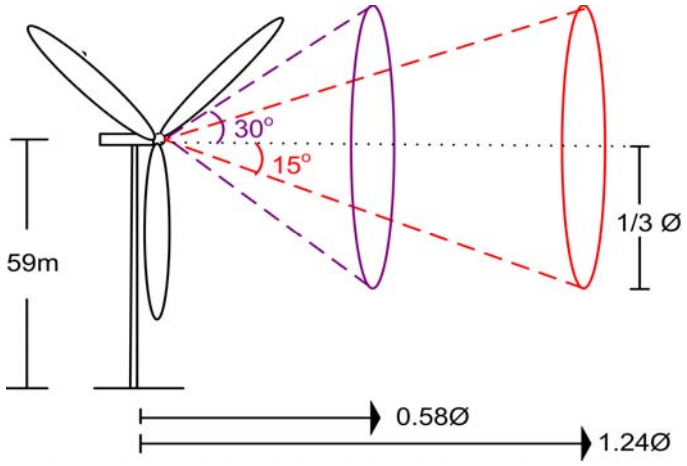

Figure 5.1 Representation of the lidar measurements.

Table 1: Lidar operation parameters

	Phase #2	*Phase #4*
Wedge Prism Angle (Degree)	15	30
Focus Distance (m)	103	53
[3]**Probe volume length (m)**	27.6	7.3
Distance from the rotor (Ø)	1.24	0.58

[3]The radial extent of the probe volume length in the radial pointing direction is defined as twice the Rayleigh length (z_R). The Rayleigh length is estimated to be $z_R \simeq 0.0013 \cdot r^2$, where r the radial distance (Wagner et al., 2009).

5.1 15° optical wedge prism

The 15° optical wedge prism was equipped to the lidar on April 22th 2009 and measurements were acquired until April 30th. During this period the wind turbine was working, however the position of the spinner was measured only from 22:50 on April 28th until 10:00 on April 30th (see Figure 5.2).

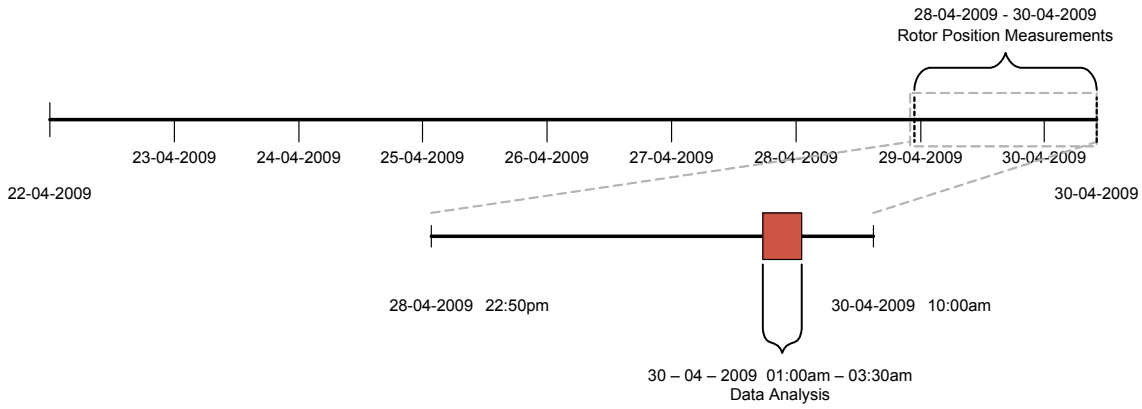

Figure 5.2 Period of the SpinnerEx 2009 experiment when the 15° wedge prism was used.

The wind direction and speed were measured by wind vanes, sonic and cup anemometers installed in the adjacent MET mast. The wind speed was observed to be relatively low, around ~4 ms^{-1}. The only exception with higher wind speeds was found between 00:00 and 06:00, on the 30th of April, when also a relative strong shear due to stably stratified temperature conditions appeared (see Figure 5.3, a). During that period the atmosphere was characterized by stable conditions as it is observed from the time series of the potential temperature difference between the heights 93 m and 57 m as well as between 93 m and 5.7 m (see Figure 5.3, c). The wind direction for that period is varying from 0° till 50° at the 57 m. Simultaneously, at the 90 m level the wind directions was found to be approximately 10° shifted clockwise (see Figure 5.3, b). For these directions, it can be assumed that the wind is flowing over flat terrain as it was blowing from Tjæreborg city towards the location of the wind turbines.

a) Wind Speed

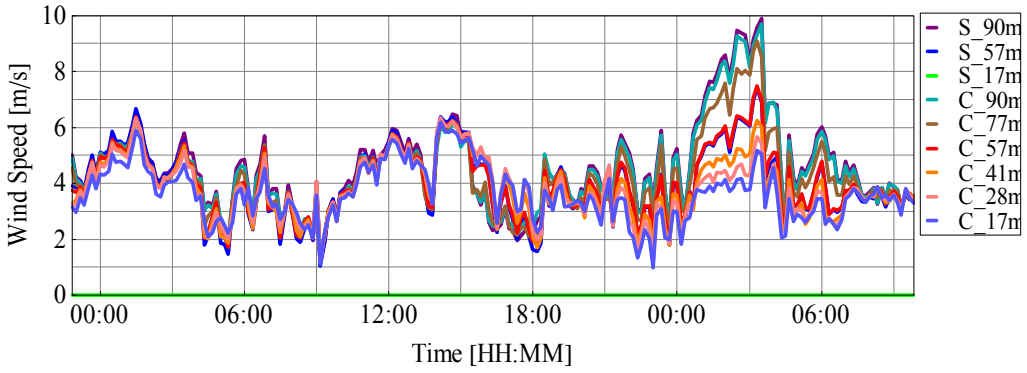

b) Wind Direction (sonic)

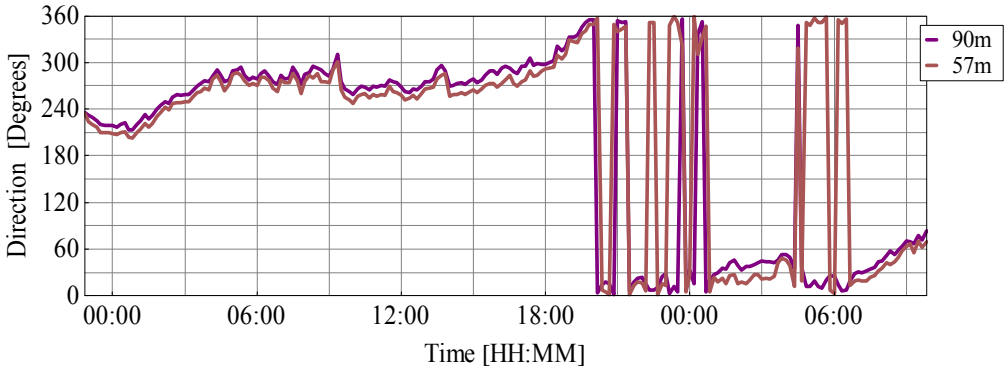

c) Potential Temperature

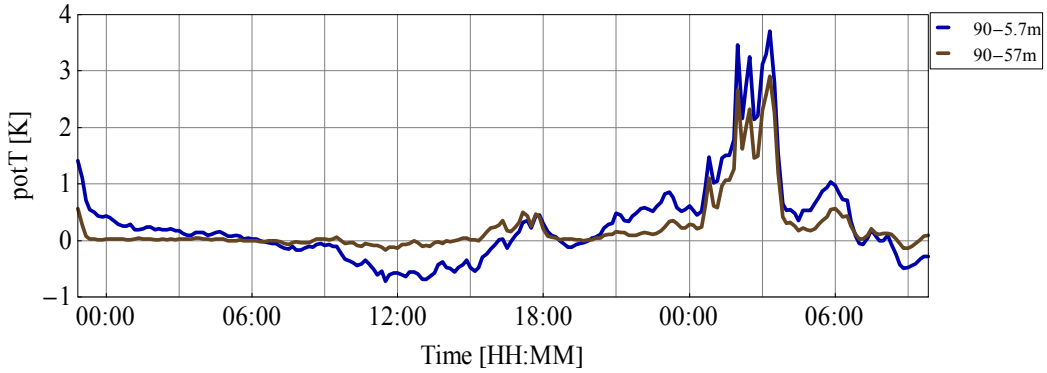

Figure 5.3 Time series of the speed and direction of the wind (a and b, respectively) and of the potential temperature (c), during the period when the 15° wedge was used.

In this section data from the period between 01:00 until the 03:30 of the 30th of April 2009 will be presented. The aforementioned period was characterized with the highest wind speeds. Moreover for wind directions between 0° and 50° it is expected that neither the wind turbine nor the MET mast were located in the wake of the adjacent wind turbines (see landscape, at Figure 1.3 and Appendix B).

Radial Wind Speed

Using the radial wind speed of each measurement and the corresponding azimuth angle it is now possible to construct a representation of the incoming wind flow towards the wind turbine. In the following figures, samples of the aforementioned representations as measured in two consecutive 10-minute periods are presented. The radial wind speeds are depicted in polar plots. In the left plot (2009-04-30 01:30) the distribution of the radial wind speed is observed to be partly homogenous (view towards the wind turbine). Additionally higher turbulence is measured in the lower part of the scanning circle. In contrast, in the consecutive time period (2009-04-30 01:40) it seems that higher wind speeds are measured in the left part of the polar plot. This could indicate a yaw misalignment of the wind turbine.

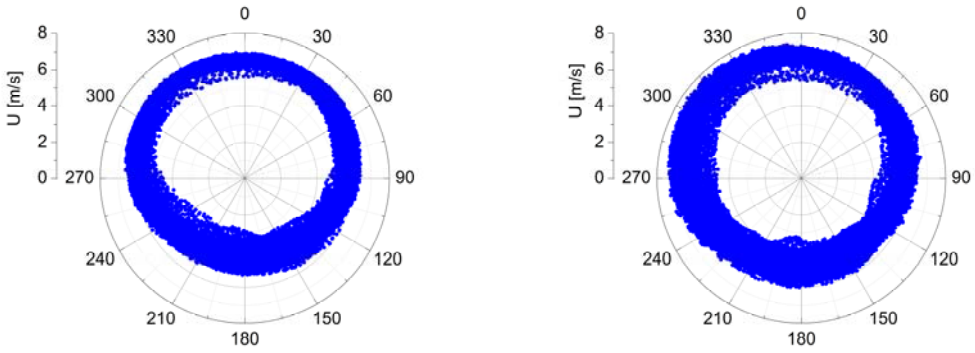

Figure 5.4 Polar plots of radial wind speeds.

As already mentioned it seems like the winds measured at the lower heights are more turbulent than the ones measured at the higher heights. By investigating the distribution of the wind speeds in this 10 minute period (2009-04-30 01:30) , it was found that the less turbulent the incoming wind flow is, the sharper is the distribution of the wind speeds. On the contrary, when the turbulence levels increases the distribution broadens with larger values of standard deviation.

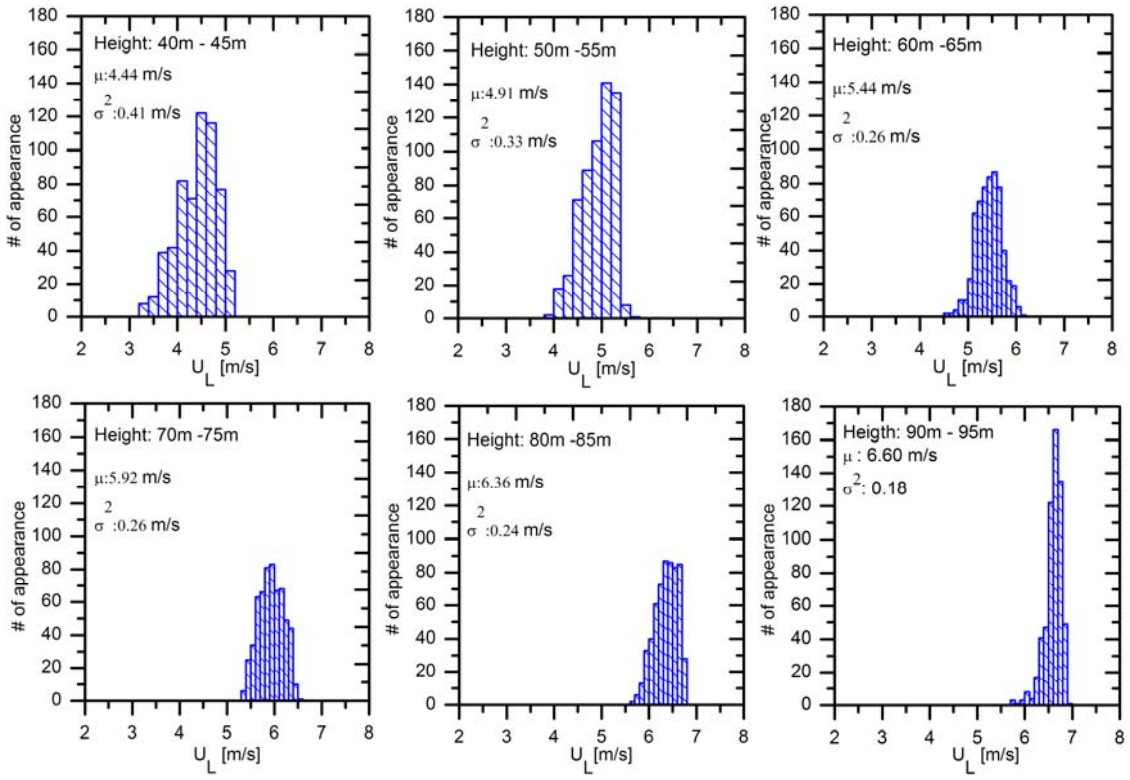

Figure 5.5 Distribution of the radial wind speed measurements for 6 different height layer, as measured at 01:30 on April 30th 2009.

In order to investigate the relationship between the lidar's signal power and the azimuth angle of the measurements, the Doppler spectrum was integrated. The area under the Doppler peak represents the total return signal power. It was consistently observed a difference of the power of the backascattered signal between the lower and the higher heights (Figure 5.6).

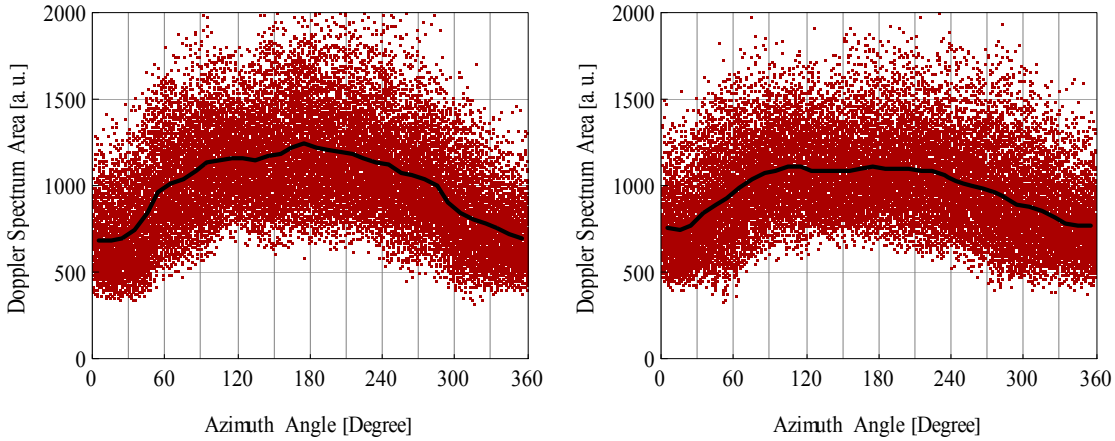

Figure 5.6 Area of the Doppler spectrum for 10-minute time series of lidar measurements, 2009-04-30 01:30 (left) and 2009-04-30 01:40 (right).

Yaw misalignment

From the data of the measured radial wind speed and azimuth angle, the yaw misalignment (θ_w) is estimated following the procedure which has been described at the section 4.2. This method is used to calculate the vertical distribution of the wind direction fluctuations, having as a reference the horizontal axis of the wind turbine. Averaged values of the radial wind speed over 6 different time steps (0.5, 1, 2, 3, 5, 10 minutes) were used. The vertical spatial resolution is 5 m. In the following figure (Figure 5.7) the vertical profile of the yaw misalignment is presented, as calculated for the data set acquired on the 2009-04-30 01:50 using 10-minute average radial wind speed values. It can be observed that the angle of the yaw misalignment is increasing, following a clockwise shift moving from the low to the high heights. This is in accordance with the stable conditions that describe the atmosphere during that period, where a height dependent clockwise shift of the wind direction is expected [Stull, 1988].

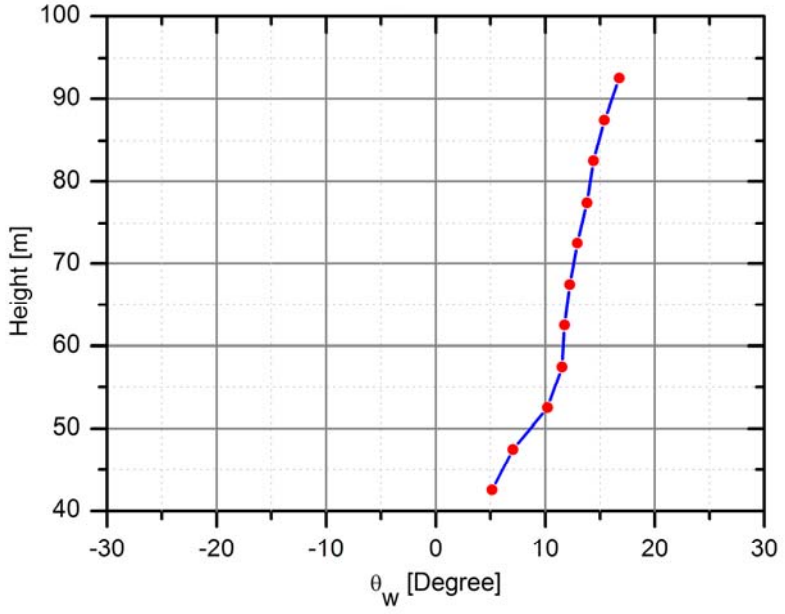

Figure 5.7 Yaw misalignment vertical profile (10-minutes average values).

Furthermore, we investigated the dependence between the yaw misalignment and the length of the time period over which the radial wind speeds were averaged. In the two following figures (Figures 5.8 and 5.9) the measured instantaneous yaw misalignment at two different heights (57 m and 93 m) are being presented. Each figure contains 6 different time series, one for each applied running averaging time (0.5, 1, 2, 3, 5, 10 minutes). It can be observed that for the 10-minute average radial wind speeds, a difference (yaw error) between the direction of the wind turbine and the direction of

the wind of approximately 10^{o} is appearing, at both heights. The shorter the averaging period is, the more scattered are the values of the yaw error.

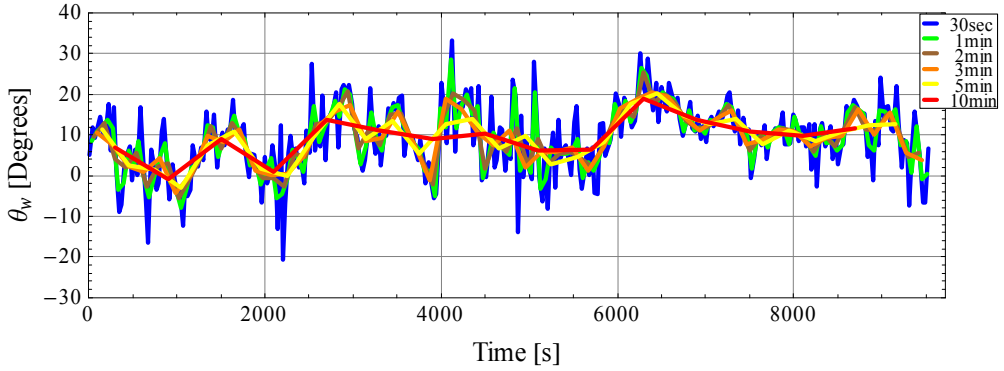

Figure 5.8 Yaw error calculated using the lidar radial wind speed measurements for the height of 57 m.

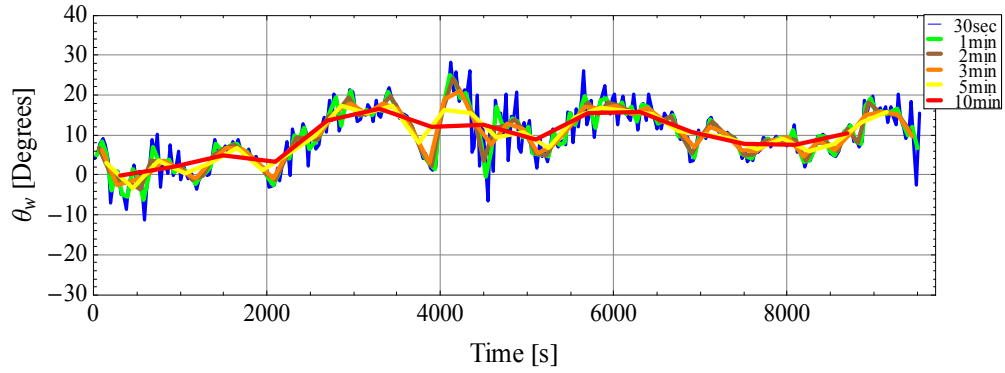

Fig. 5.9 Yaw error calculated using the lidar radial wind speed measurements for the height of 93 m.

Using the data logged by the NM80 wind turbine controller, it was furthermore possible to compare the calculated yaw errors with the difference between the wind direction as measured by sonic anemometers and wind vanes and the direction of the wind turbine as recorded by the wind turbine controller. As already mentioned, the wind turbine yaw direction data were not calibrated in an absolute frame of reference. However, a calibration offset was later calculated to be equal with 17.9^{o} (see Appendix D).

$$\theta_{w_i} = W_{Dir_i} - (Yaw_{\text{wind turbine}} - \text{offset}) \tag{5.1}$$

Where W_{Dir_i}, is the wind direction as measured either from the sonic anemometer or the wind vane.

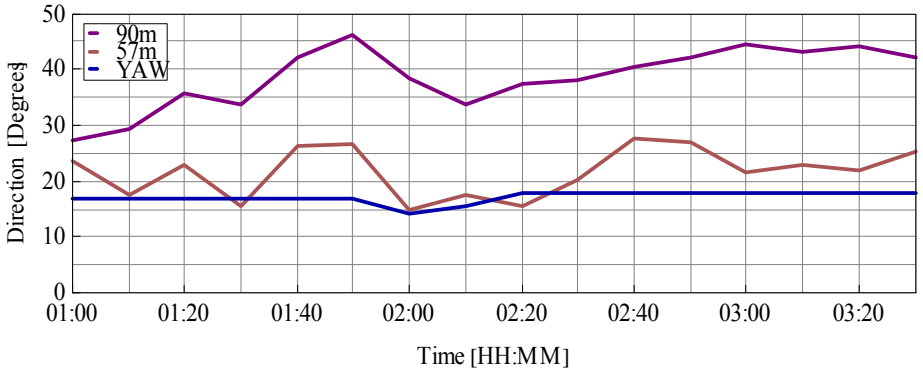

Figure 5.10 Wind direction at two heights (57 m and 93 m) and wind turbine yaw direction.

The wind direction measurements along with calibrated measurements of the yaw angles are being presented in the above graph (see Figure 5.10). The comparison was done at 57 m with both sonic anemometer and wind vane measurements, while at 93 m only the sonic anemometer was used (see Appendix C). In the following figure (Figure 5.11) the correlation between the yaw error relative to the direction as measured by the lidar (blue line with red dots) and the difference between the wind direction and the yaw of the wind turbine are presented. The calculations have been done using the 10-minute average values of the lidar radial wind speed measurements. The correlation is found to be of the order of 0.74. Furthermore it appears that the turbine has both a mean yaw gain factor different from unity and a non-zero mean offset during this period.

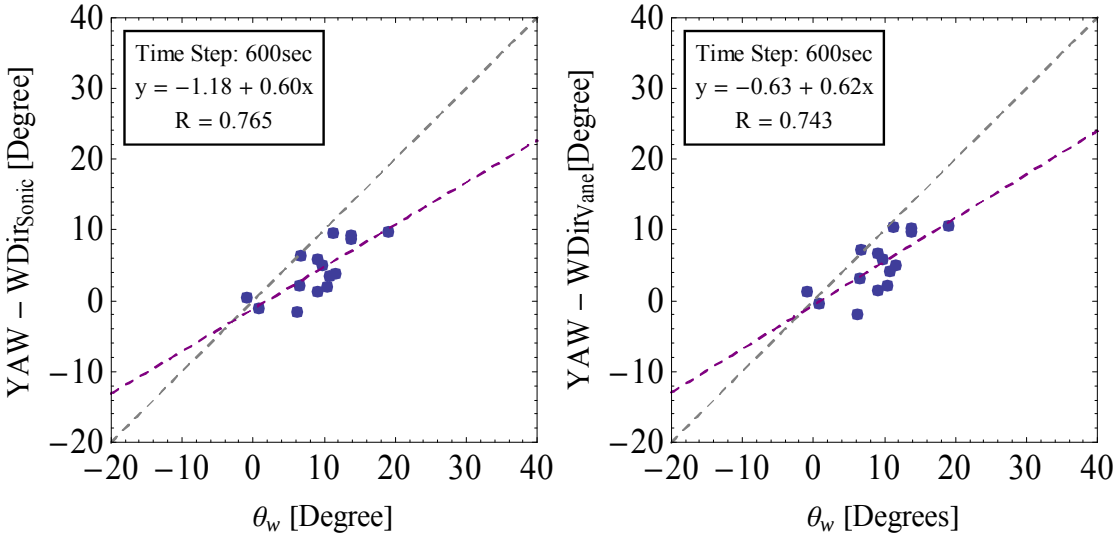

Figure 5.11 Correlation plots between the yaw error as measured from the lidar with the difference between the direction of the wind turbine and the wind direction measurements from the sonic anemometer (left) and the wind vane (right).

Figure 5.12 presents the time series of the calculated yaw misalignment angles based to the lidar data (blue line with red dots) and the difference of the wind and yaw direction. From the plots it appears that the lidar can measure the yaw misalignment relatively accurate for approximately the first ~3600 seconds. While for the rest of the period the lidar is overestimating the yaw error. This is can be connected to the drift of the wind direction which was observed. In the Appendices E and F, both the correlation plots and the time series figures are presented.

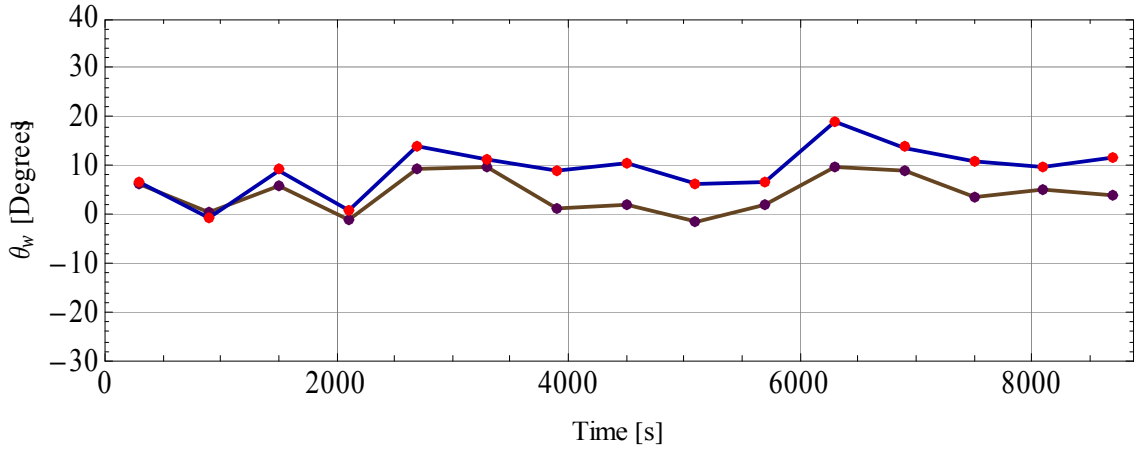

(a)

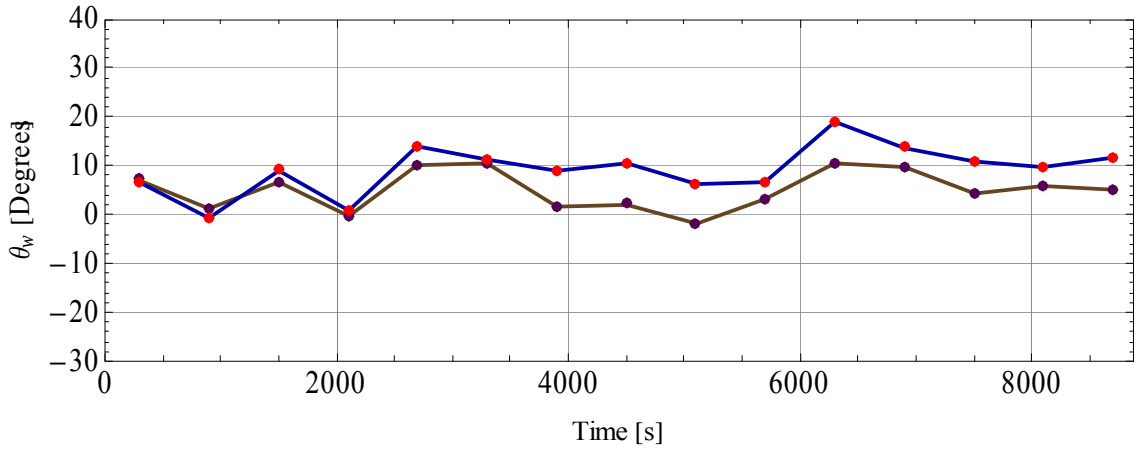

(b)

Figure 5.12 Comparison of the time series of the yaw error as measured from the lidar (blue) with the difference between the direction of the wind turbine and the wind direction measurements from the sonic anemometer (a) and the MET tower wind vane (b).

Table 2 presents the mean and the standard deviation of the: (a) absolute calculated yaw misalignment angles (θ_w) and (b) the measured difference between the yaw of the turbine and the wind direction measurements of the sonic anemometer. The calculations are done for each running mean averaging time (0.5, 1, 2, 3, 5, 10 minutes). A yaw misalignment between 10^o and 9^o appears to be measured by the lidar. As the running mean averaging time increases it is observed that both the mean and the standard deviation are decreasing. A difference between 4^o and 5^o is observed between the mean values of the yaw misalignment of the angle. However these values could be affected by errors during the calibration of the yaw position measurements.

Additionally Table 2 includes values of the correlation between the calculated and the measured yaw misalignment angles, for each length of the running average period. It appears that the correlation improves with increasing length of the running averaging period.

Table 2 Yaw misalignment angles

Averaging Time	**Lidar [θ_w]**		**Yaw - $W_{dirSonic}$**		**Correlation**
	Mean [^{o}]	StD [^{o}]	Mean[^{o}]	StD[^{o}]	
30sec	10.45	6.50	5.32	3.89	0.47
1min	9.74	6.13	5.26	3.81	0.58
2min	9.54	5.64	5.18	3.74	0.69
3min	9.30	5.64	5.13	3.68	0.71
5min	9.48	5.13	4.92	3.70	0.75
10min	9.30	4.72	4.67	3.35	0.76

Times series of the horizontal wind speed

For the calculation of the projection of the radial wind speed to the horizontal axis, the yaw misalignment angles calculated from the 10-min running average times, where implemented to the equation (3.10).

$$U_L = u_x(\cos\theta_w \cos\theta_i \cos\theta_c - \cos\theta_w \sin\theta_i \sin\theta_c \cos\varphi - \sin\theta_w \sin\theta_c \sin\varphi) \quad (3.10)$$

Figure 5.13 presents the 1-min average values, with a spatial resolution of 5 meters for the 3.5 hour period between 01:00 and 03:30 on 2009-04-30. In this plot it is observed that

layers of different wind speed are appearing over the 90 m of the boundary layer, indicative of an atmosphere characterized by stable stratified atmospheric conditions.

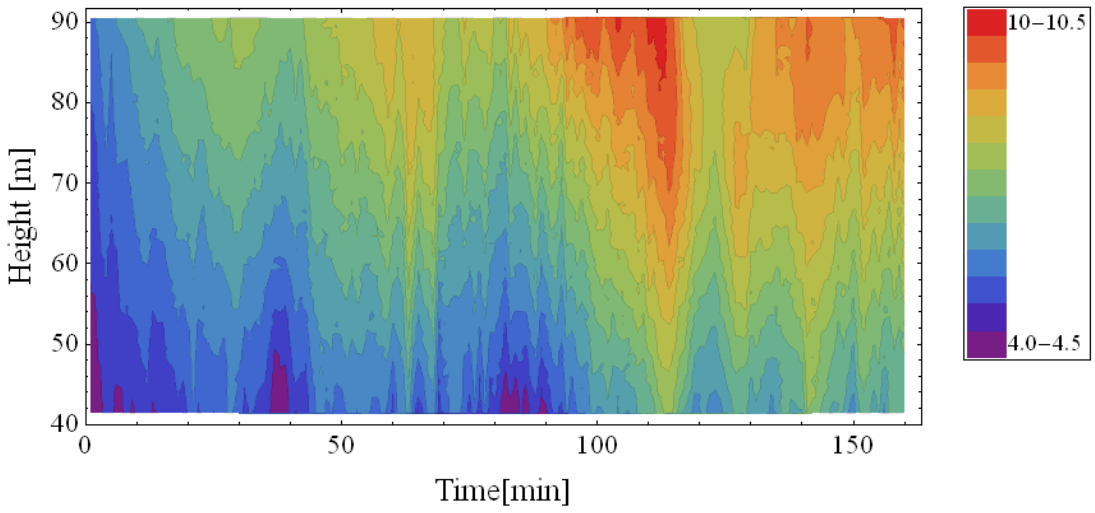

Figure 5.13 Horizontal wind speeds measurements from 2009-04-30 01:00 until 03:30.

The lidar based wind measurements presents good correlation with the MET mast wind speed data, even though the lidar was acquiring measurements in a distance approximately 400 meters away from the MET mast. Figure 5.14 presents the mean values of the wind speed measured by a cup at 6 different heights (17, 28.5, 41, 57, 77 and 93 m) along with the mean horizontal wind speed calculated from the lidar, over a 10-minute period (2009/04/30 02:30). The lidar values are extending approximately from 40 until 93 m and the spatial resolution in this graph is 1 m.

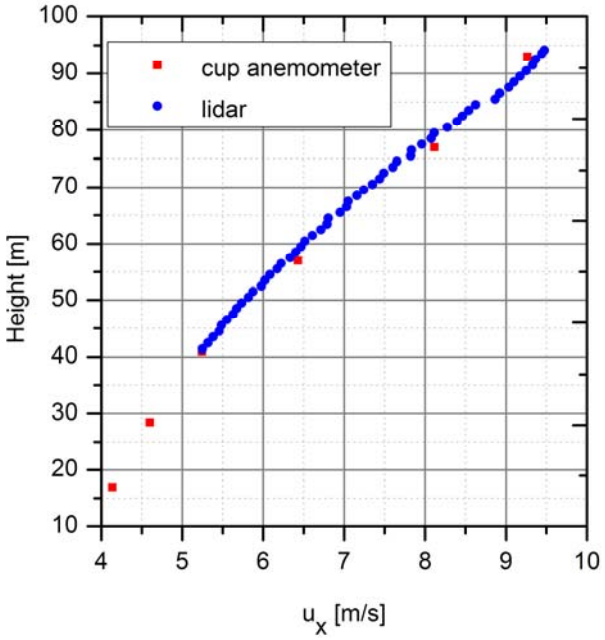

Figure 5.14 Vertical profile of the wind speed.

5.2 30° optical wedge prism

The ZephIR lidar was acquiring wind speed measurements, using an optical wedge prism with a deflection angle of 30°, from the 8th July until the 28th August 2009 (phase #4, Section 1.1). During this period the wind turbine operated on 7 occasions, which coincide with the DAN –Aero experiments. However only for four of those, both lidar and MET mast data are available. For each one of these occasions the wind turbine operation was often interrupted and adjustments of the wind turbine operation parameters (rpm, pitch and yaw offset) were made. Table 3 presents periods of undisturbed wind turbine operation for each individual day. Information are included concerning the wind direction at hub height (57 m), the yaw measurement of the wind turbine, as well as the status regarding the possibility that either the wind turbine or the mast are found inside the wake of one of the adjacent wind turbines.

Table 3 Periods of undisturbed wind turbine operation

Period				Not in a wake(1)	
Day	**Hour**	**$W_{Dir\ (57m)}$**	**Yaw**	**Turbine**	**Mast**
2009/07/16	12:30pm – 13: 10pm	~230°	238° – 248°	✓	✓
2009/07/21	15:10pm – 15: 50pm	~250°	245° – 265°	×	✓
2009/08/06	15:10pm – 16: 50pm	~130°	185° – 220°	×	×
2009/08/07	09:30am – 12: 30pm	~115°	170° - 210°	×	×

(1) × inside a wake, ✓ not in a wake

Data for the 40-minute period between 12:30 and 13:10 on July 16th 2009 are presented in this section. During this period the wind direction, as measured from sonic anemometers and wind vanes, was observed to vary between 225° – 250° at 57 m (see Figure 5.15a). For these South, South-West directions the wind was coming from the sea, passing first from the MET mast before arriving at the wind turbine. According to the terrain description (see section 1.2), for wind directions above 245° there is anticipated that the NM80 wind turbine would be affected from wind turbine wakes.

Figure 5.15b presents the time series of the wind speed sonic anemometer measurements. It appears that the wind speed fluctuates around the value of 6.5 ms^{-1} for all heights. Since the distance between the wind turbine and the MET mast is about 310 m, the changes of wind speed and direction measured by the MET mast will affect the wind turbine with a time lag of approximately 48 s. Figure 5.16 presents the 10-minute average values of the wind speed, as measured from cup anemometers at 6 different heights (17, 28.5, 41, 57, 77 and 93 m, respectively). The wind profile generally appears linear with homogenous speed. Furthermore, it can be seen that the vertical profile of the wind speed is presenting steps with a

varying slope. This can be attributed to the fact that the wind is being affected from changes in the roughness of the surface, as it flows from the sea to the mainland.

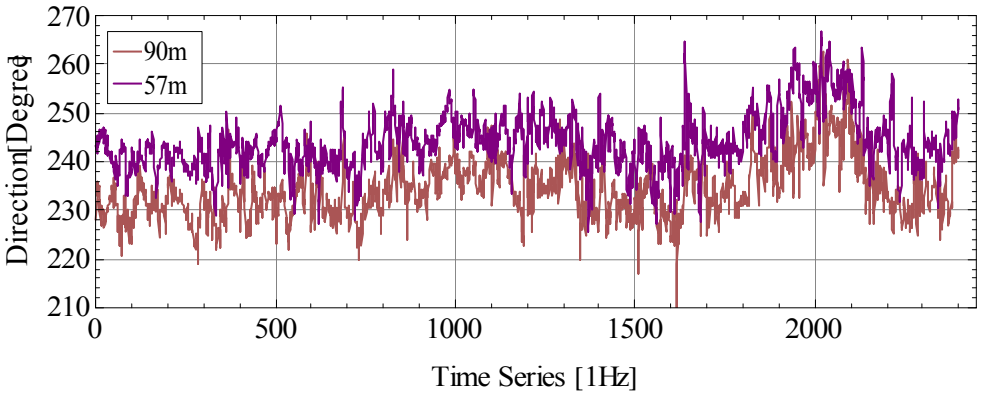

(a)

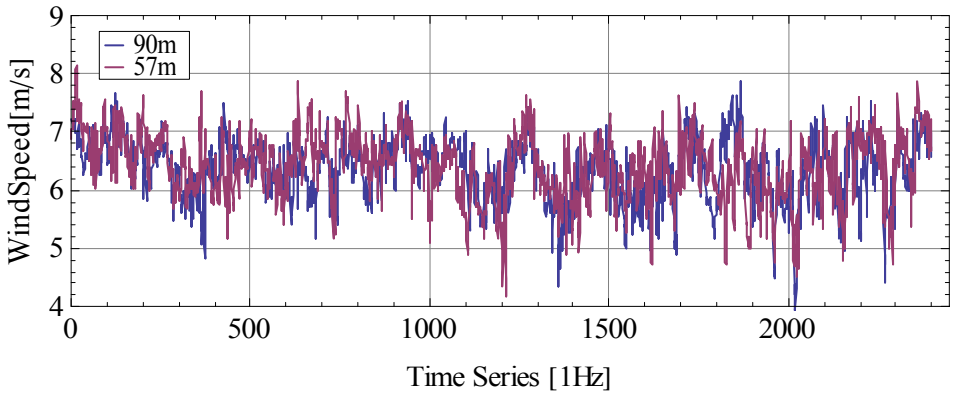

(b)

Figure 5.15 Time series of the wind direction (a) and speed (b), as measured by the instrumentation of the MET mast.

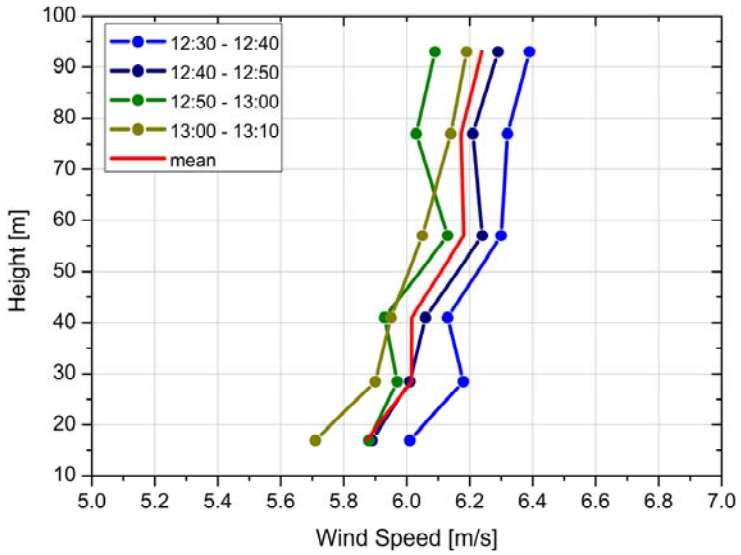

Figure 5.16 Vertical profile of the 10-min mean wind speed (cup anemometer).

Radial Wind Speed

Radial wind speed measurements were acquired from the ZephIR lidar during the period between 12:30 – 13:10 on the 16th of July 2009. Problems with the availability of data appeared only for 34 seconds between 12:57:59 and 12:58:23, due to issues concerning the rotor position measurements. Figure 5.17 presents these radial wind speed measurements in polar plots. It is observed that in general during these 40 minutes, the wind speed is characterized by roughly homogeneous distribution. Furthermore, the radial wind speeds acquired for azimuth angles between 0° and 180° are presenting slightly higher turbulence.

Moreover in the forth plot (13:00 – 13:10) higher wind speed were measured at the azimuth angle region of 0° – 180° in comparison with those in the region 180° – 360°. This could be an indication of a yaw misalignment of the wind turbine or the presence of wake that covers only a part of the wind turbine rotor.

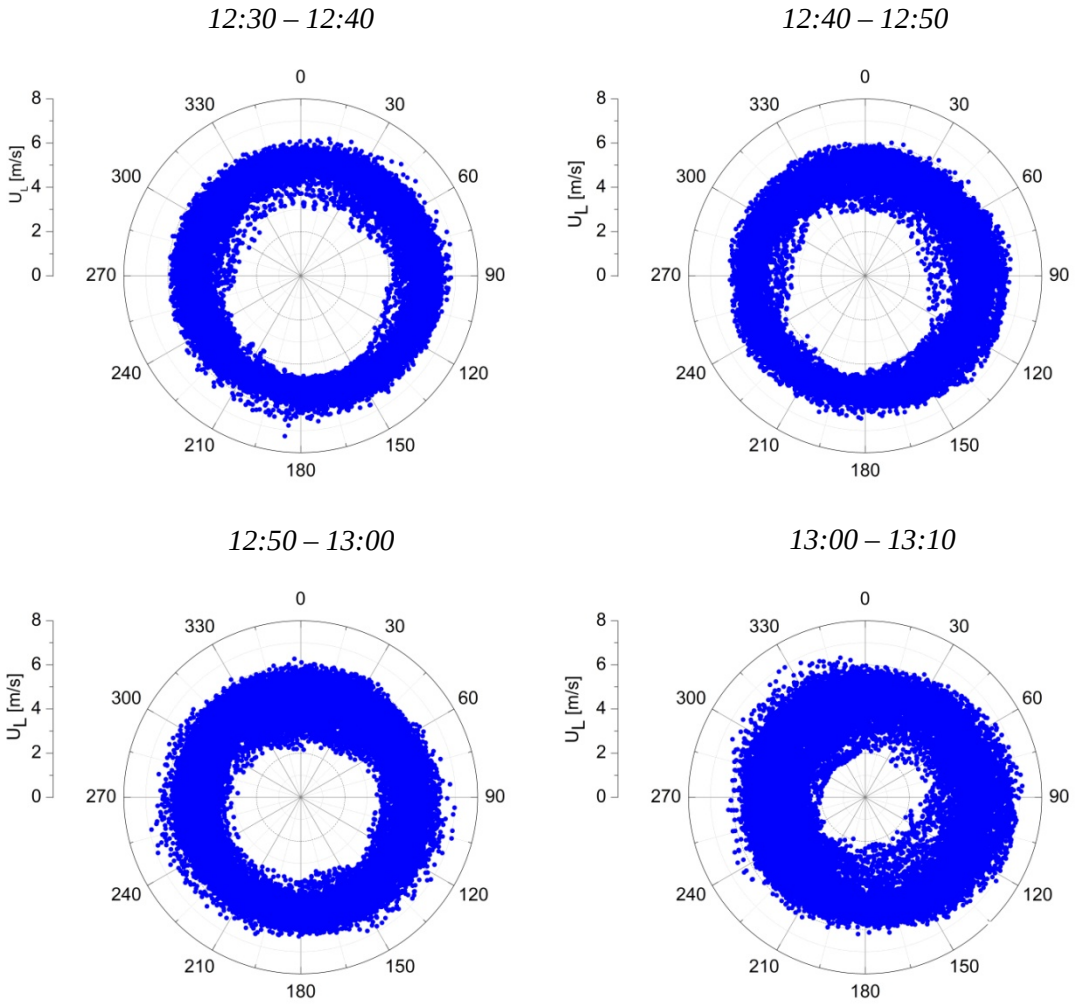

Figure 5.17 Polar plots of radial wind speeds (view towards the wind turbine).

Yaw misalignment

For this period, according to the 1-Hz sonic measurements, the wind direction was measured to be around 220° – 250° at 57 m and 240° – 260° at 90 m (see Figure 5.18). Through the yaw measurements it was found that the wind turbine during this period, yawed from 238° to 248°, following the clockwise drift of the wind direction. The wind turbine was expected to be inside a wake (from the wind turbine #8, see Figure 1.3), for wind directions beyond 245°. This fact could justify the characteristics of the radial wind speed measurements acquired between 13:00 and 13:10, where it can be seen that lower wind speed measurements are appearing for azimuth angles in the interval between 180° and 360°.

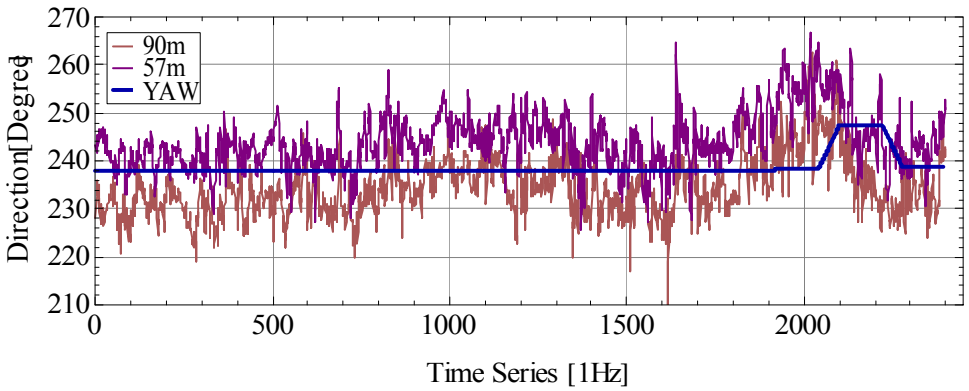

Figure 5.18 Time series of the wind and yaw direction.

Figure 5.19 presents the difference between the 1-Hz radial wind speeds measurements $\left(U_{L_{z,\varphi(o^0-180^o)}},\ U_{L_{z,\varphi(180^o-360^o)}}\right)$ acquired from the lidar between 13:00 and 13:10, for data which were acquired at a height layer z, but for two different conjugate azimuth angles $\left(\varphi_{(0^o-180^o)},\ \varphi_{(180^o-360^o)}\right)$. It can be seen that after approximately 300 s the lidar started to measure lower values of the radial wind speed in the azimuth region between 180° – 360°.

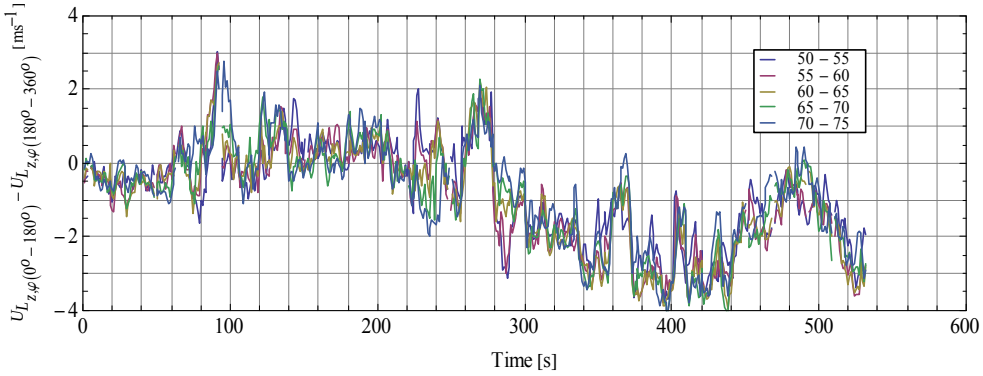

Figure 5.19 Time series of the difference between radial wind speed measurements for different conjugated angles at 5 different height layers (50 – 55, 55 – 60, 60 – 65, 65 – 70 and 70 – 75 m).

The corresponding radial wind speed measurements to the period between 120 s – 360 s of the Figure 5.19 are presented in the above polar plots (see Figure 5.20). Each polar plot contains 70 consecutive scans (approximately 0.85 s are needed for the completion of one scanning azimuth circle).

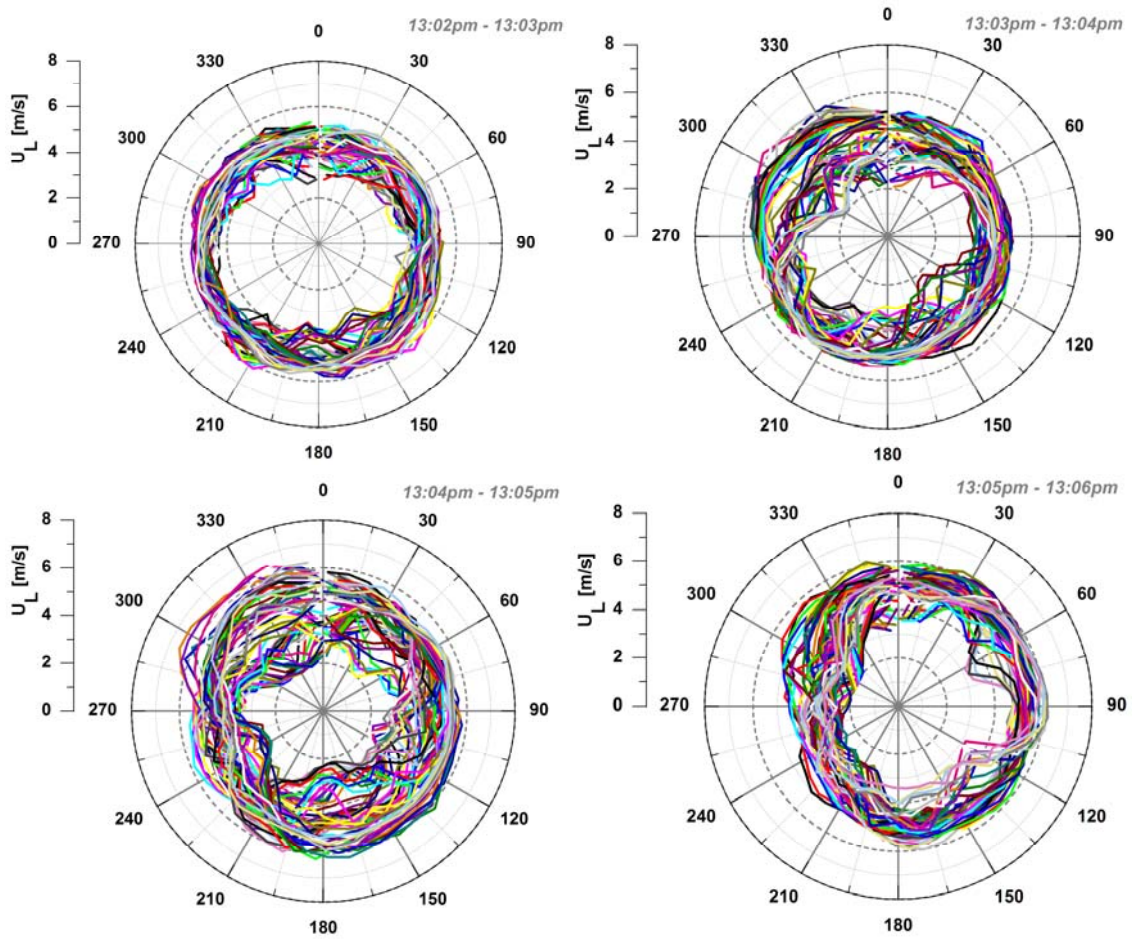

Figure 5.20 Polar plots of radial wind speeds measurements of the period between 13:02 and 13:06 (view towards the wind turbine).

The presence of a part of the rotor, and subsequently a part of the lidar scanning circle, inside the wake of the wind turbine is expected to affect the yaw misalignment method. In particular, according to the geometrical model and the method described in chapter 4, the presence of a wake in the region of azimuth angles between 180^{o} and 360^{o} would be misinterpreted as a counterclockwise rotation of the wind turbine from the direction of the wind, giving larger yaw misalignment angles.

Figures 5.21 and 5.22 present the yaw misalignment angles of the wind turbine at two heights (57 m and 93 m, respectively) for the period between 12:30 and 13:10 on the 16^{th} of July 2009. During this period the yaw misalignment angle at hub height was found to be varying

between 0° and -10°. An exception is observed in the end of the period were larger variations are occurring.

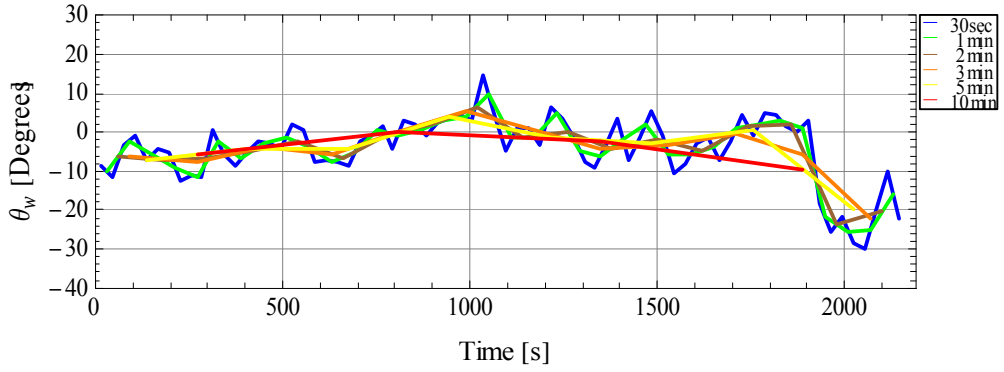

Figure 5.21 Yaw error calculated using the lidar radial wind speed measurements for the height of 57 m.

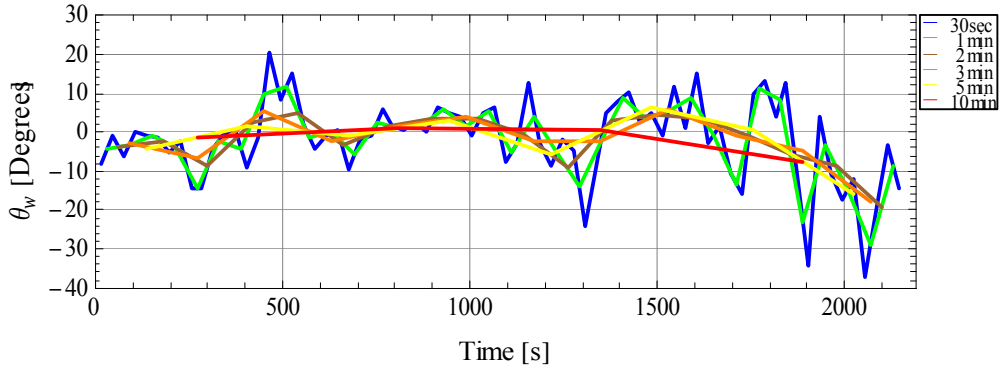

Figure 5.22 Yaw error calculated using the lidar radial wind speed measurements for the height of 93 m.

Table 4 presents the mean and the standard deviation of the: **(a)** absolute yaw misalignment angles (θ_w) and **(b)** the absolute difference between yaw and sonic wind direction measurements over the whole period (12:30 – 13:10, 2009-07-16). The analysis has been made for different lengths of the averaging period (30 sec, 1, 2, 3, 5 and 10 min). As the time step increases it is observed that both the mean and the standard deviation of θ_w are decreasing, from 6.59° to 4.46°. The differences between the calculated values of θ_w and the measured yaw misalignment were found to be less than 1° for all the lengths of the averaging period. However, despite the small deviation, the correlation between them doesn't appear to be high. This can be justified by the fact that due to the presence of a wake, the lidar is overestimating the yaw error the last 10 minutes of the period. Figure 5.23 presents the 2-min yaw misalignment time series, where this overestimation of the yaw error is visible. All the correlation plots and the time series can be found in Appendices E and F.

Table 4 Yaw misalignment angles

Time Period	Lidar [θ_w]		Yaw - $W_{dirSonic}$		Correlation
	Mean [°]	StD [°]	Mean[°]	StD[°]	
30sec	6.59	6.67	5.66	3.64	0.42
1min	6.10	6.50	5.48	3.50	0.49
2min	5.72	6.40	5.26	3.13	0.59
3min	5.41	5.76	5.22	3.36	0.56
5min	5.53	6.11	4.86	2.40	0.60
1min	4.46	4.25	4.22	2.14	-0.17

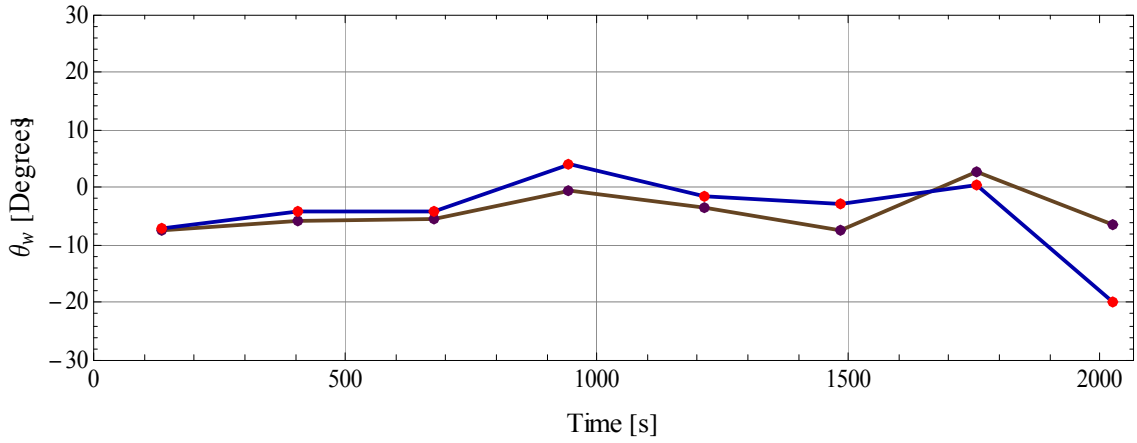

(a)

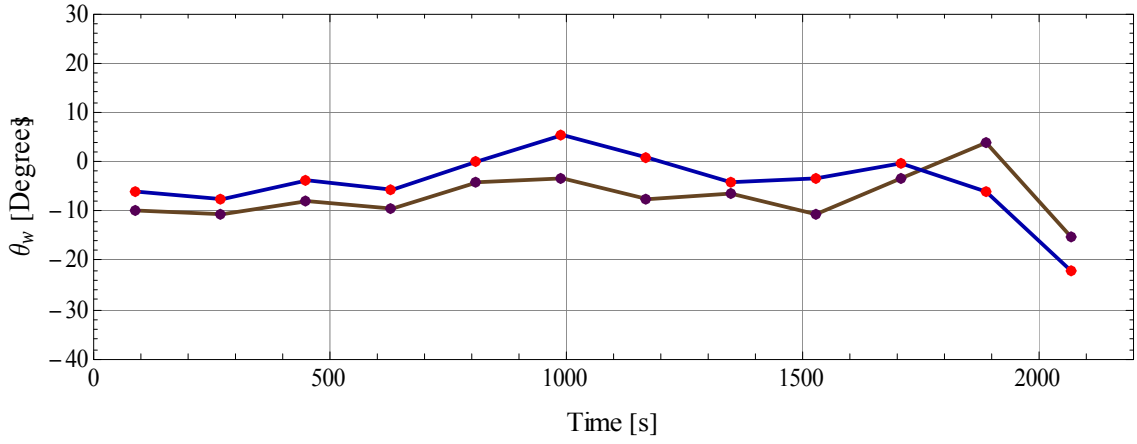

(b)

Figure 5.23 Time series of the yaw misalignment angles as calculated from the lidar data (blue) and as measured from the difference between the direction of the wind turbine and the wind direction measurements from the sonic anemometer (a) and the wind vane (b).

Time series of the horizontal wind speed

The horizontal wind speed was calculated through Equation (3.10) by taking into account the yaw misalignment angles. Figure 5.24 presents the 10-min average yaw misalignment angles (at 11 different heights). While Figure 5.25 presents the corresponding vertical profile of the u component of the wind, as measured by the lidar and the cup anemometers of the MET mast. It seems that during the last period (13:00 – 13:10), the largest variation between the lidar and the MET mast measurements is occurring. In the same way the yaw misalignment is overestimated, which probably is due to the influence of a wake produced by one of the other wind turbines.

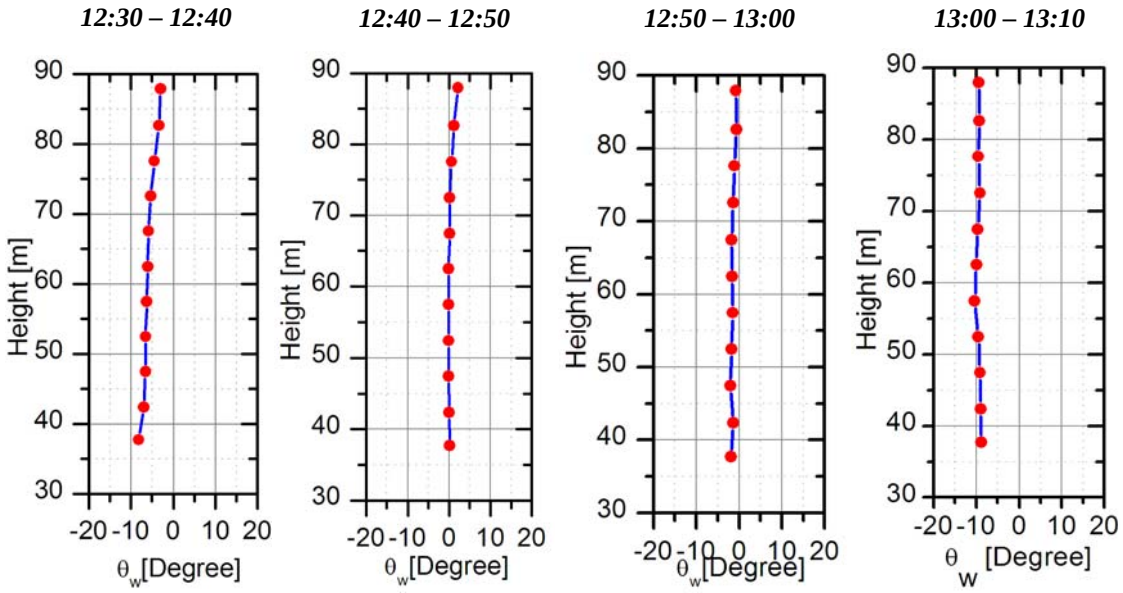

Figure 5.24 Vertical profiles of the yaw misalignment angles

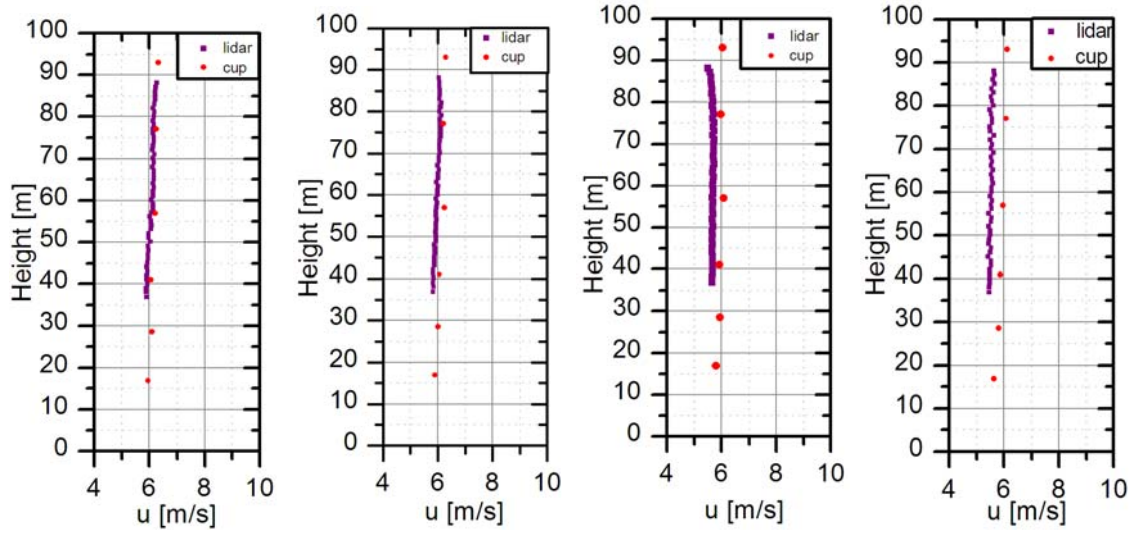

Figure 5.25 Vertical profile of the horizontal wind speed.

6 Conclusions

Observations of the upwind approaching wind field using a remote sensing continuous wave wind lidar system were accomplished during the SpinnerEx 2009 experiment. A standard ZephIR wind lidar was modified and installed into the rotating spinner of a NM80 wind turbine, scanning upwind. Based on the line-of-sight radial wind speed measurements and the corresponding extracted azimuth position of each lidar measurement, it was possible to investigate the structure of the incoming wind field in front of the wind turbine.

A methodology has been described for the calculation of the yaw misalignment of the wind turbine. The calculations are based on the mean values of the radial wind speed measurements at a given height, over a period of time. In this report the duration of this period varied from 30 s to 10 min. Results from two different test cases were presented, where mean yaw misalignment angles of 9.5^{o} and 5^{o} were observed. Data from an adjacent located MET mast and from the NM80 wind turbine's control were used to evaluate this to our knowledge first wind turbine spinner lidar integration data acquisition methodology. In both cases the calculated values of the yaw misalignment angles were following the fluctuations of the wind direction in reference with the wind turbine yaw. However differences in the absolute values were observed. Limitations to this technique appeared when the wind turbine rotor was found in a wake of a wind turbine. The presence of a wake led to variations in the radial wind speed values, which were interpreted as a change of the wind direction.

Concluding, the integration of the lidar in the spinner of a wind turbine has proven very useful for the research of the incoming wind towards the rotor plane. Furthermore this innovative measurement concept offers the possibility of active control of a wind turbine through a wind lidar. Incorporation of remote sensing wind data into the turbine control system can lead to improved energy yield and load reduction, through yaw, rpm and pitch control. However several parameters have to be taken into account during the lidar data processing, such as meteorological conditions (e.g. rain, mist), wake effects and terrain limitations (horizontal shear). Therefore further studies are planned that will include the investigation and modeling of the effect on the lidar measurements of those aforementioned parameters. Implementation of enhanced control algorithms utilizing real-time upwind measured wind data of different wind flow conditions is envisioned to contribute to the improvement of active control of wind turbines in the near future.

References

Harris M., M. Hand and A. Wright, *"A Lidar for turbine control"*, Tech. Rep. NREL/TP – 500 – 39154 National Renewable Energy Laboratory, NREL, Golden, Colorado, US, (2006).

Harris M., D. J. Bryce, A. S. Coffey, D. A. Smith, J. Birkemeyer & U. Knopf, *"Advance measurement of gusts by laser anemometry"*, J. Wind Eng. 95, 1637 – 1647, (2007).

Mikkelsen, T., C. Michael; I. Antoniou, J.Mann. *"WindScanner: A full-scale laser facility for wind and turbulence measurements around large wind turbines",* EWEC (2008).

Smith D.A. and Harris M. and Coffey S. and Mikkelsen T. and Jørgensen H.E. and Mann J. and Danielian R., *"Wind Lidar Evaluation at the Danish Wind Test Site in Høvsøre"*, Wind Energ., 9:87 – 93, (2006).

Stull Roland B., "*An Introduction to Boundary layer Meteorology"*, Kluwee Academic Publishers, (1988).

Wagner R., Mikkelsen T., Courtney M., *"Investigation of turbulence measurements with a continuous wave, conically scanning LiDAR"*, Risø-R-1682, (2009).

Appendix A: Data Files

The lidar measurements were stored in data files, whose labels contained the following information:

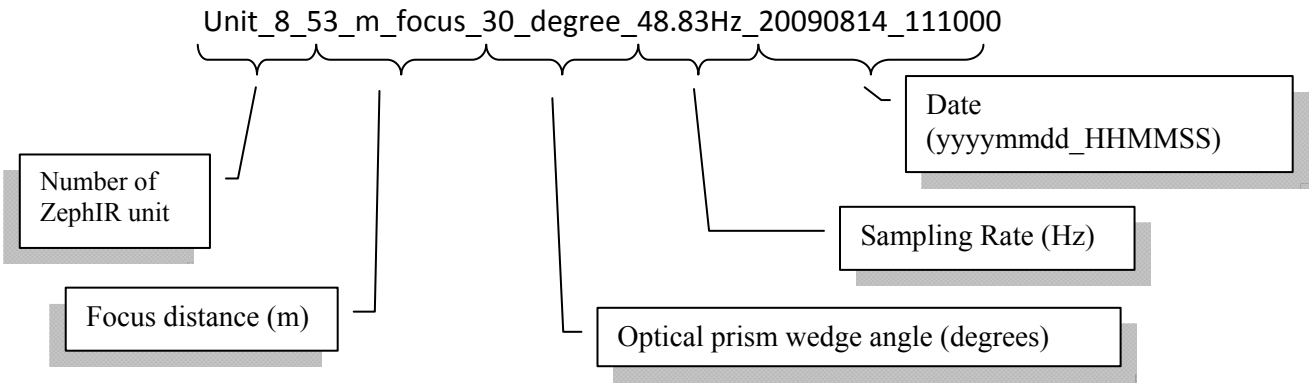

The format of the file is presented in the following Table:

Name	Position	Type	Size	Meaning	Min	Max	Source
Reference	0	int	4				ZephIR
Phase	4	float	4	Phase of the wedge.	0	2π	ZephIR
Height	8	float	4				ZephIR
Scaling	12	float	4	255/maximum value in spectrum.			ZG software
Time	16	int	4				ZephIR
Ms	20	int	4				ZephIR
Status	24	int	4				ZephIR
Number of FFT bins	28	int	4	Fixed to 255.	255	255	ZephIR
FFT data	32	byte[255]	255	Doppler Spectrum.	0	255	ZG software
Rotor position	287	float	4	Rotor position blade.	0	2π[4]	ZG software
Analog channel x	291	ushort	2	Accelerometer x (along yaw direction).	0	65535	DAU
Analog channel y	293	ushort	2	Accelerometer y (perpendicular to yaw direction).	0	65535	DAU
Analog channel yaw	295	float	4	Yaw angle.	0	2π	ZG software

4 Only true when rotor is running normally.

Appendix B: Wind Speed Vertical Profile

Wind speed vertical profiles as measured from cup anemometers

Filters: u_{min} =5 m/s (at 57m), 10^o wind direction sectors, stable atmospheric conditions

(with red color is depicted the mean profile of each sector)

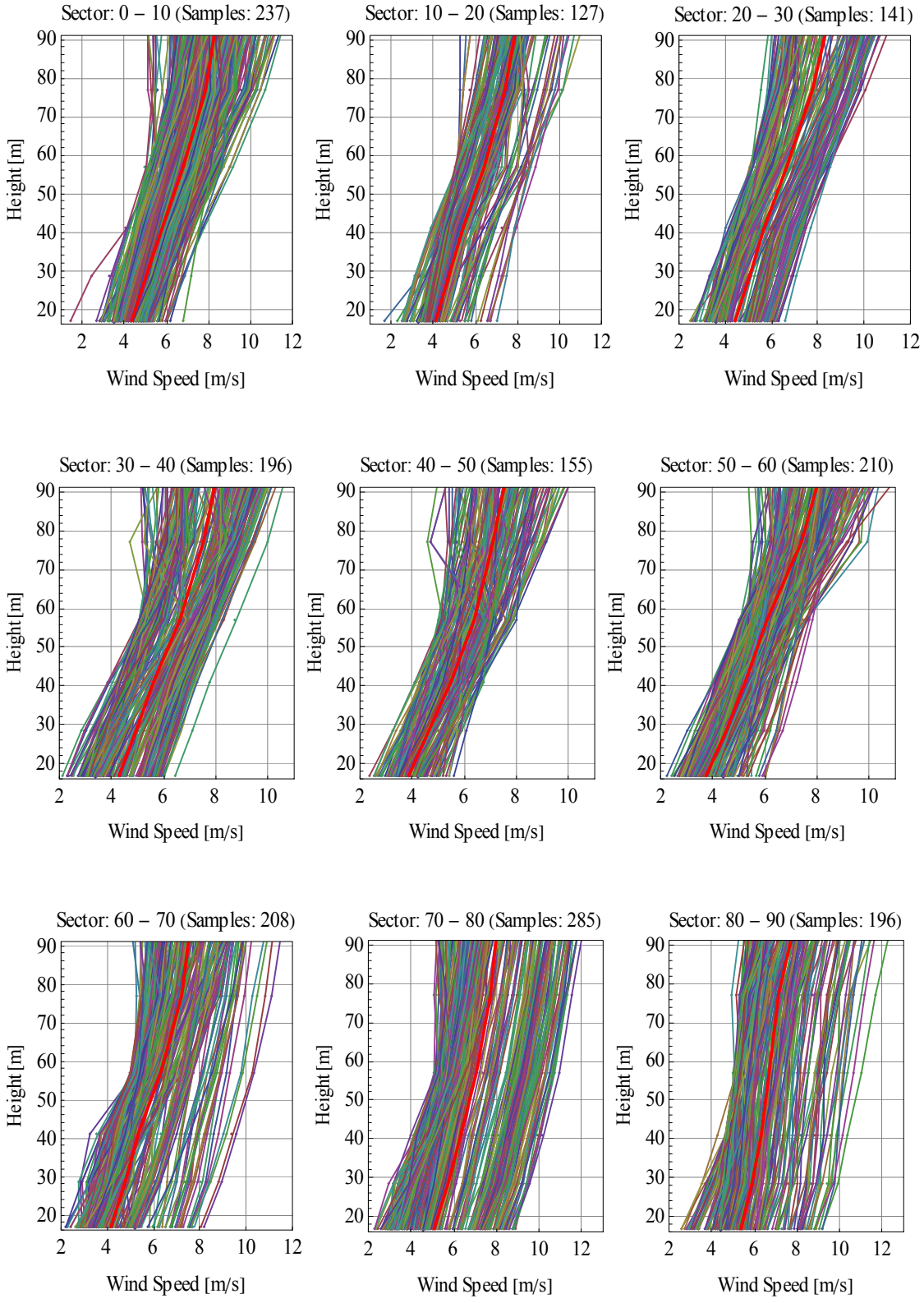

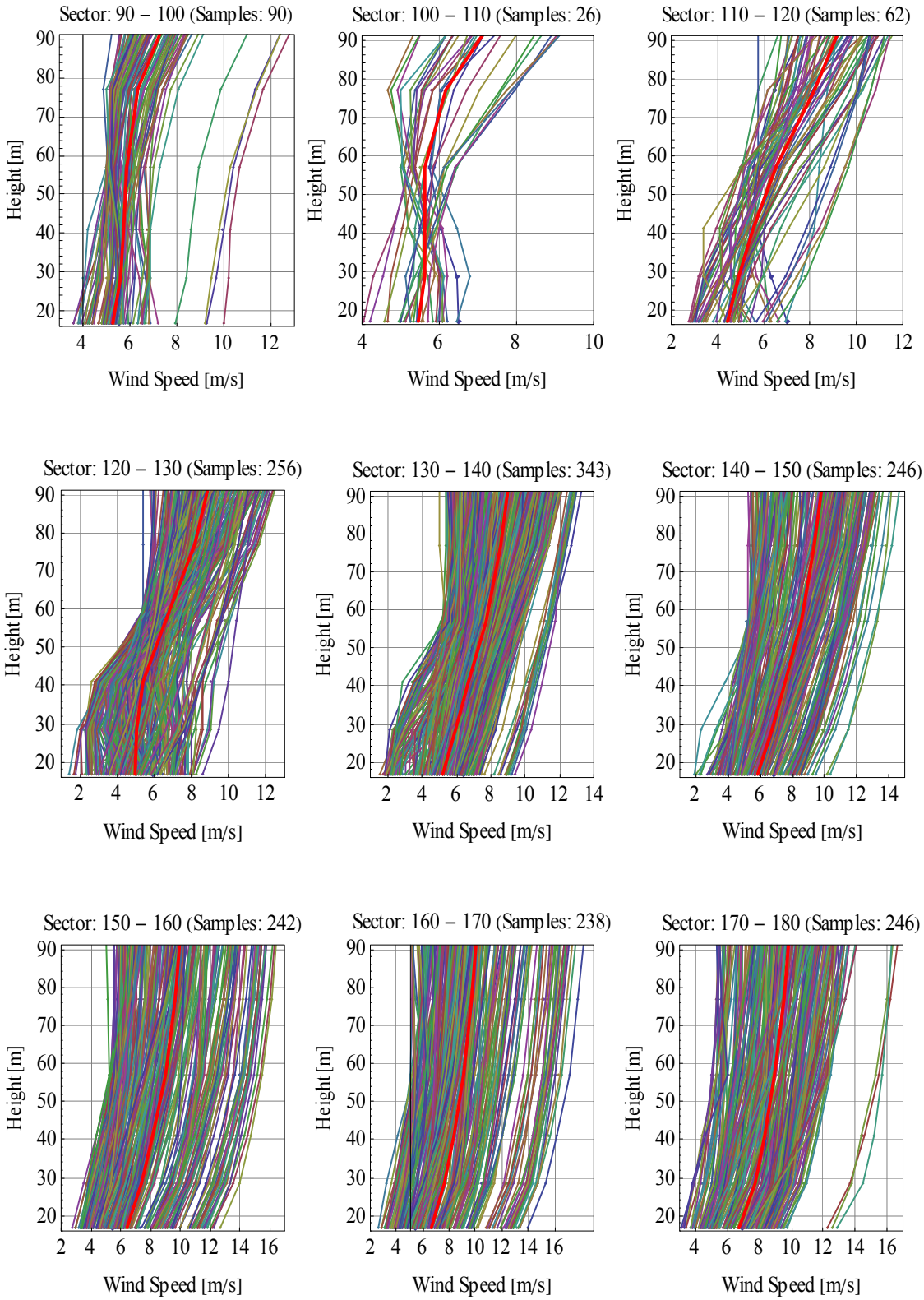
Sector: 90 – 100 (Samples: 90)
Sector: 100 – 110 (Samples: 26)
Sector: 110 – 120 (Samples: 62)
Sector: 120 – 130 (Samples: 256)
Sector: 130 – 140 (Samples: 343)
Sector: 140 – 150 (Samples: 246)
Sector: 150 – 160 (Samples: 242)
Sector: 160 – 170 (Samples: 238)
Sector: 170 – 180 (Samples: 246)
Height [m]
Wind Speed [m/s]

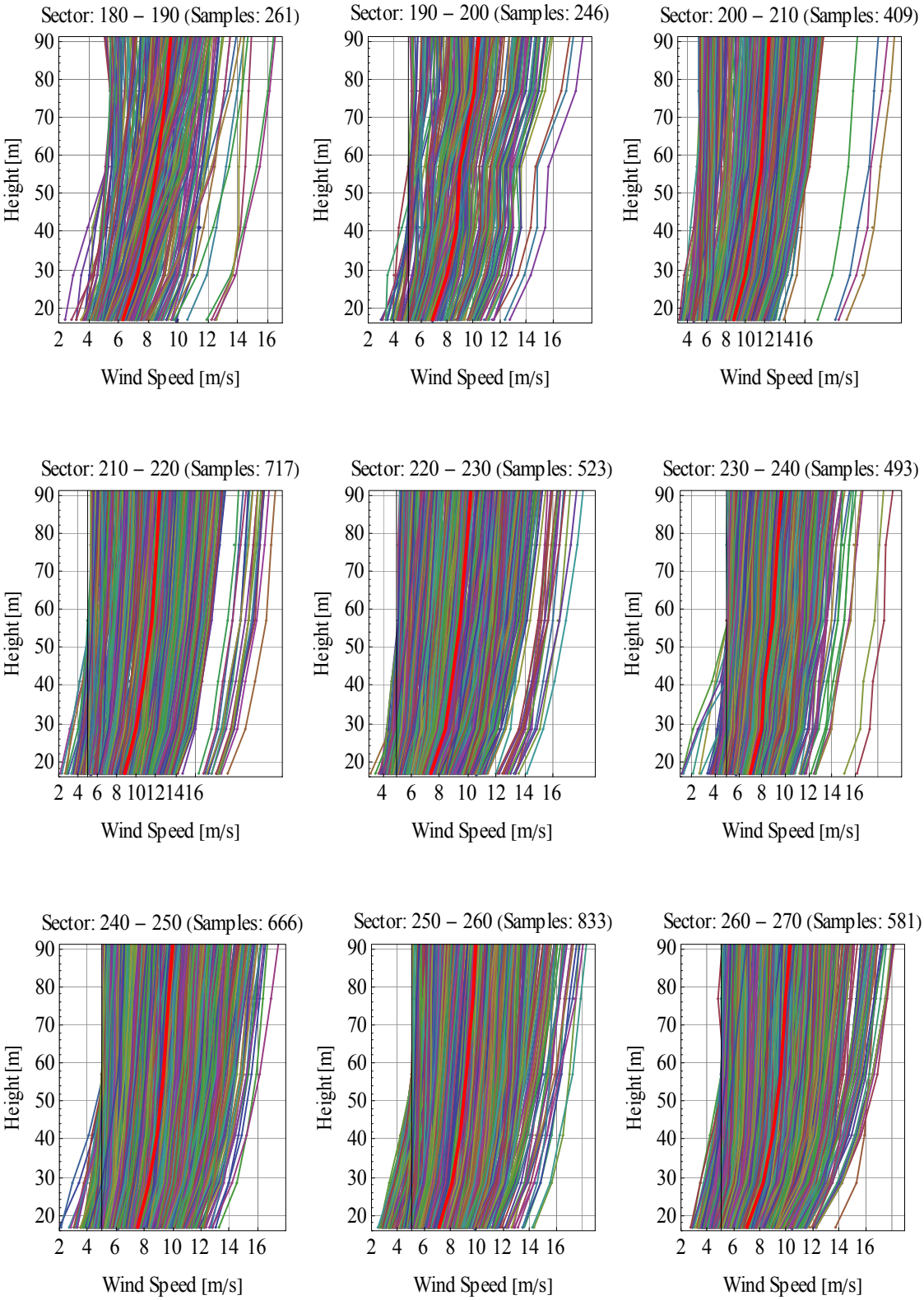
Sector: 180 – 190 (Samples: 261)
Sector: 190 – 200 (Samples: 246)
Sector: 200 – 210 (Samples: 409)
Sector: 210 – 220 (Samples: 717)
Sector: 220 – 230 (Samples: 523)
Sector: 230 – 240 (Samples: 493)
Sector: 240 – 250 (Samples: 666)
Sector: 250 – 260 (Samples: 833)
Sector: 260 – 270 (Samples: 581)
Height [m]
Wind Speed [m/s]

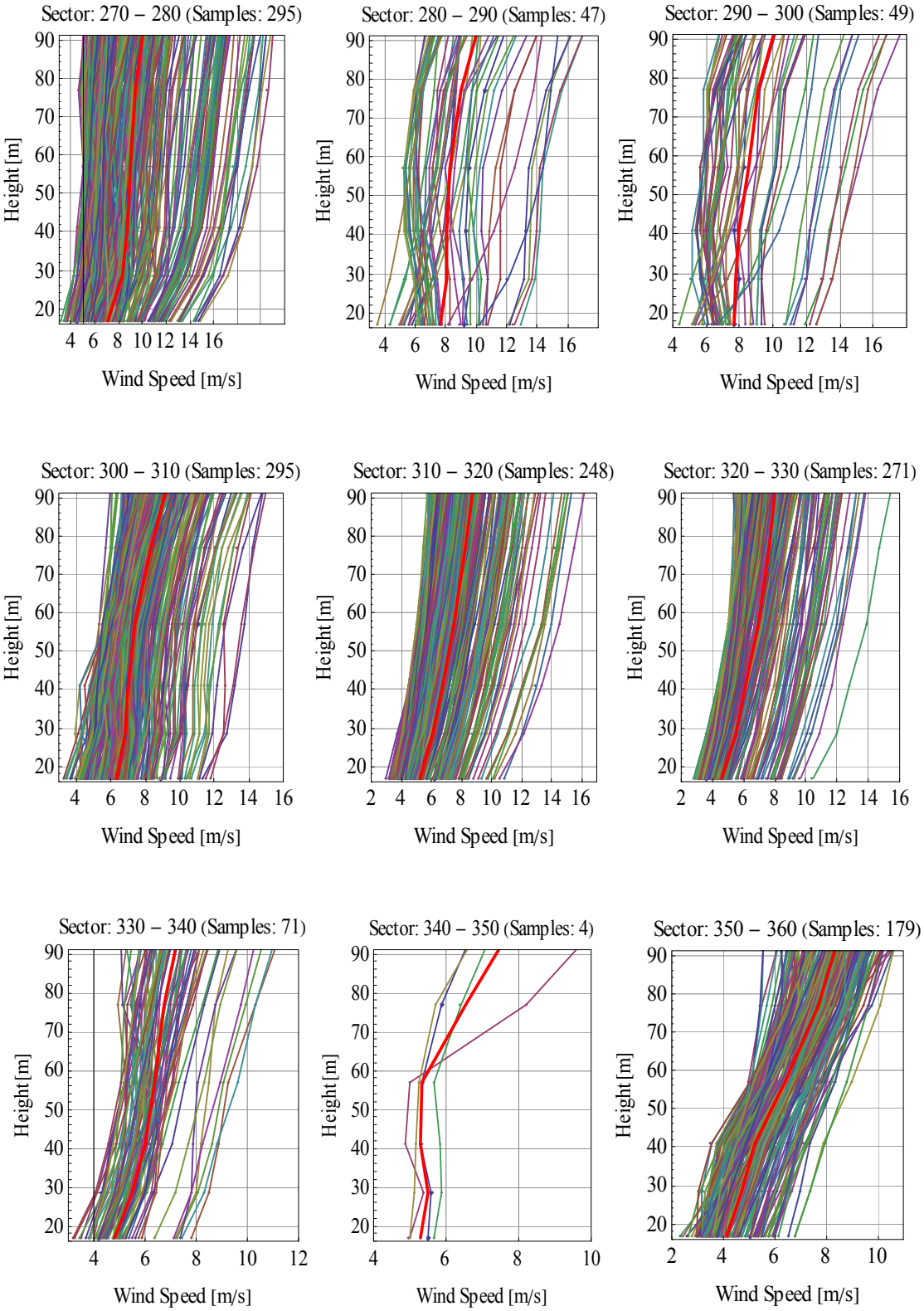
Sector: 270 – 280 (Samples: 295)
Sector: 280 – 290 (Samples: 47)
Sector: 290 – 300 (Samples: 49)
Sector: 300 – 310 (Samples: 295)
Sector: 310 – 320 (Samples: 248)
Sector: 320 – 330 (Samples: 271)
Sector: 330 – 340 (Samples: 71)
Sector: 340 – 350 (Samples: 4)
Sector: 350 – 360 (Samples: 179)
Height [m]
Wind Speed [m/s]

Appendix C: Sonic - Cup Comparison

The ratio between the 10-min average values of the wind speed as measured by sonic and cup anemometers in two different heights (57 m and 90 m) was calculated by taking into account almost one year of data (from the 2008-07-30 00:00 until the 2009-05-15 00:00). The data were filtered by only using wind speed measurements above 4 ms^{-1}. The objective was to investigate the "shadow" effect of the MET mast to the wind speed measurements.

At 90 m it is observed that for wind directions between 100° and 130° the sonic was measuring higher than the cup, while the contrary is observed in the region between 280° and 320°. Therefore the sonic anemometer measurements were selected for comparison with the lidar, for wind directions 100° - 130° and the cup for directions 280° - 320°. Similarly behavior of the ratio at 57 m is observed. The only difference is the sonic is measuring slightly higher wind speeds between 190° and 260°.

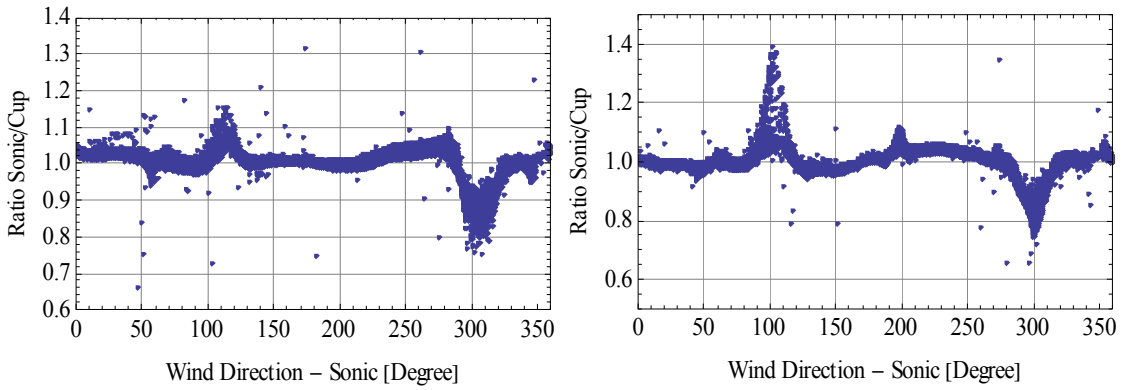

Figure C1 Sonic – Cup wind speed measurements ratio at 90m (left) and 57 (right).

In the same context the correlation between the wind directions as measured both from the sonic and the wind vane were calculated at 57 m and 90 m. It was observed that the vanes both at 57 m and 90 m were not calibrated well.

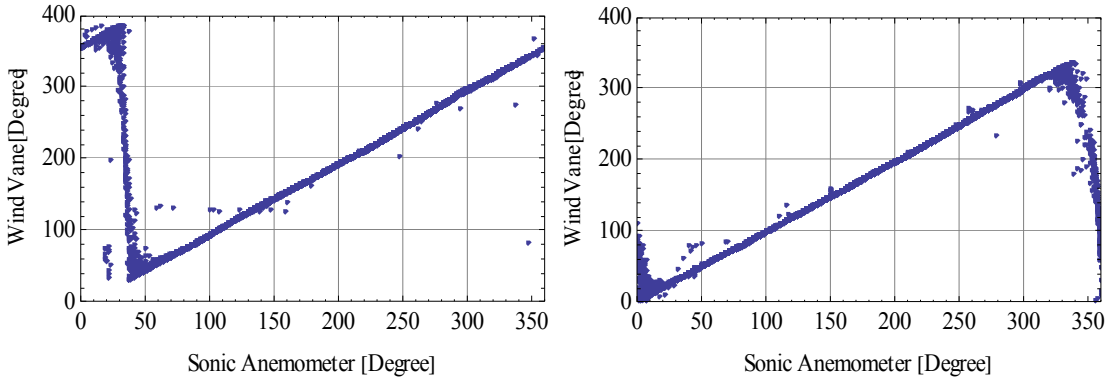

Figure C2 Vane – Sonic wind direction measurements correlation at 90 m (left) and 57 m (right).

Appendix D: Yaw Measurements Calibration

The measurements of the yaw direction started to be acquired on the 16th of July 2009. Using these values it was possible to calibrate the yaw direction data which were streamed from the wind turbine control, in the previous period. In the following figure, the time series (1 Hz) of the wind direction (as measured from the wind vane and sonic, both at 57 m, Vdir57m and Sdir57m, respectively), the yaw direction measurement (YawM) and the streamed position of the wind turbine (YawC) are presented. The plot corresponds to a 10 minute period, from 12:40 to 12:50. It can be observed that the wind direction is between 230° and 240°. The offset between the yaw measurements and the indication of the wind turbine control was found to be equal with -17.9°. This offset value was used to correct the wind turbine control data, so as to be possible to have an indication of the direction of the wind turbine during the period which corresponds to the second phase of the experiment.

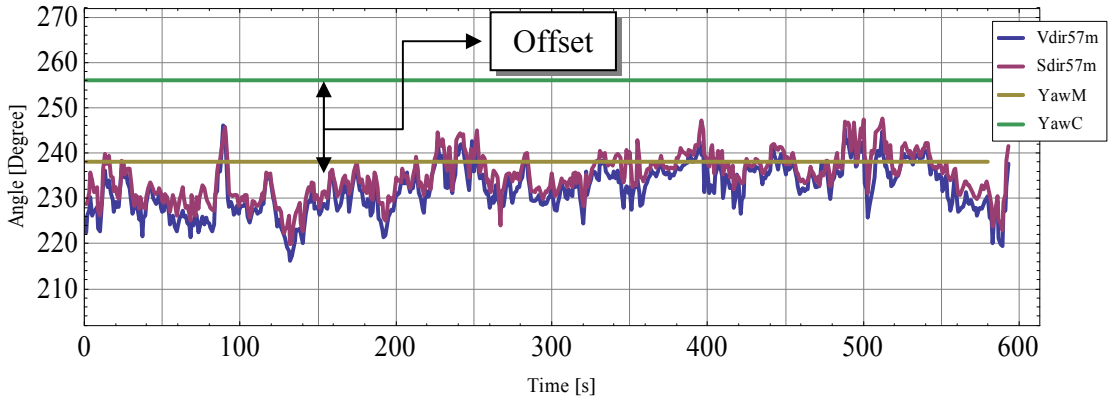

Figure D.1 Time series of the direction of both the wind and the wind turbine.

Appendix E: Yaw misalignment correlation

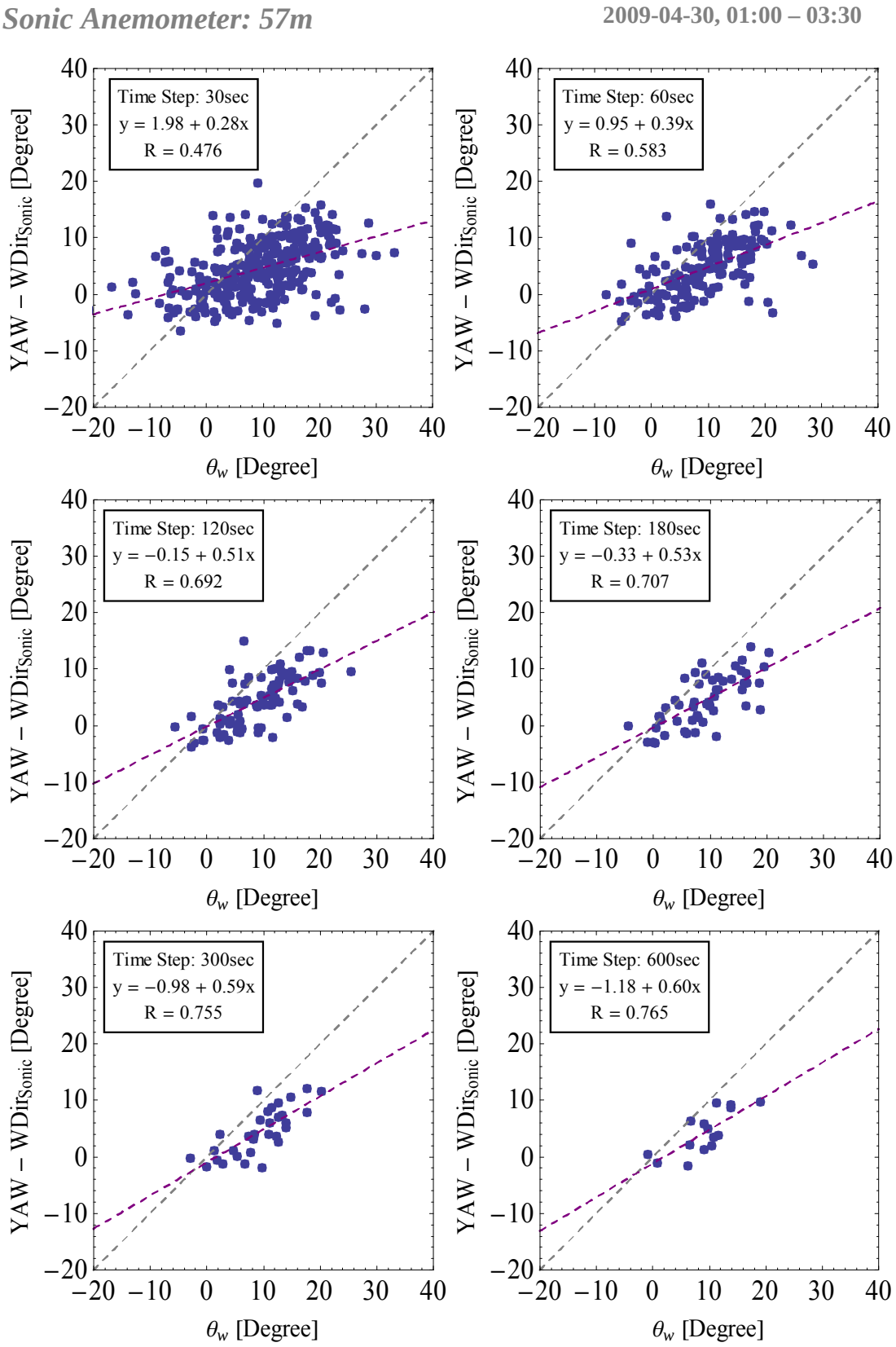

Figure E.1 Correlation plots of the yaw misalignment as calculated from the lidar and the difference between the wind turbine yaw and the wind direction (sonic) at 57 m.

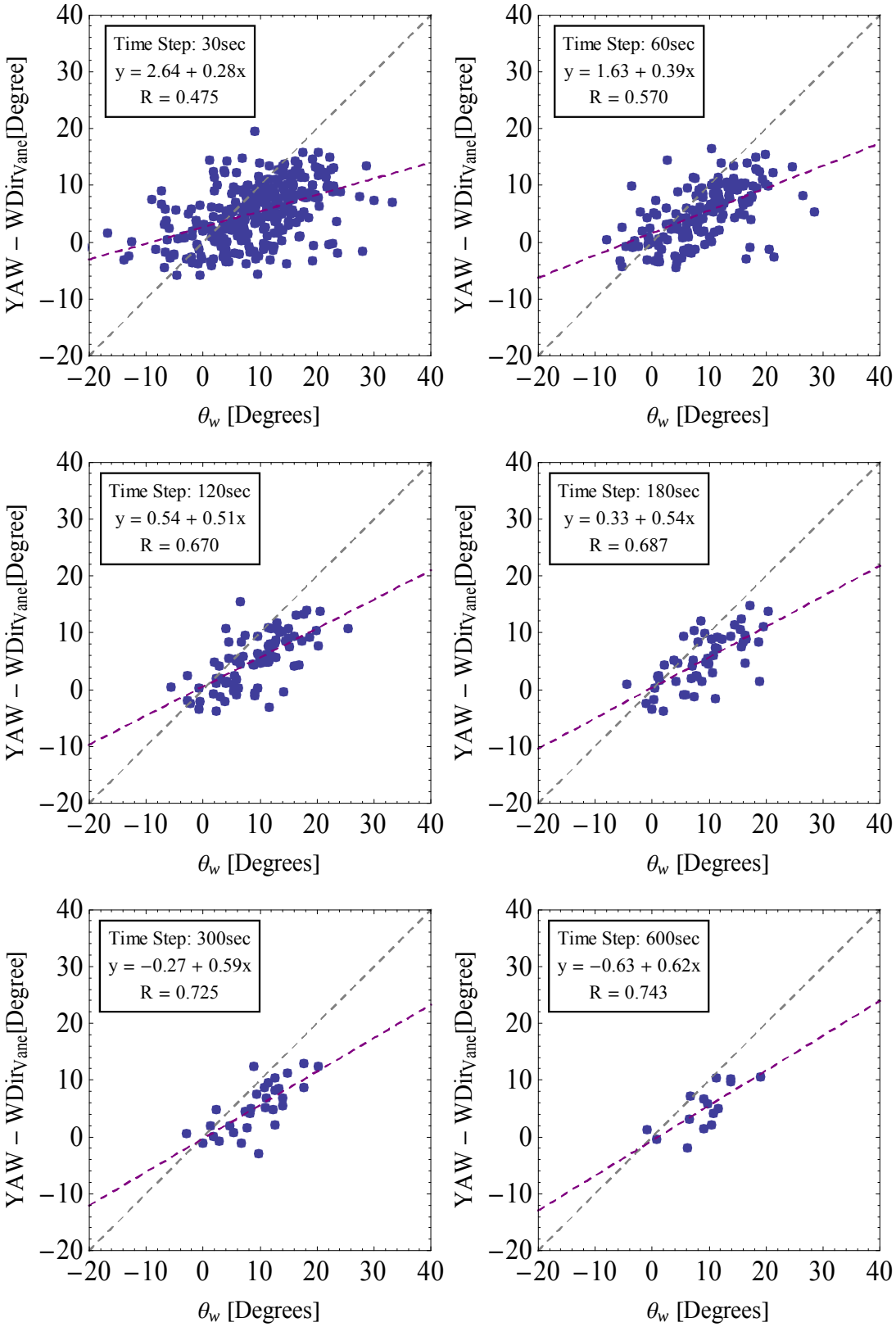

Figure E.2 Correlation plots of the yaw misalignment as calculated from the lidar and the difference between the wind turbine yaw and the wind direction (vane) at 57 m.

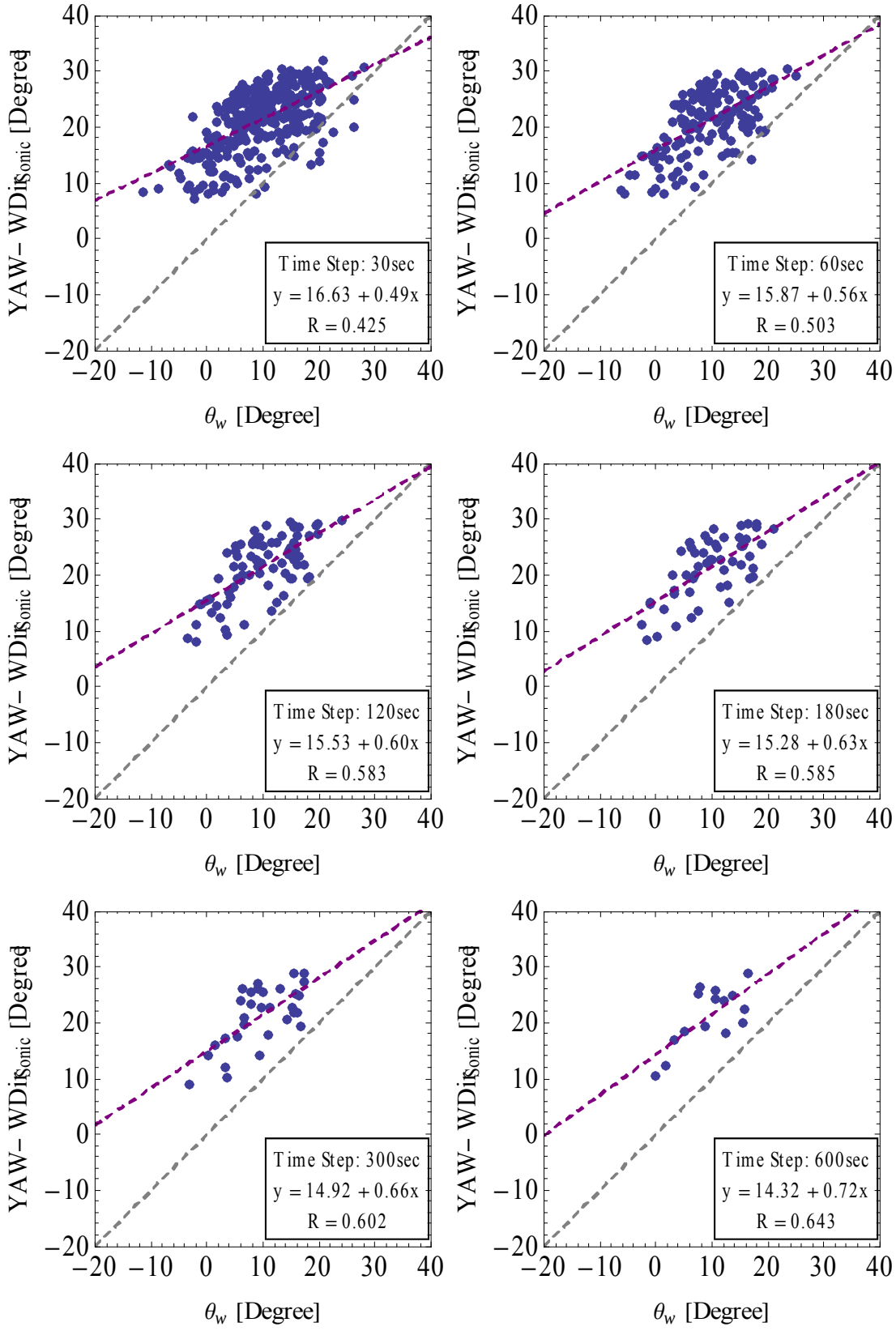

Figure E.3 Correlation plots of the yaw misalignment as calculated from the lidar and the difference between the wind turbine yaw and the wind direction (sonic) at 93 m.

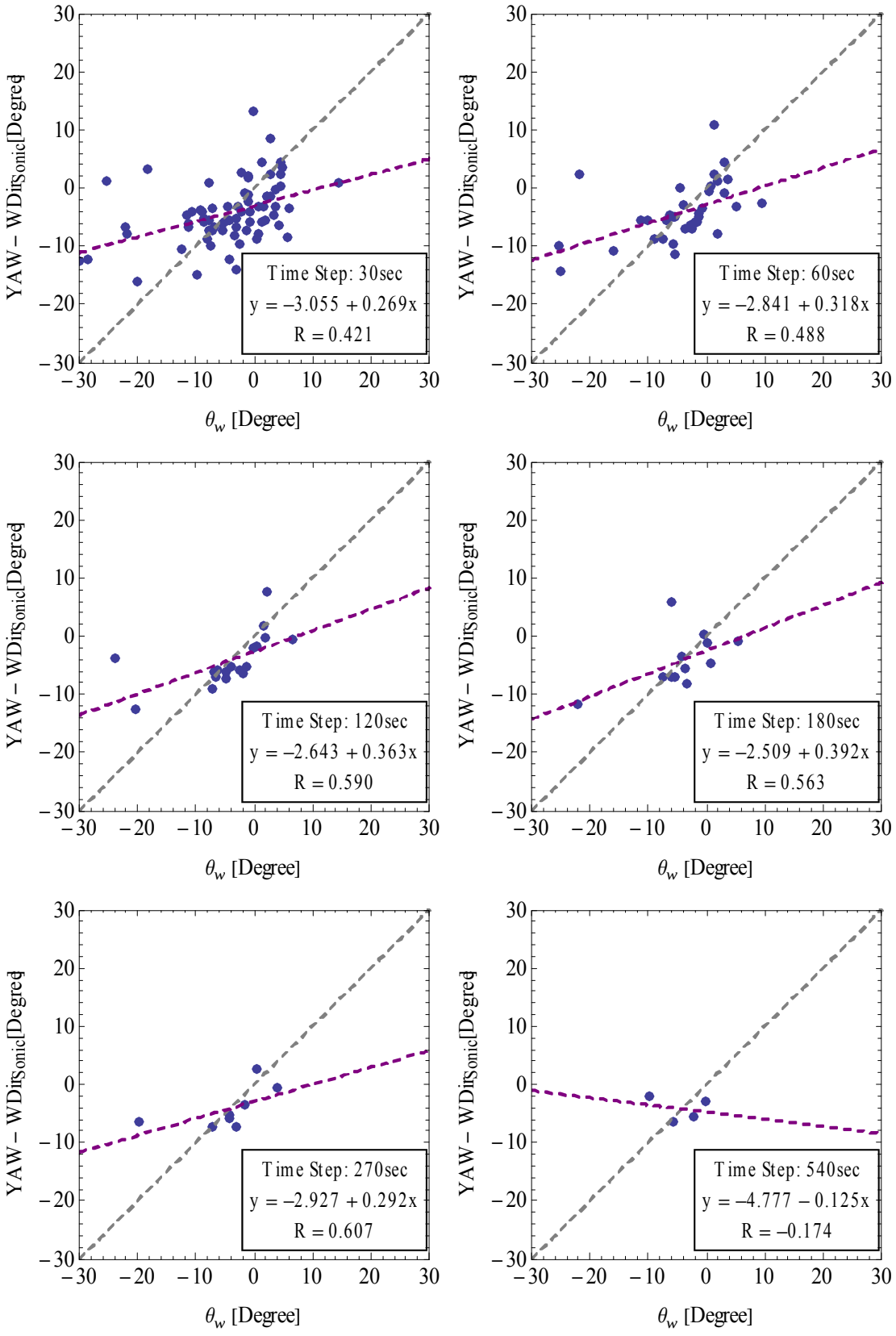

Figure E.4 Correlation plots of the yaw misalignment as calculated from the lidar and the difference between the wind turbine yaw and the wind direction (sonic) at 57 m.

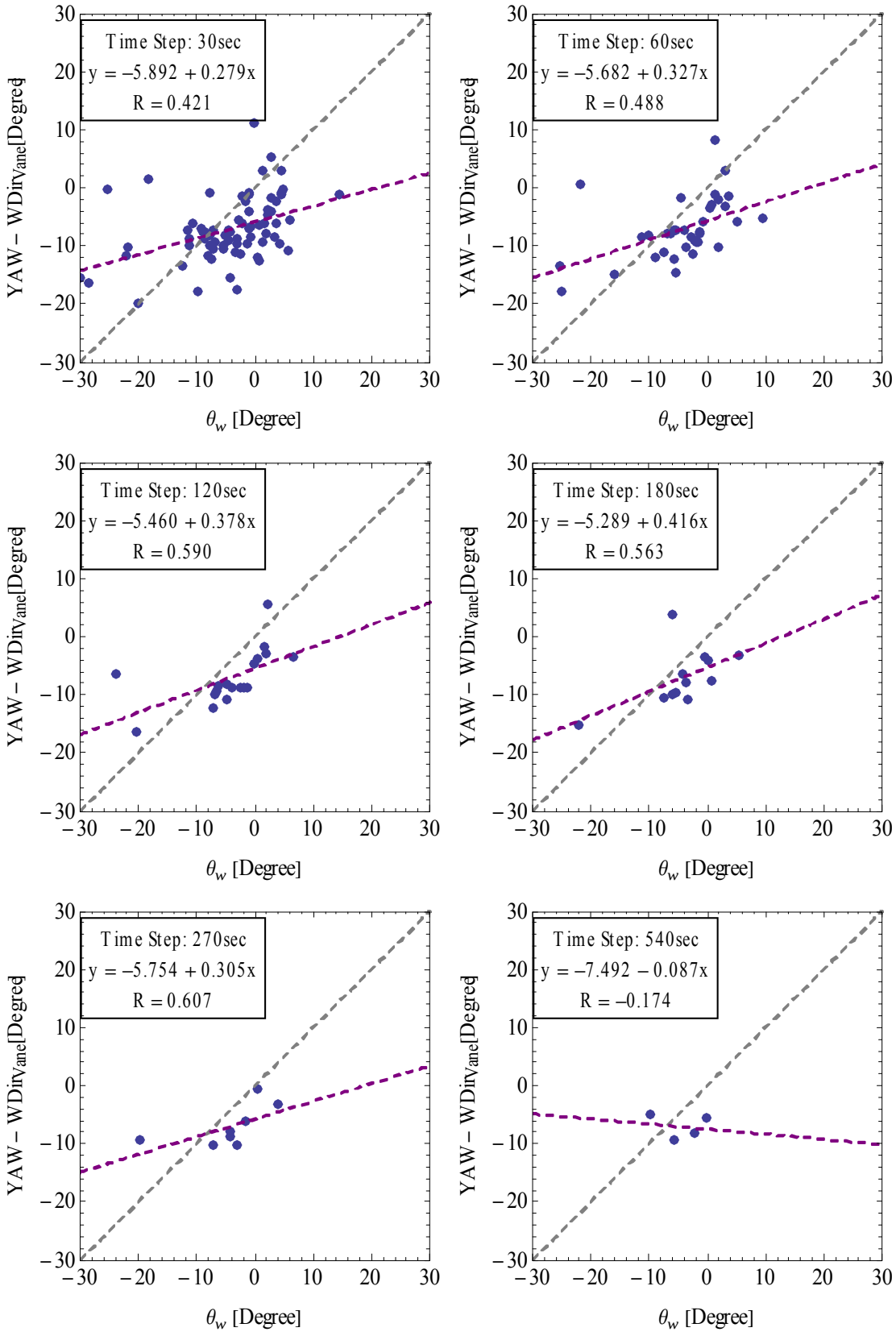

Figure E.5 Correlation plots of the yaw misalignment as calculated from the lidar and the difference between the wind turbine yaw and the wind direction (vane) at 57 m.

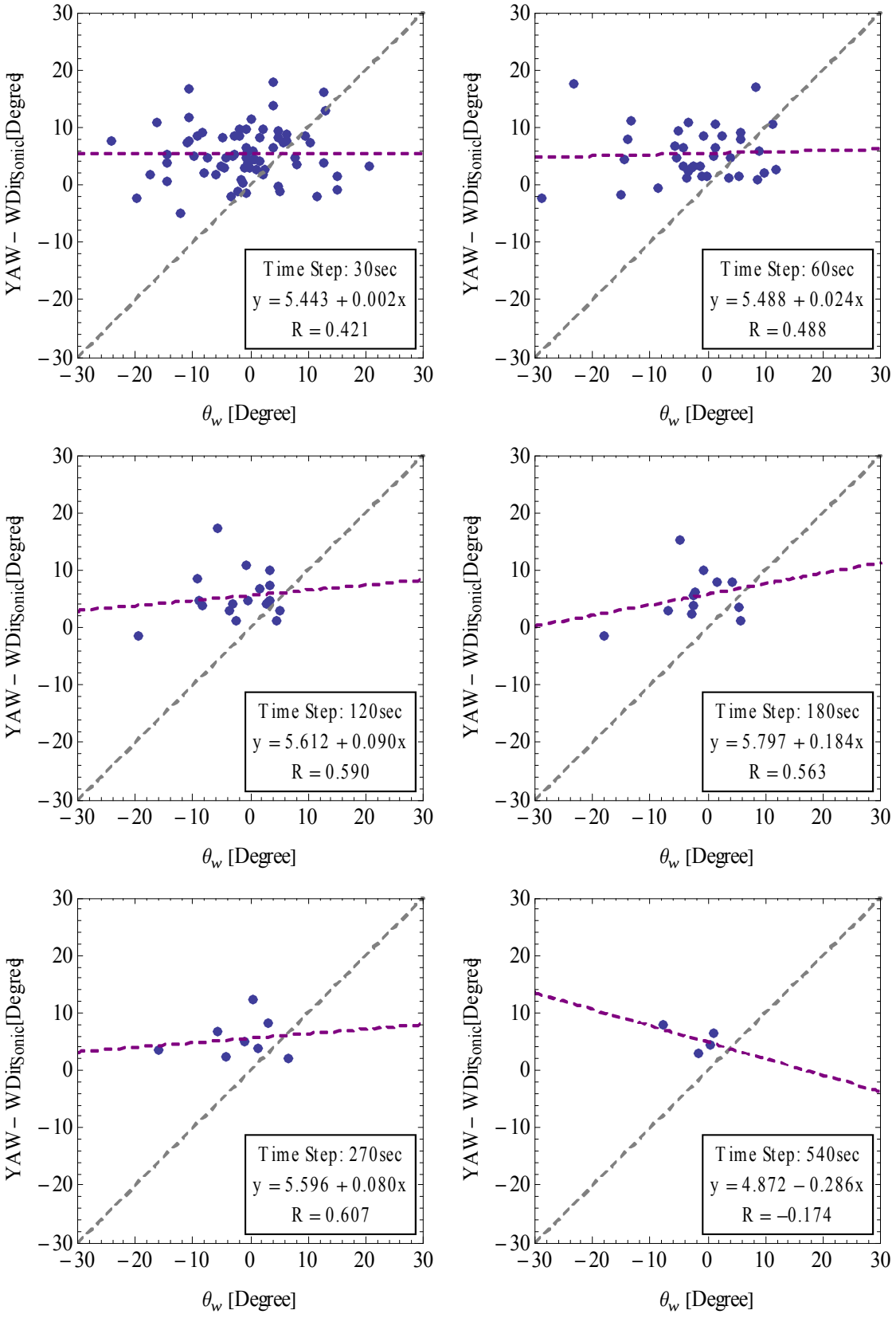

Figure E.6 Correlation plots of the yaw misalignment as calculated from the lidar and the difference between the wind turbine yaw and the wind direction (sonic) at 93 m.

Appendix F: Time series of the yaw misalignment

Sonic Anemometer: 57m **2009-04-30, 01:00 – 03:30**

Frequency: 30sec

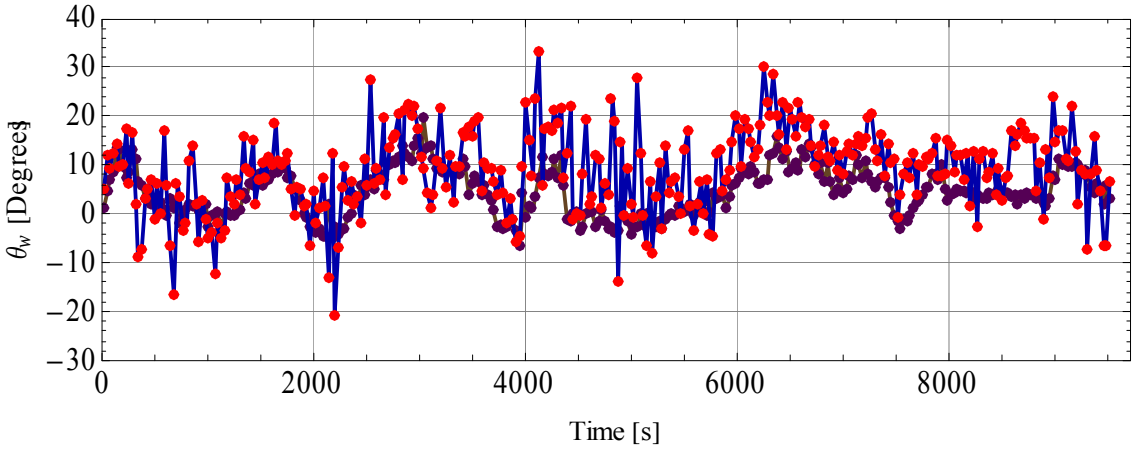

Frequency: 1min

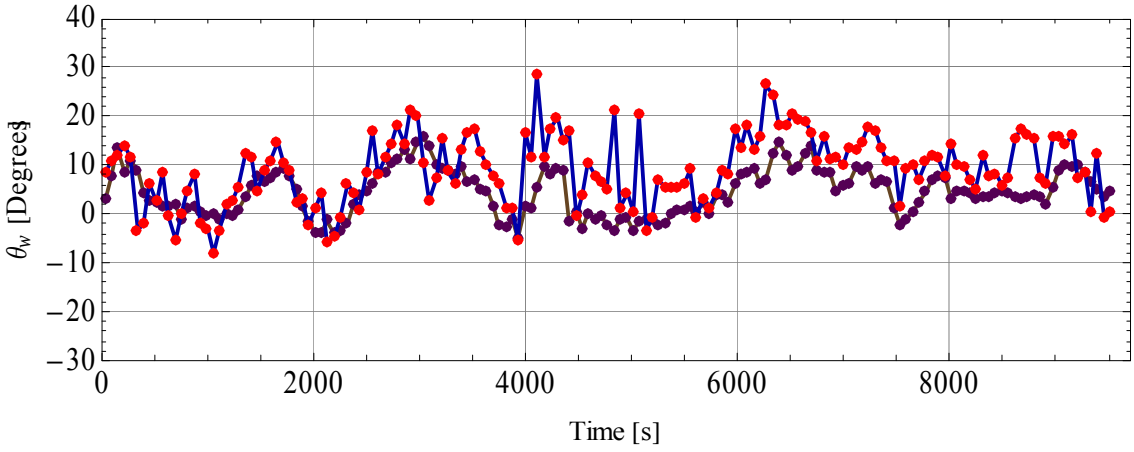

Frequency: 2min

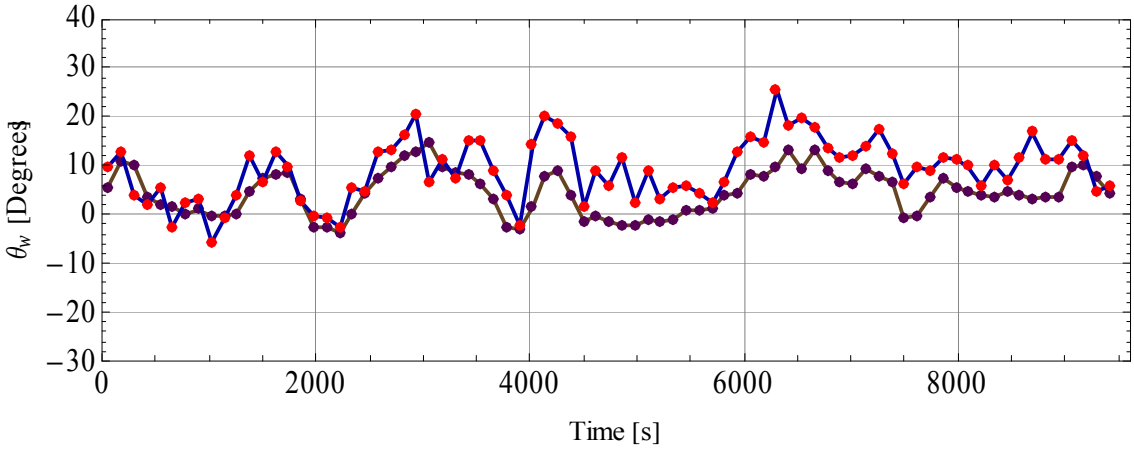

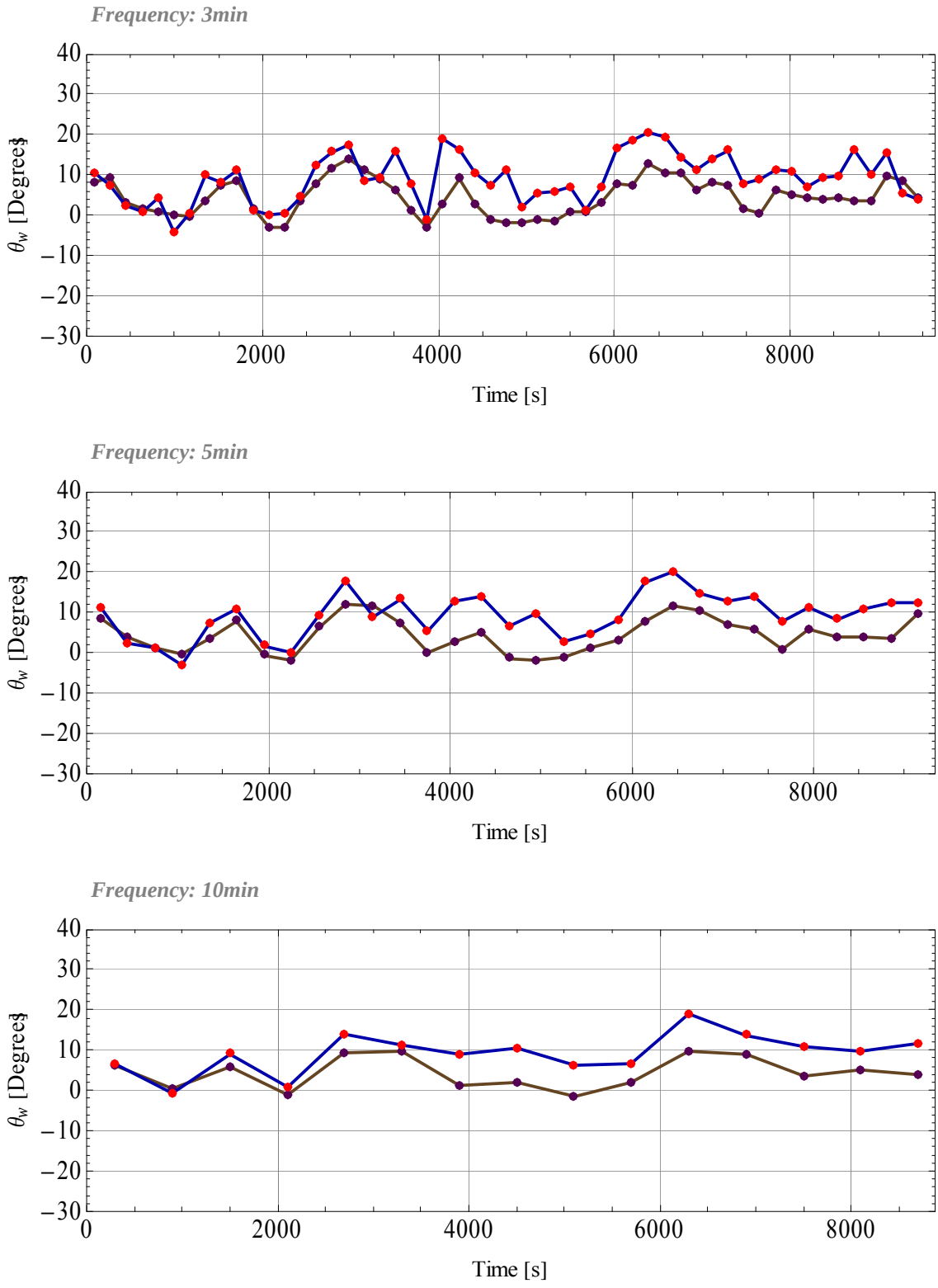

Figure F.1 Time series of the yaw misalignment as calculated from the lidar (blue curve) and the difference between the wind turbine yaw and the wind direction (sonic, brown curve) at 57 m.

Frequency: 30sec

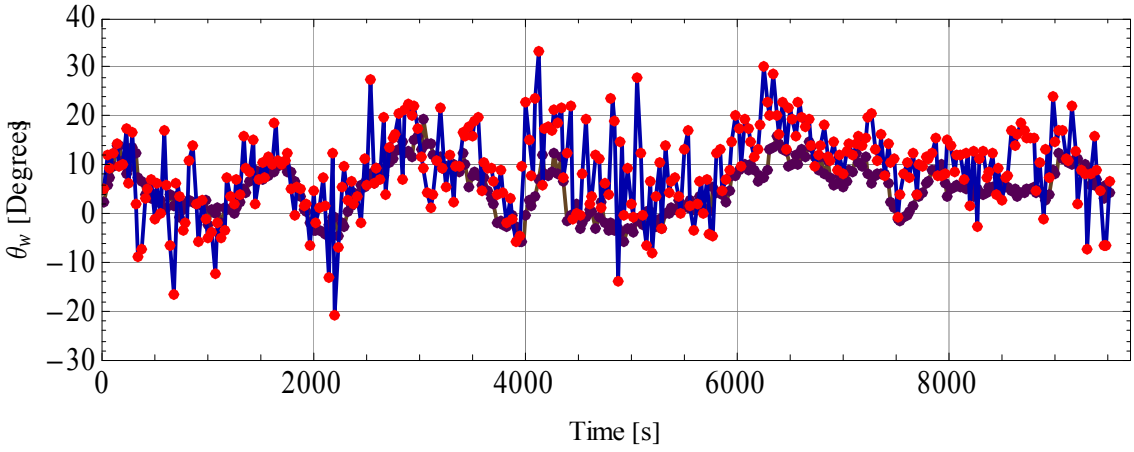

Frequency: 1min

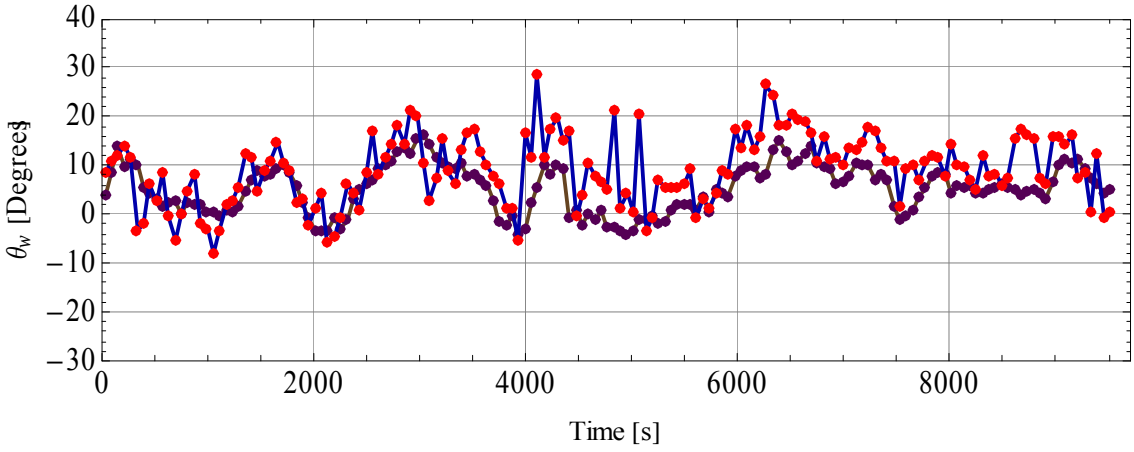

Frequency: 2min

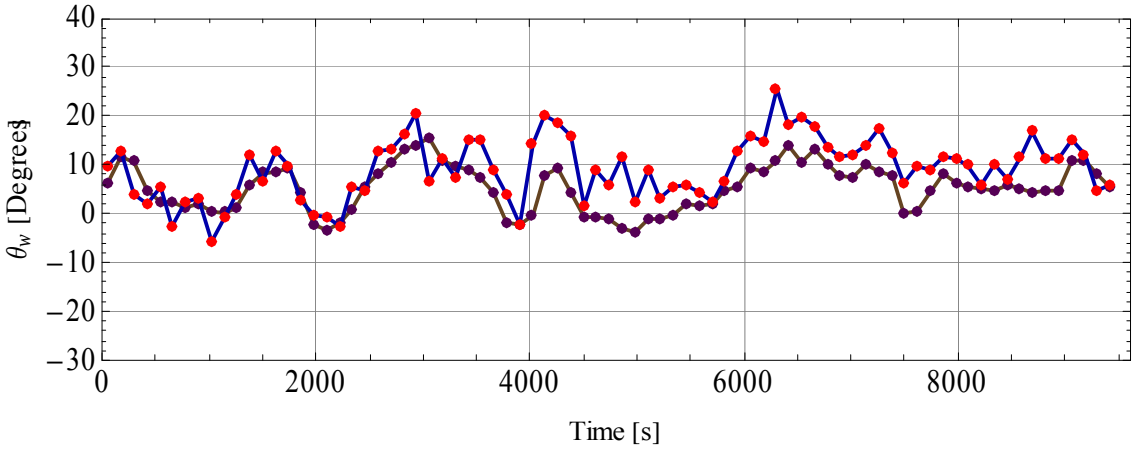

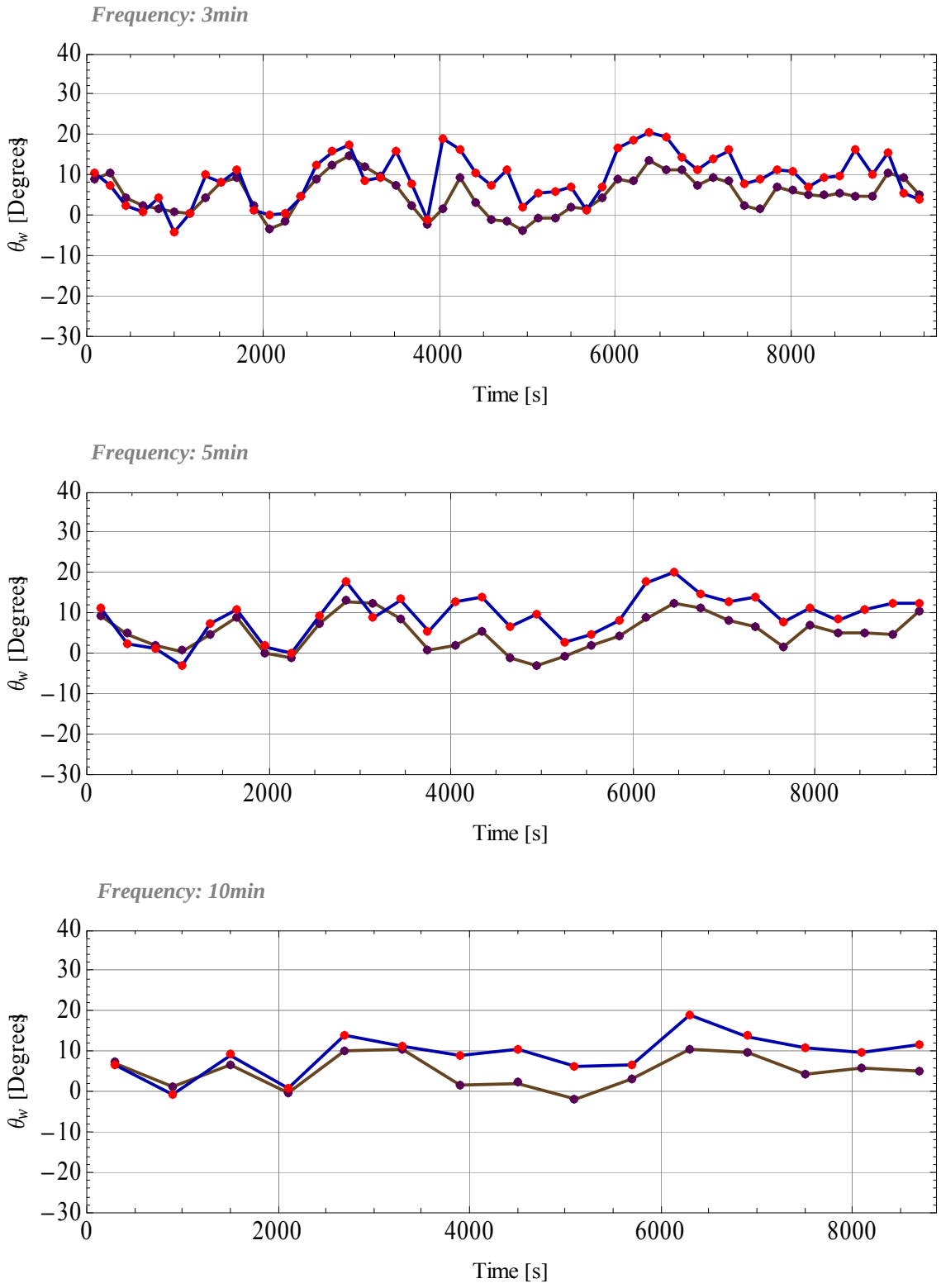

Figure F.2 Time series of the yaw misalignment as calculated from the lidar (blue curve) and the difference between the wind turbine yaw and the wind direction (vane, brown curve) at 57 m.

Frequency: 30sec

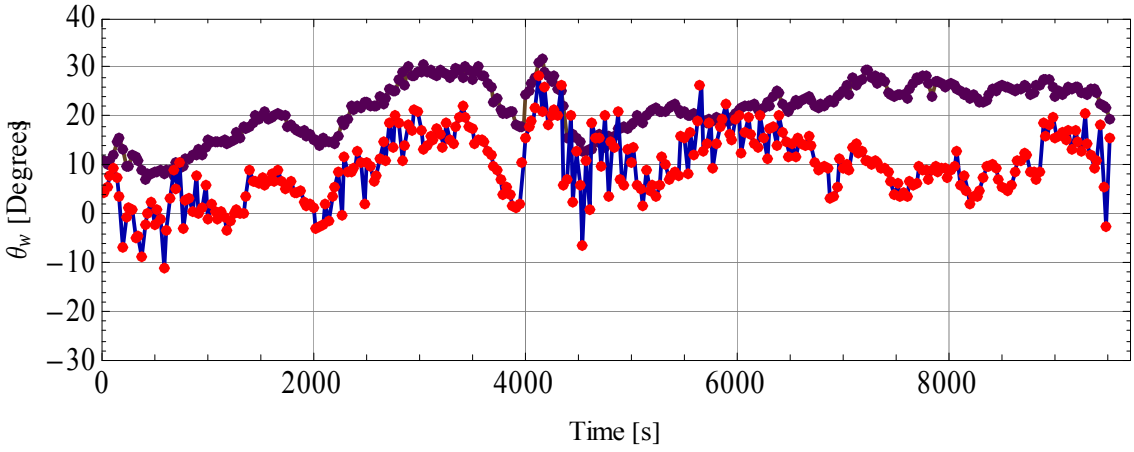

Frequency: 1min

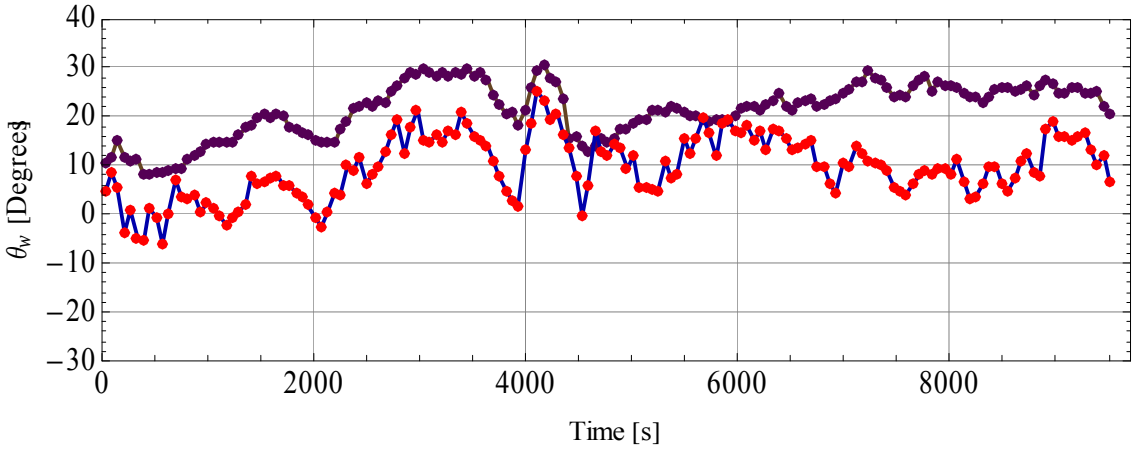

Frequency: 2min

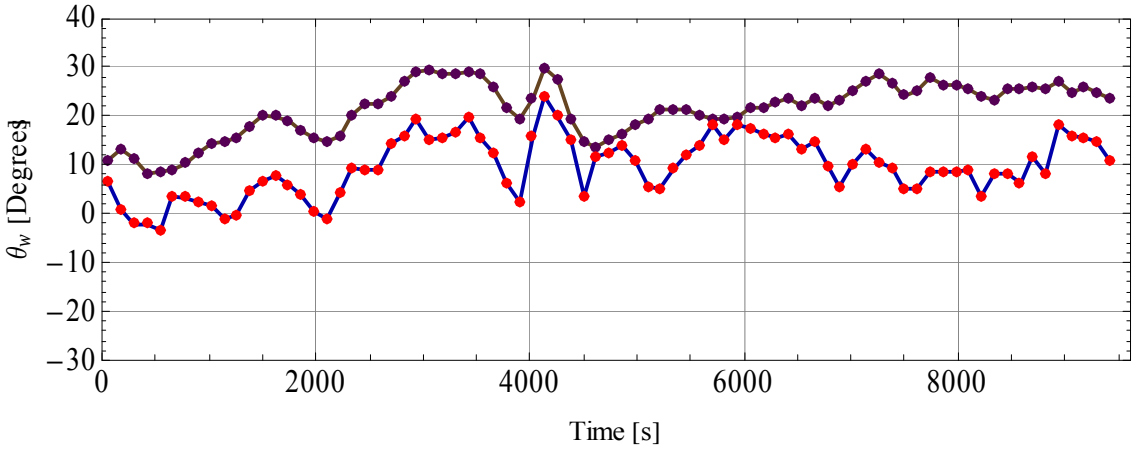

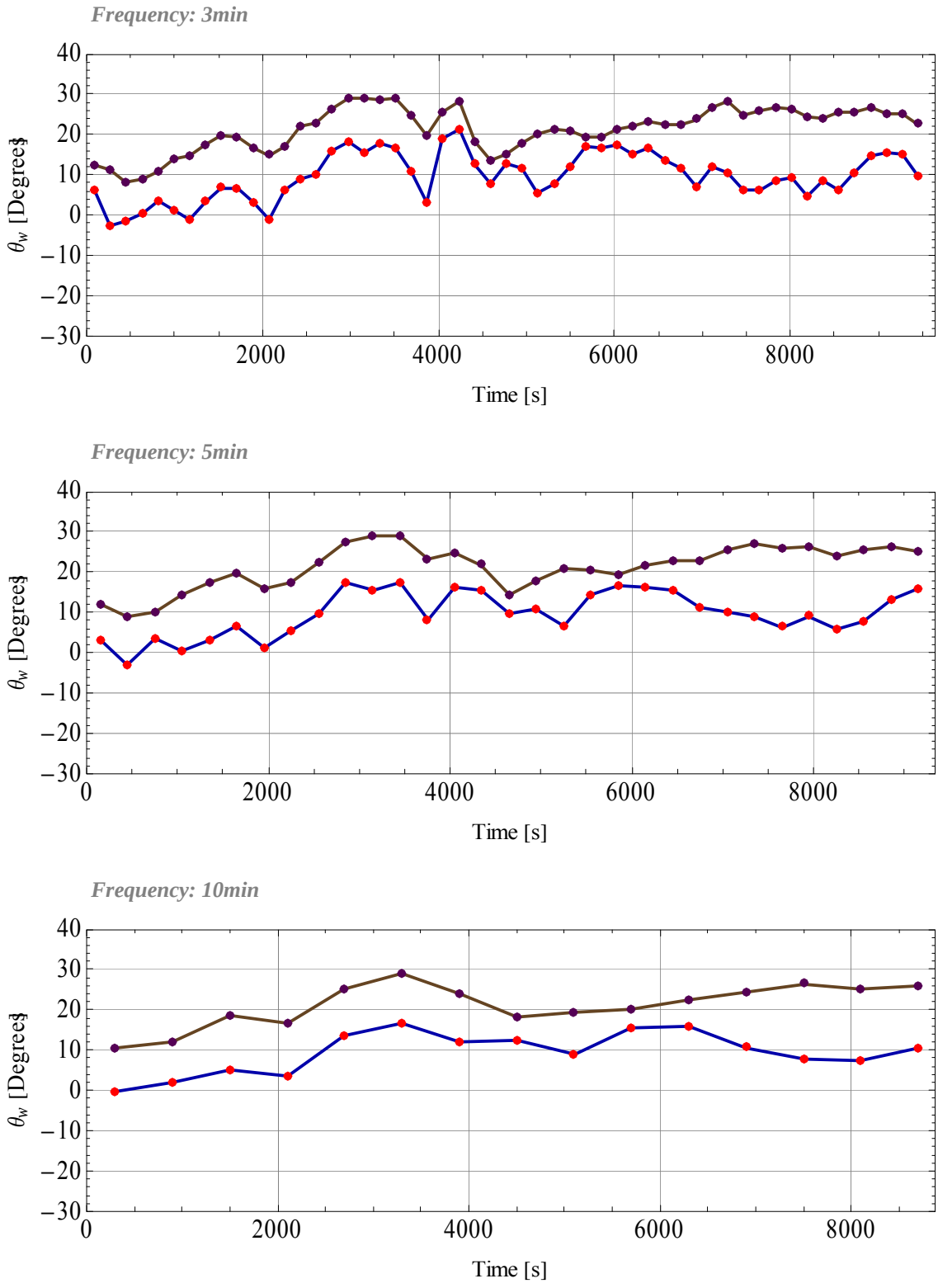

Figure F.3 Time series of the yaw misalignment as calculated from the lidar (blue curve) and the difference between the wind turbine yaw and the wind direction (vane, brown curve) at 93 m.

Frequency: 30sec

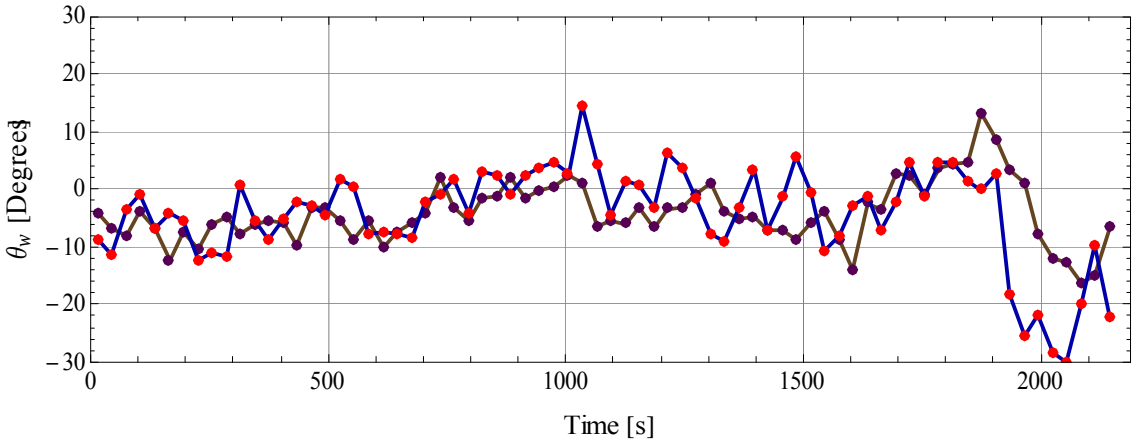

Frequency: 1min

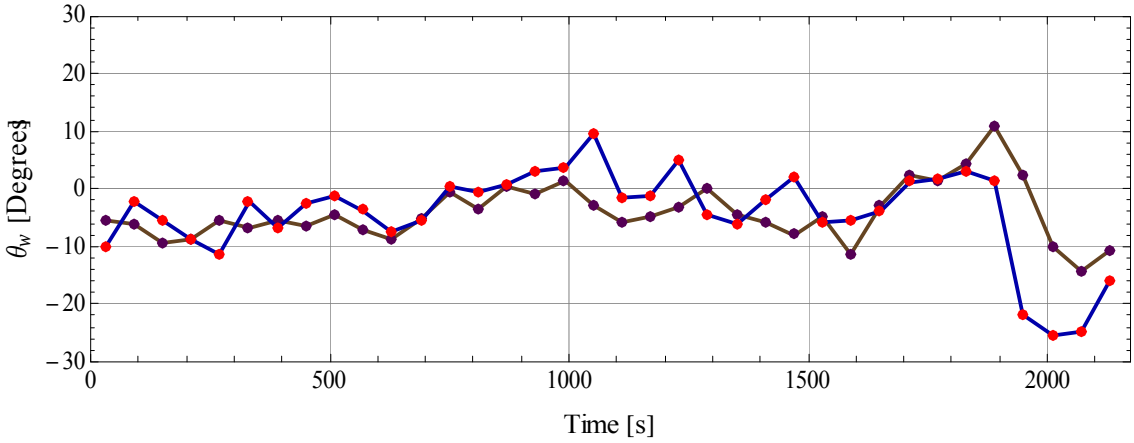

Frequency: 2min

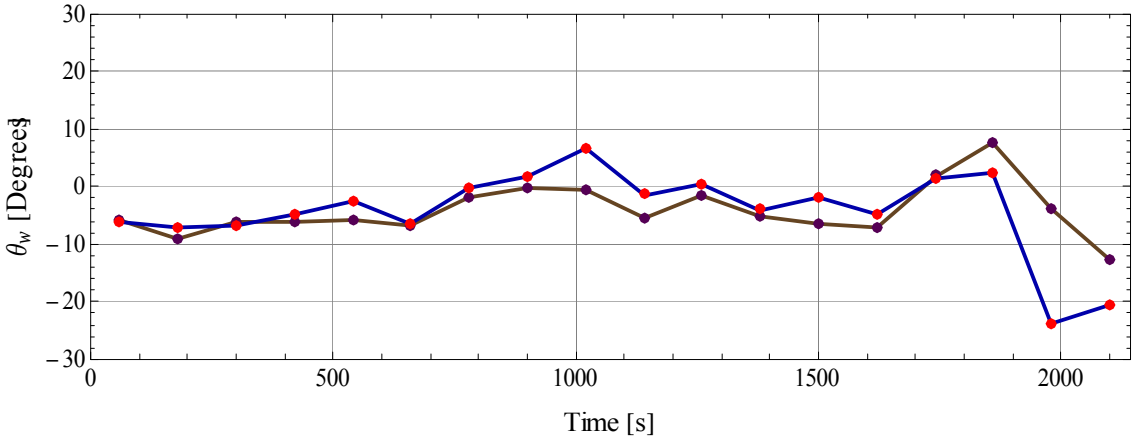

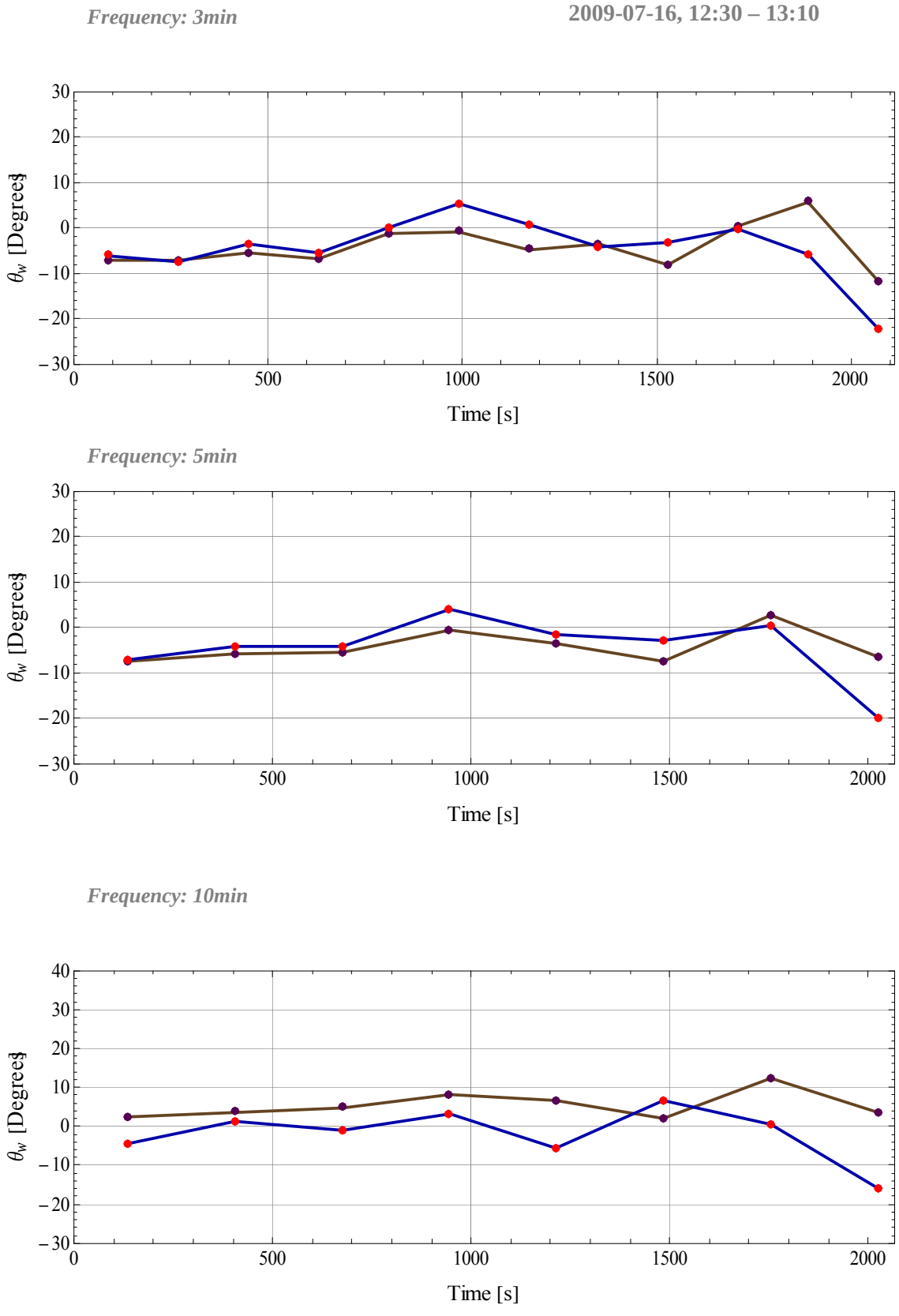

Figure F.4 Time series of the yaw misalignment as calculated from the lidar (blue curve) and the difference between the wind turbine yaw and the wind direction (sonic, brown curve) at 57 m.

Frequency: 30sec

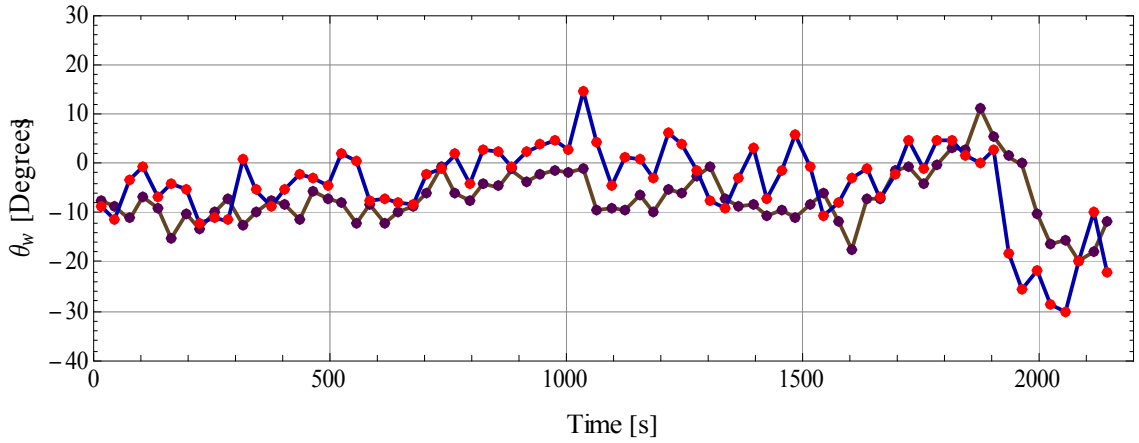

Frequency: 1min

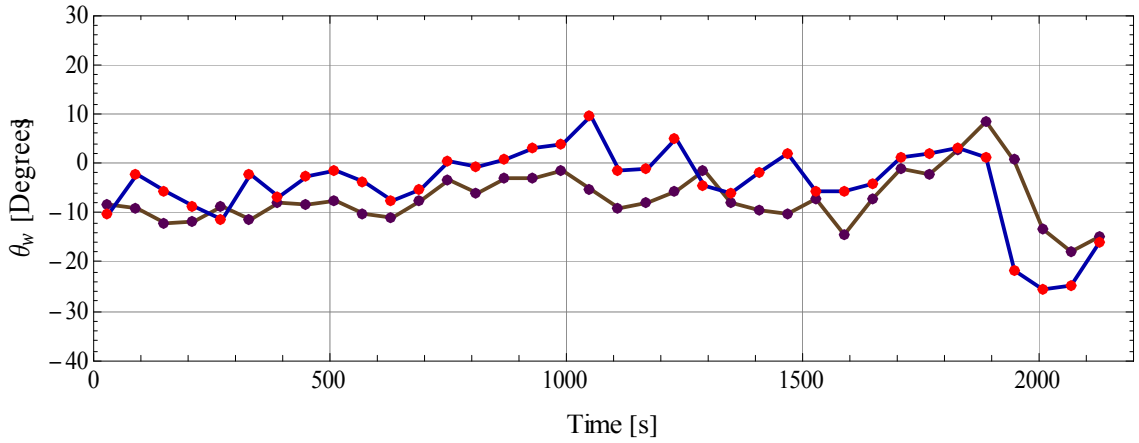

Frequency: 2min

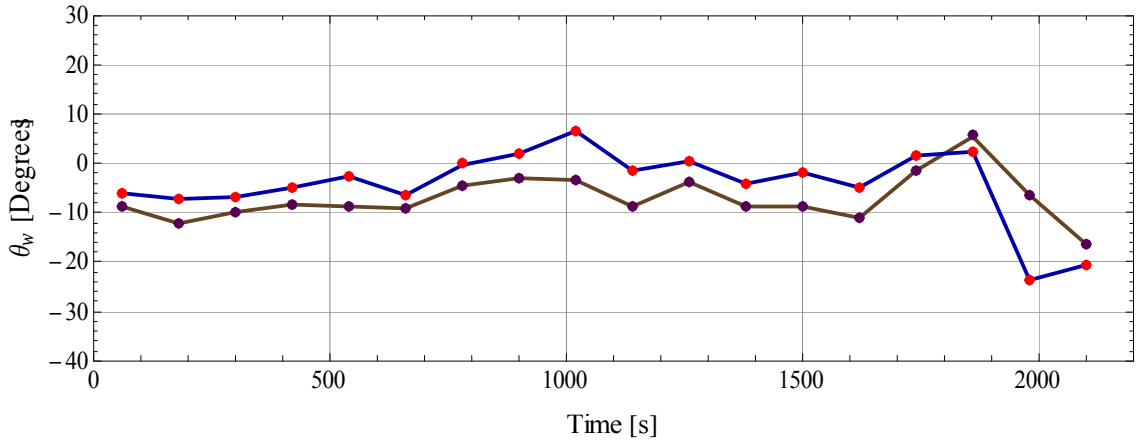

Frequency: 3min **2009-07-16, 12:30 – 13:10**

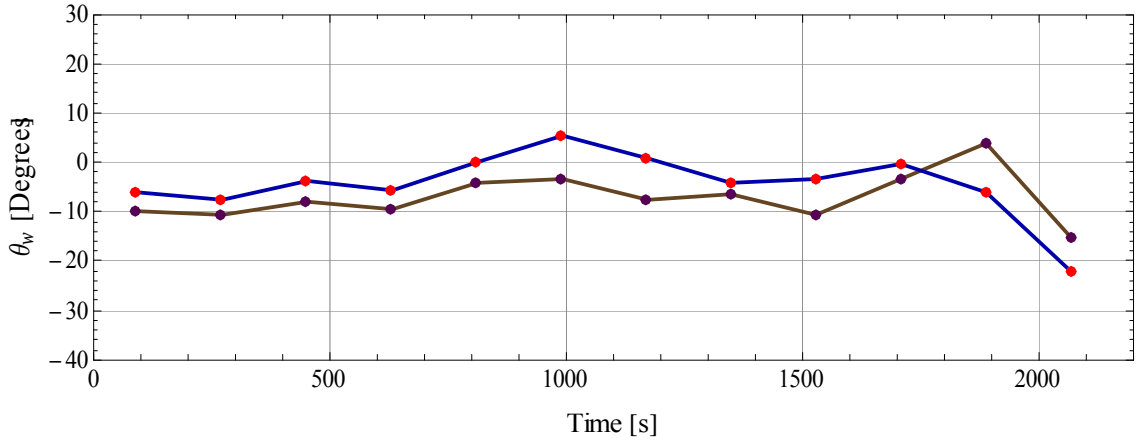

Frequency: 5min

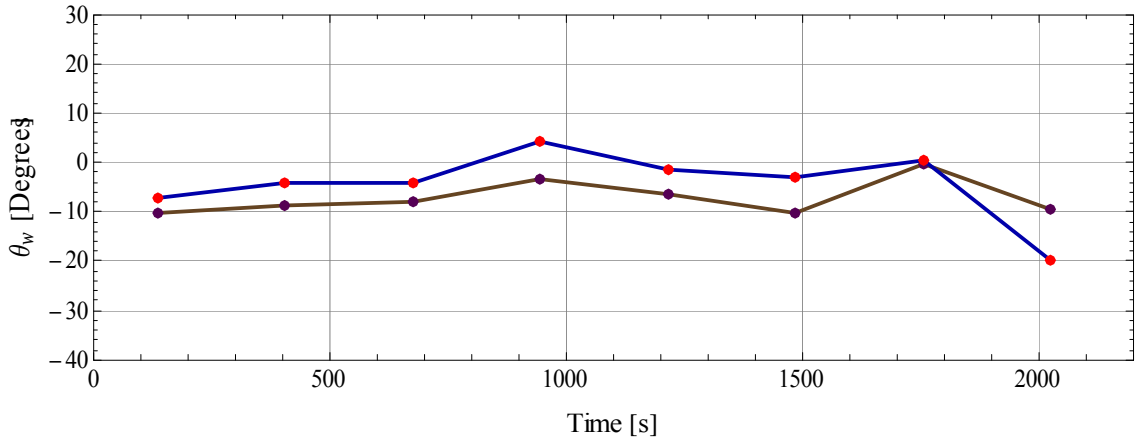

Frequency: 10min

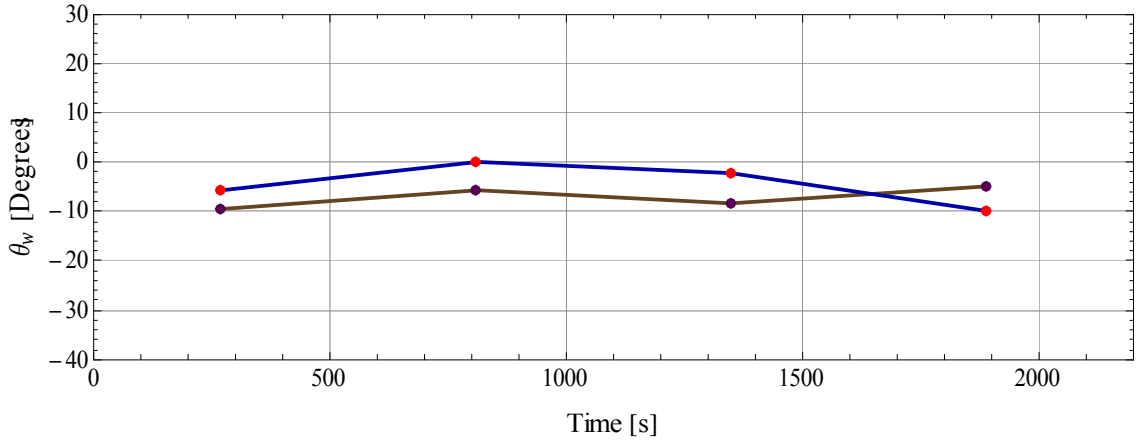

Figure F.5 Time series of the yaw misalignment as calculated from the lidar (blue curve) and the difference between the wind turbine yaw and the wind direction (vane, brown curve) at 57 m.

Frequency: 30sec

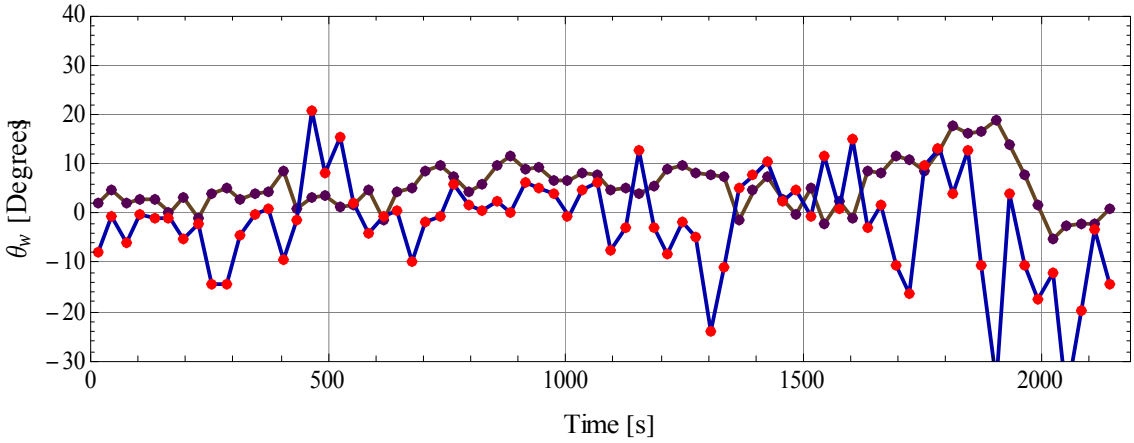

Frequency: 1min

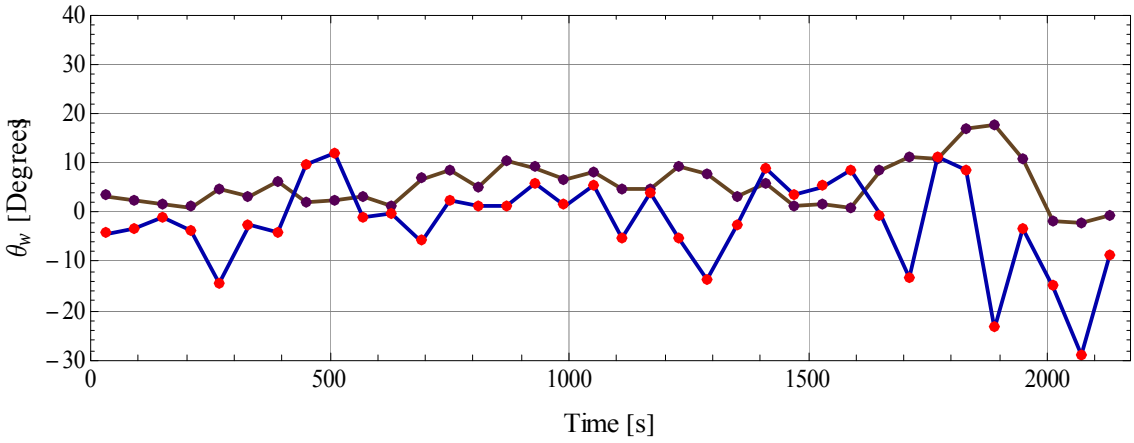

Frequency: 2min

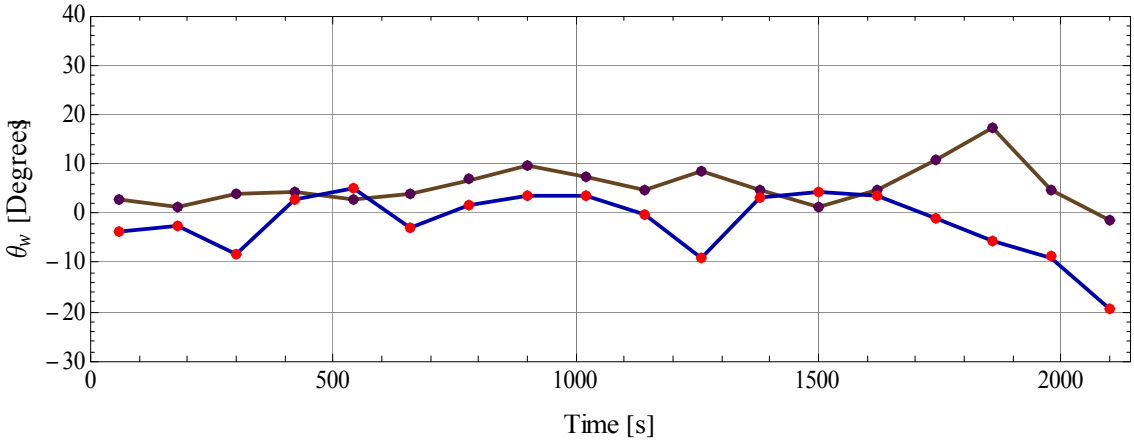

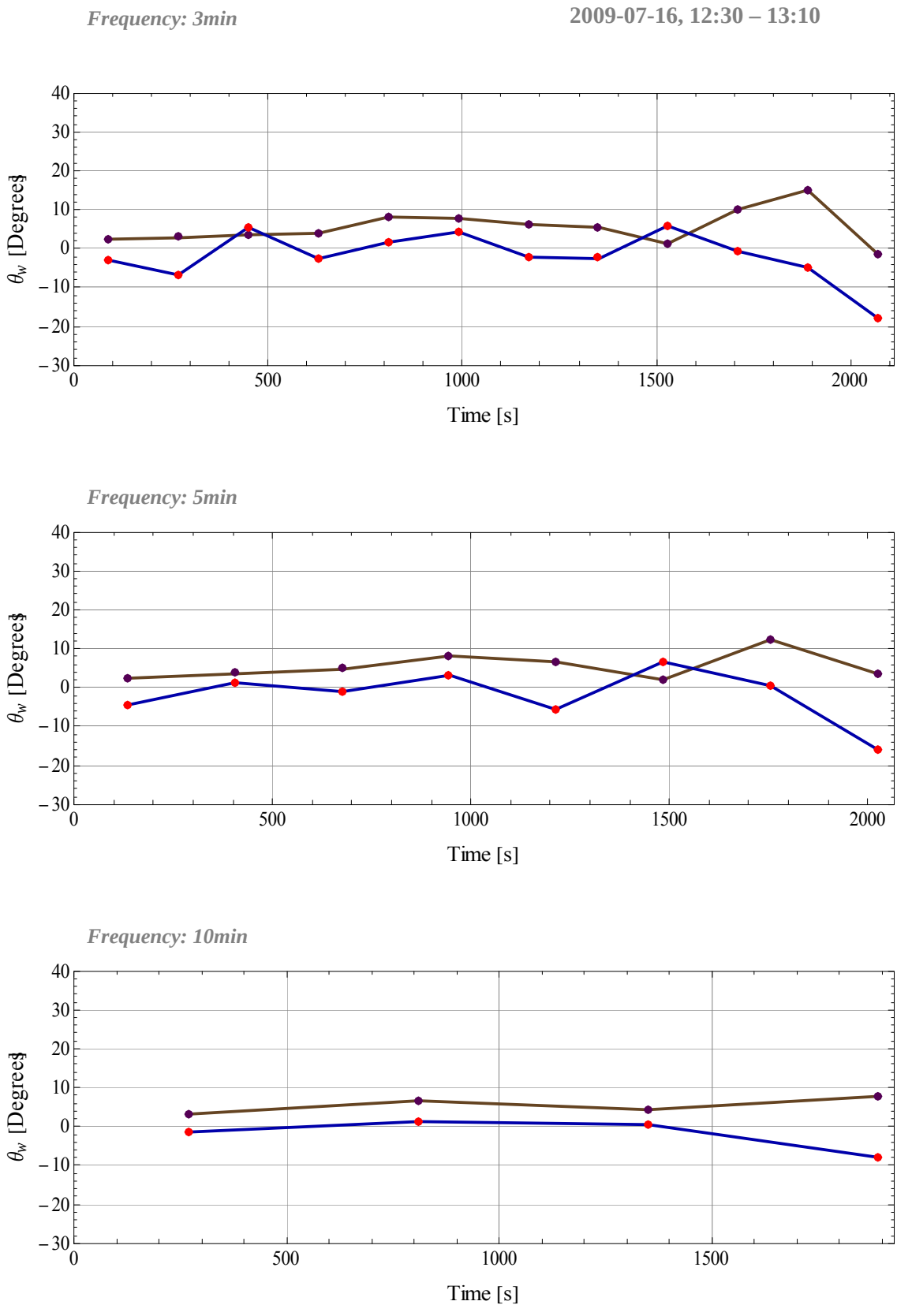

Figure F.6 Time series of the yaw misalignment as calculated from the lidar (blue curve) and the difference between the wind turbine yaw and the wind direction (sonic, brown curve) at 93 m.

Risø DTU is the National Laboratory for Sustainable Energy. Our research focuses on development of energy technologies and systems with minimal effect on climate, and contributes to innovation, education and policy. Risø has large experimental facilities and interdisciplinary research environments, and includes the national centre for nuclear technologies.

Risø DTU
National Laboratory for Sustainable Energy
Technical University of Denmark

Frederiksborgvej 399
PO Box 49
DK-4000 Roskilde
Denmark
Phone +45 4677 4677
Fax +45 4677 5688

www.risoe.dtu.dk